AD NUMBER

AD474639

NEW LIMITATION CHANGE

TO

Approved for public release, distribution unlimited

FROM

Distribution authorized to U.S. Gov't. agencies and their contractors; Critical Technology; NOV 1965. Other requests shall be referred to Air Force Aero Propulsion Laboratory, Aerospace Power Division, Wright-Patterson, AFB, OH.

AUTHORITY

afapl ltr, 12 apr 1972

SECURITY MARKING

The classified or limited status of this report applies to each page, unless otherwise marked.
Separate page printouts MUST be marked accordingly.

THIS DOCUMENT CONTAINS INFORMATION AFFECTING THE NATIONAL DEFENSE OF THE UNITED STATES WITHIN THE MEANING OF THE ESPIONAGE LAWS, TITLE 18, U.S.C., SECTIONS 793 AND 794. THE TRANSMISSION OR THE REVELATION OF ITS CONTENTS IN ANY MANNER TO AN UNAUTHORIZED PERSON IS PROHIBITED BY LAW.

NOTICE: When government or other drawings, specifications or other data are used for any purpose other than in connection with a definitely related government procurement operation, the U. S. Government thereby incurs no responsibility, nor any obligation whatsoever; and the fact that the Government may have formulated, furnished, or in any way supplied the said drawings, specifications, or other data is not to be regarded by implication or otherwise as in any manner licensing the holder or any other person or corporation, or conveying any rights or permission to manufacture, use or sell any patented invention that may in any way be related thereto.

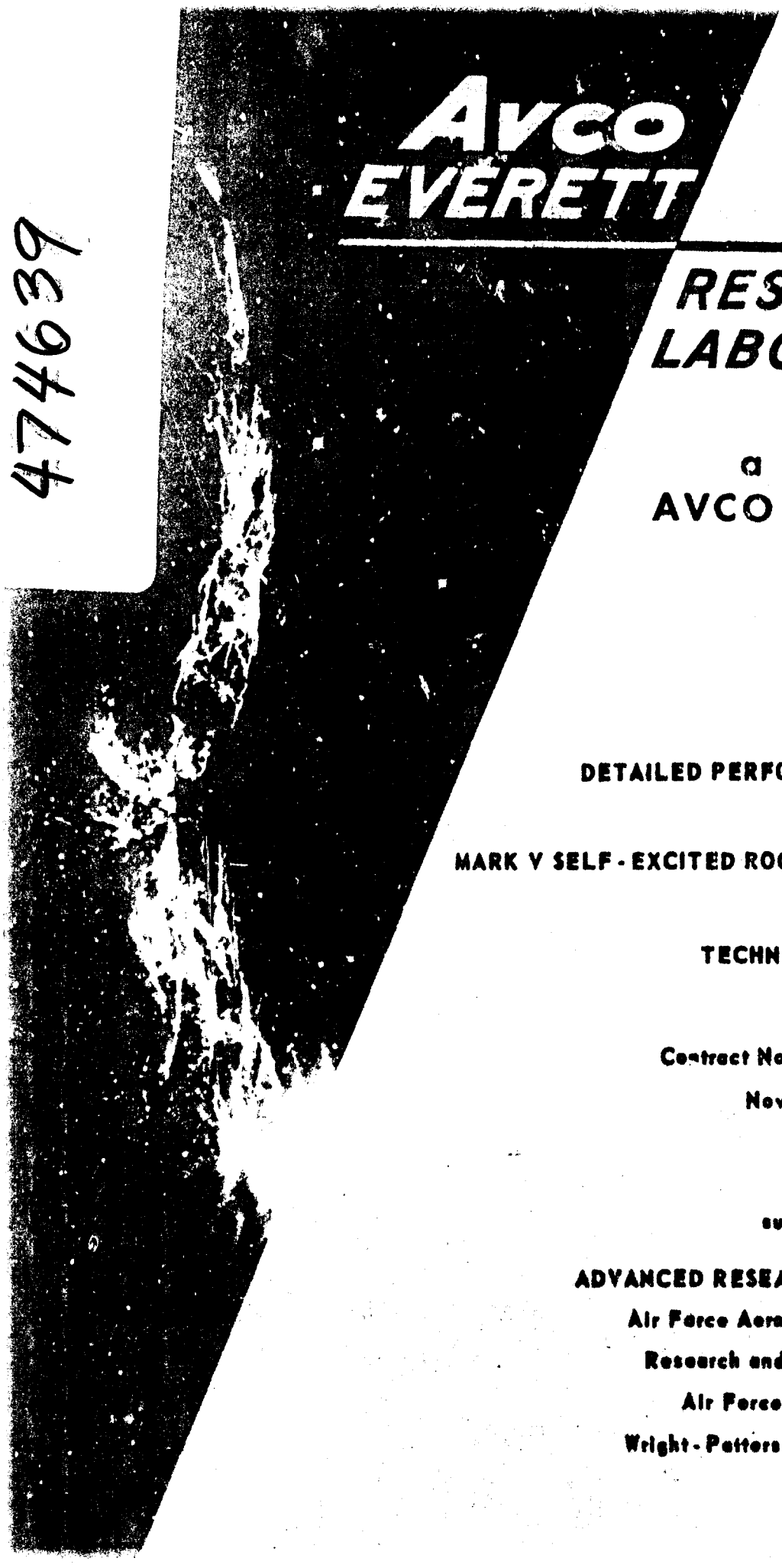

AVCO EVERETT

RESEARCH LABORATORY

a division of
AVCO CORPORATION

DETAILED PERFORMANCE EVALUATION of the MARK V SELF-EXCITED ROCKET DRIVEN MHD GENERATOR

TECHNICAL REPORT

Contract No. AF 33(615)-1862
November 1965

supported by

ADVANCED RESEARCH PROJECTS AGENCY
Air Force Aero Propulsion Laboratory
Research and Technology Division
Air Force Systems Command
Wright-Patterson Air Force Base, Ohio

NOTICES

When Government drawings, specifications, or other data are used for any purpose other than in connection with a definitely related Government procurement operation, the United States Government therby incurs no responsibility nor any obligation whatsoever; and the fact that the Government may have formulated, furnished, or in any way supplied the said drawings, specifications, or other data, is not to be regarded by implication or otherwise as in any manner licensing the holder or any other person or corporation. or conveying any rights or permission to manufacture, use or sell any patented invention that may in any way be related thereto.

This document is subject to special export controls and each transmittal to foreign governments or foreign nationals may be made only with prior approval of the Aerospace Power Division, Air Force Aero Propulsion Laboratory, Wright-Patterson Air Force Base, Ohio.

Copies of this report should not be returned to the Research and Technology Division unless return is required by security considerations, contractual obligations, or notice on a specific document.

AFAPL-TR-65-112

DETAILED PERFORMANCE EVALUATION
of the
MARK V SELF-EXCITED ROCKET DRIVEN MHD GENERATOR

AVCO-EVERETT RESEARCH LABORATORY
a division of
AVCO CORPORATION
Everett, Massachusetts

TECHNICAL REPORT

November 1965

supported by

ADVANCED RESEARCH PROJECTS AGENCY
Air Force Aero Propulsion Laboratory
Research and Technology Division
Air Force Systems Command
Wright-Patterson Air Force Base, Ohio

ARPA Order No. 291
Project Code No. 6329

FOREWORD

This final report was perpared by the Avco-Everett Research Laboratory, Everett, Massachusetts. The work was performed for the Advanced Research Projects Agency, ARPA Order No. 291, Project Code No. 6329, and monitored by the Air Force Aero Propulsion Laboratory under Air Force Contract No. AF 33(615)-1862, "Detailed Performance Evaluation of the Mark V Self-Excited Rocket-Driven MHD Generator," Task No. 535004 of Project Number 5350.

This research was performed under the technical monitorship of Air Force Project Engineer Lt. Robert R. Barthelemy, Plasma Dynamics Technical Area of the Aerospace Power Division. The work was accomplished in May 1965 and the report was submitted in October 1965.

The work covered by this report is sponsored by the Advanced Research Projects Agency and managed by the Air Force under Air Force Contract AF 33(615)-1862. However, this report is being published and distributed prior to review by either agency. The publication of this report, therefore, does not constitute approval by the Advanced Research Projects Agency or the Air Force of the findings or conclusions contained herein. It is published for the exchange and stimulation of ideas.

ABSTRACT

A rocket-driven self-excited MHD generator designed for a net power output of 20,000 kilowatts has been tested. The generator was designed to demonstrate the feasibility of using an MHD device to provide power at very high levels with relatively simple equipment. This report describes the generator and the testing program performed to study the characteristics of self-excitation and the combined operation of self-excitation and power output.

The initial test period was devoted to achieving self-excitation which is described together with the major problems involved. The stress is placed on the effect of L di/dt, loading, control of battery bank and test firing point, together with end effects experienced in the channel. After obtaining sufficient knowledge of the self-excitation and the control thereof, the major effort was concentrated on the production of net power output.

The dynamics of the generator working fluid are discussed, together with the effects of various loadings of the generator. The transverse voltage distributions on the channel, together with the axial voltage and Hall voltage measurements taken, and their influence on generator performance, are presented. Power and current density and their variation are shown with power and magnet current relationships.

Significant results of the generator testing program were the production of a net power of 23,600 kilowatts with a gross power output of 32,000 kilowatts.

TABLE OF CONTENTS

TABLE OF CONTENTS
(Continued)

TABLE OF CONTENTS
(Continued)

TABLE OF CONTENTS
(Continued)

LIST OF FIGURES

LIST OF FIGURES
(Continued)

LIST OF FIGURES
(Continued)

LIST OF FIGURES
(Continued)

LIST OF FIGURES
(Continued)

I. INTRODUCTION

The exhaust of a modern chemical rocket engine is an impressive source of energy. As an example, the thermal heat flux of the Atlas booster is the equivalent of approximately six thousand (6000) megawatts, four times that of the largest public utility electric generating units now in operation. On the other hand, the operating duration of these rockets, that is to say, fractions of a second to many minutes (and even longer) is appropriate to a number of demand requirements for high level electrical power. Thus, if a significant fraction of the rocket exhaust energy flux could be converted into electrical power, it would represent an important new capability.

The combustion products of conventional rocket propellants at temperatures between 2000 and 3000°K can be made to conduct electricity by adding a small amount of easily ionizable impurity called seed to the combustion chamber. In practice, the seed is usually a salt of potassium. Thus, the process of converting the rocket exhaust energy into useful electrical power may be accomplished in a magnetohydrodynamic (MHD) generator. Further, the natural "fit" between the very high energy level of the rocket engine and the suitability of the MHD generator to single unit operation at high power level makes it possible to envisage units with relatively simple equipment at low cost and potential light weight. The situation is perhaps best illustrated in Figures I-1 and I-2. Figure I-1 shows the power-operating time characteristics of available "standard" power sources (shaded area), and Figure I-2 shows the power output-weight characteristics for rocket-driven MHD generators.

In its simplest form, the rocket-driven MHD generator consists of a combustion chamber, MHD channel, and magnet which may be self or separately excited, superconducting, or cryogenically cooled by the propellants and suitable auxiliaries. The channel exhausts to the atmosphere. Figure I-3 illustrates the basic components of a typical ground based fixed installation. Other equipment performing essentially the same functions but designed for light weight could be appropriate for mobile and air or space borne applications.

Because of the basic simplicity of the apparatus, it is expected that a rocket-driven MHD generator installation would represent a relatively modest investment compared with other power sources at comparable level, and this advantage will increase with size. A rough estimate of the installed cost of such installations as a function of power output is shown in Figure I-4.

The design, construction, and initial test of a self-excited, rocket-driven MHD generator which would demonstrate the suitability of such a generator (the Mark V) to produce electrical power at high level for limited duration was the object of the ARPA sponsored Contract AF 33(657)-

8380. The final report for the work was submitted in April 1964.* The detailed test program with the Mark V was conducted under the present Contract AF 33(615)-1862, and the results of that test program are the subject of this report.

Figure I-5 is a photograph of the self-excited Mark V generator. The combustion chamber burning gaseous oxygen and seeded alcohol is on the left. The structural steel encloses the heat sink, room temperature copper magnet winding that is driven by a portion of the generator output. The channel is inside the magnet. Above the magnet are the power take-offs from the individual segmented electrodes. The exhaust duct on the right conveys the spent gases to the atmosphere. The Mark V was designed for a net power output of twenty (20) megawatts for three (3) minutes at a mass flow of sixty (60) Kg/second with a maximum magnet power requirement of twenty (20) megawatts or a maximum gross power output of forty (40) megawatts. In power capability it is the largest direct conversion device known to be in existence, and dwarfs the Mark II experimental MHD generator, which previously was the largest device of its kind.

Fifty-six power generation tests were conducted with the Mark V generator during the testing program and generator self-excitation was found to be easily and reliably achieved. A maximum net power output of 23,600 kilowatts was produced, exceeding the design value of 20,000 kilowatts. The maximum gross power output required was only 32,000 kilowatts.

*"Design, Development, and Test of a Prototype Self-Excited MHD Generator," Final Technical Report, Contract AF 33(657)-8380, April 1964.

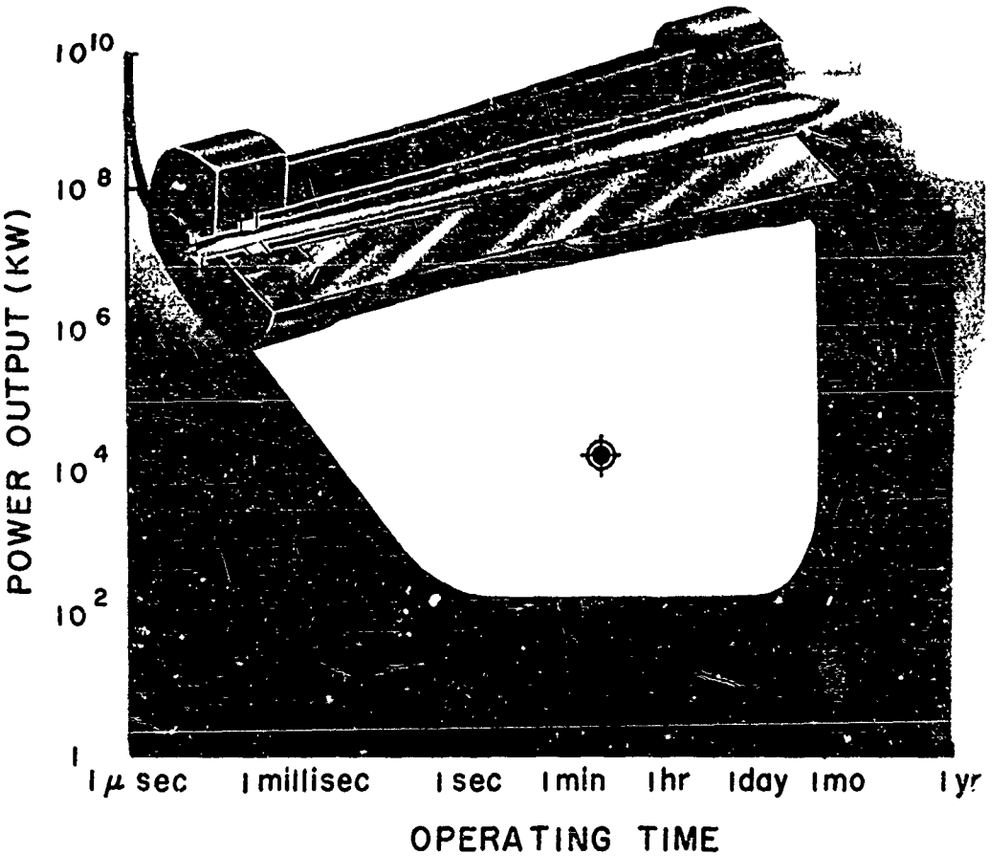

Figure I-1 Power Output vs Operating Time for D.C. Power Sources

Power sources in the unshaded area are not generally available, but the existence of a few costly and bulky sources in the unshaded area may be taken as an indication of future need. It is believed that the rocket-driven MHD generator can fulfill a majority of such needs. The mark in the unshaded portion of the chart indicates the design point of the generator which has been tested under the present program.

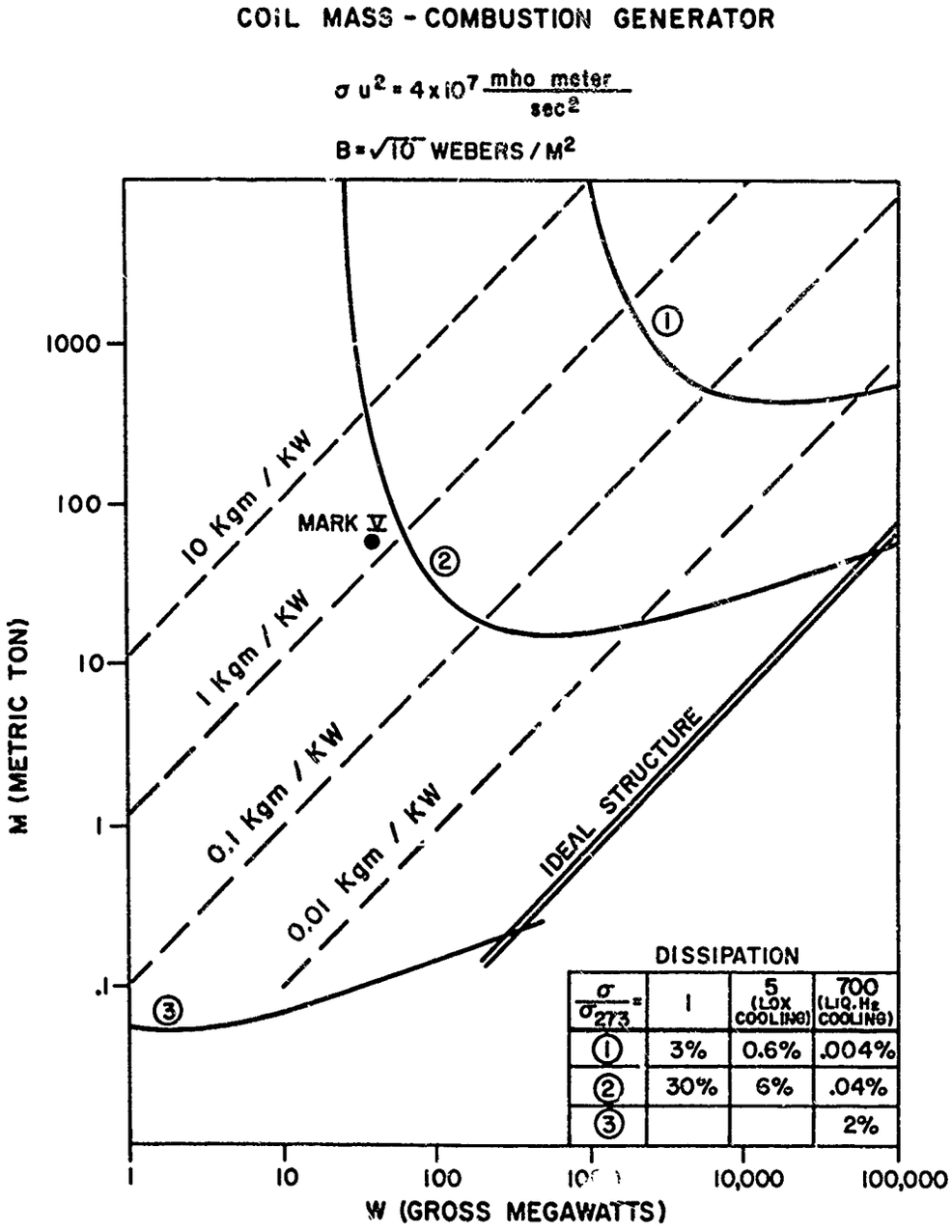

Figure I-2 Power Output-Weight Characteristics for Rocket-Driven MHD Generators

Figure I-2 shows the power output-weight characteristics for rocket-driven MHD generators with varying percentages of the generator output dissipated in the field coil and with various field coil coolants which may also serve as propellant. It is clearly seen that mobile and air or space borne systems are a distinct possibility. Again, the point indicated by "Mark V" denotes the design conditions of the generator which has been tested under the present program.

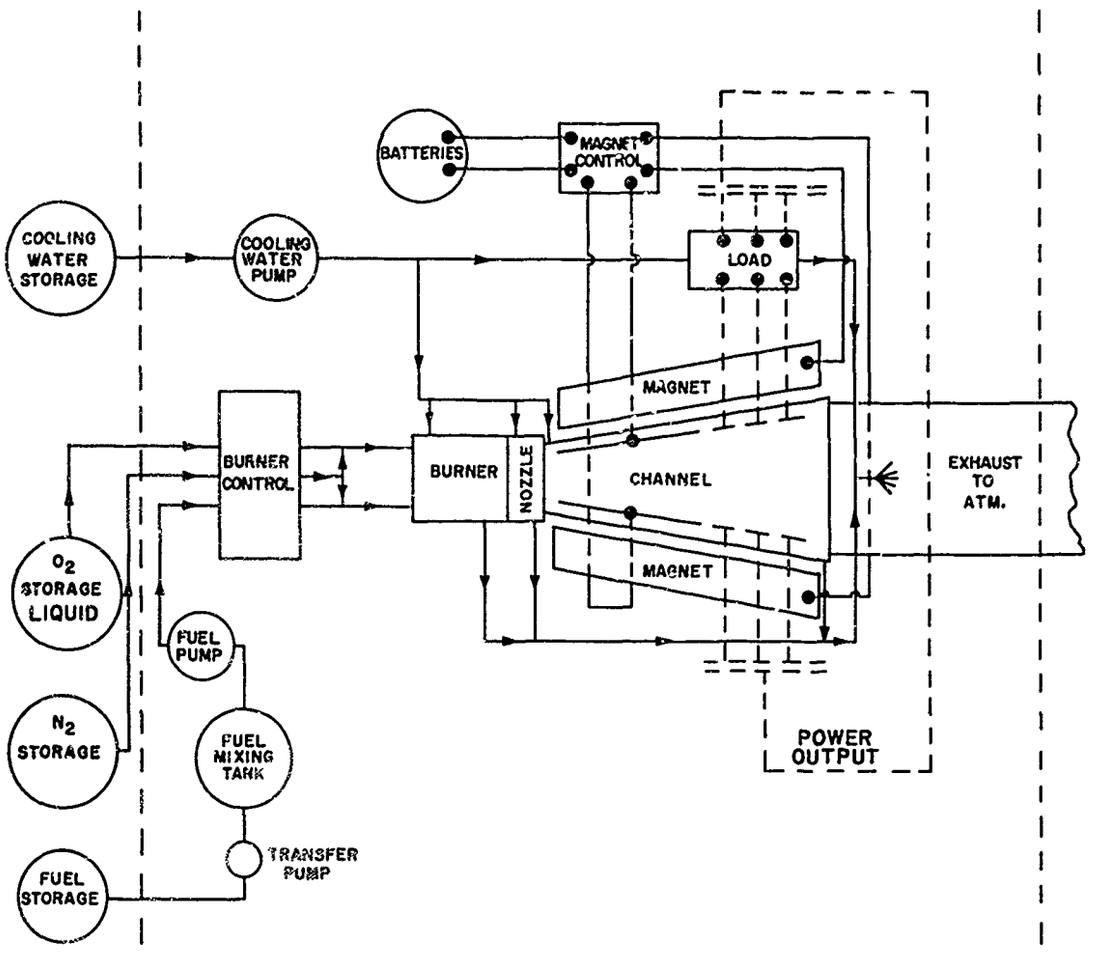

Figure I-3 Basic Components for a Typical Rocket-Driven MHD Generator Installation

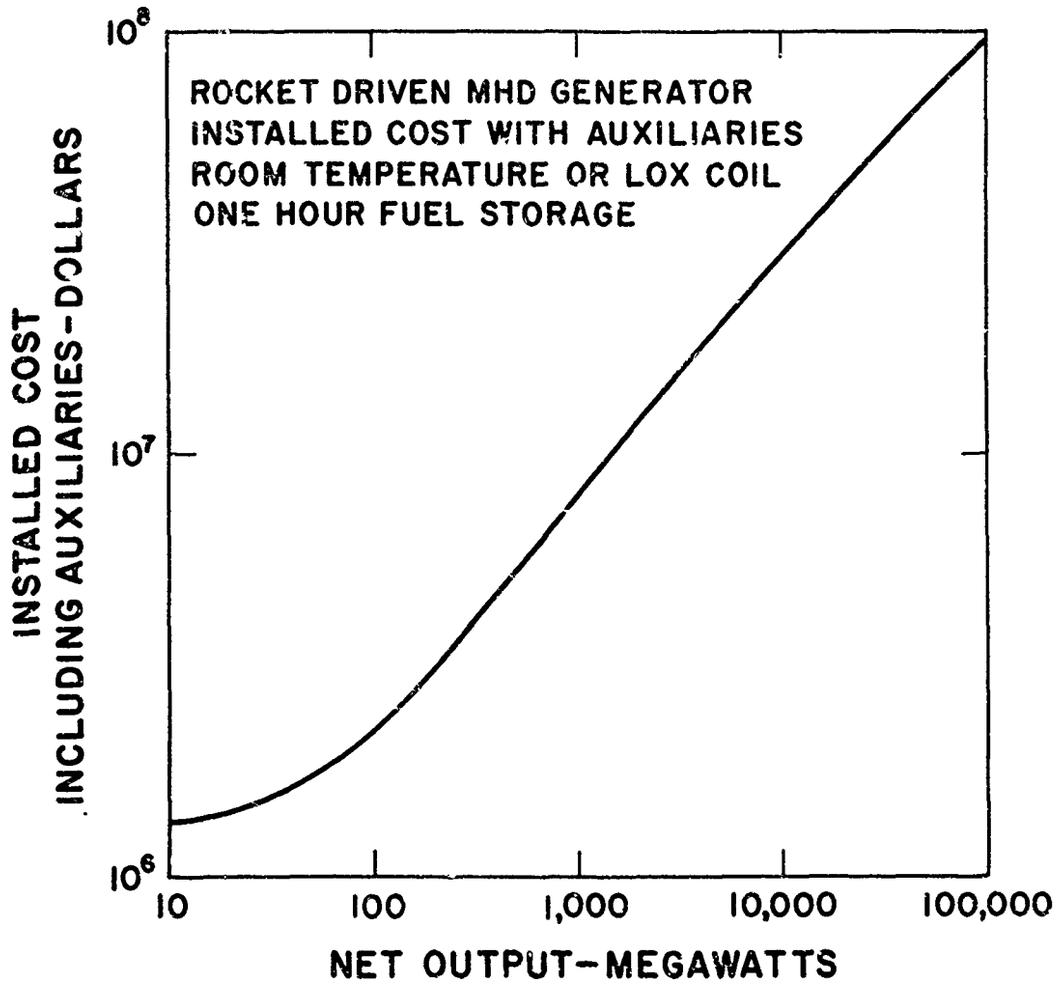

Figure I-4 Installation Cost vs Power Output for Rocket-Driven MHD Generators

Figure I-5 Photograph of the Mark V MHD Generator

II. GENERATOR DESIGN

To familiarize the reader with the design of the Mark V generator, a brief description of the design parameters and the general arrangement of the test apparatus is presented.

The components of the Mark V generator may be grouped to form four basic elements; burner, magnet, channel, and auxiliary systems. A photograph of the generator may be seen in Figure I-5.

A. GENERAL DESIGN

The working fluid used in the Mark V MHD generator is produced in a rocket type combustion chamber. The high temperature gases are then passed through a nozzle into the channel where the gas is expanded at supersonic conditions to the atmosphere. The channel is placed inside a large heat sink coil, which provides the necessary magnetic field.

The channel is divided into four sections; inlet, excitation, power, and outlet, as shown in Figure II-A1. The inlet section guides the flow from the burner nozzle, through the magnet and into the excitation section. It also serves as an electrical insulator between the combustion chamber nozzle and the excitation section.

The excitation section is that part of the MHD channel from which the power, required to energize the magnet, is extracted from the working fluid. For reasons to be described below, a single, continuous (non-segmented) electrode pair is used in the excitation section.

The power section starts from the exit of the excitation section, and ends at a point where the magnetic field strength on the centerline of the channel is 30 kG.

The power section utilizes segmented electrodes. Fifty electrode pairs are used, with each pair having a power output of approximately 0.40 Kw. Each electrode pair is connected to its individual load resistor which is made of water cooled stainless steel tubes.

The outlet section serves the same purpose as the inlet section by being an electrical insulator and a flow passage through the hole in the end of the magnet into the exhaust duct.

1. Self-Excitation

The load line diagram for the self-excitation section of the generator is shown in Figure II-A2. There is a separate voltage-current curve for each value of magnetic field B. Now the entire output current of the self-excitation section of the generator is delivered to the magnet so that each value of B in the ordinate corresponds to a unique value of current on the abscissa. On the other hand, the DC voltage-current characteristic of the magnet is given by the straight line labeled I x R_m. The output voltage of the generator is given by the curve located above the magnet characteristic, except in the region of very low current and above the operating point. In the region where the output voltage of the generator at a given current is greater than the steady state DC voltage demanded by the magnet at the same current, the Mark V will self-excite; i.e., the field will build up without external excitation.

The magnetic field variation with time may be determined from the data shown in Figure II-A2. At any time

$$IR_m + L_m \frac{di}{dt} = V_g \qquad (1)$$

where I is the generator (and magnet) current, L_m the magnet inductance, V_g the generator output voltage and t the time. A typical buildup characteristic is shown in Figure II-A3 in which magnetic field B, output voltage V_g, and DC magnet voltage V_m are shown as a function of time. The results shown in this figure are a solution of Eq. (1) using the data shown in Figure II-A2. For the purpose of the calculation, the magnet is excited by external means, until the end of the "pre-excitation" time as indicated; the open circuit generator voltage during the pre-excitation time varies as shown by the curve labeled E_g. At the end of the pre-excitation time, the magnet is switched over to the generator by starting the gas flow and disconnecting the external supply.

Following changeover from external source to generator, the magnetic field rises to the design value of 35,000 gauss (at the inlet) in a period of 44 seconds which basically is then the time required to start the Mark V. We should mention that the load on the downstream electrodes from which the output is taken, may be either connected or disconnected during the excitation period without influencing the buildup. This occurs because the generator flow is slightly supersonic.

The self-excitation process is greatly assisted by the fact that at low values of field strength during the buildup, the gas velocity is much increased over the steady state value by the absence of MHD body forces. (At zero current in the MHD generator, the channel acts like an isentropic nozzle, and velocities as high as M = 2.3 are obtained in the excitation section.) Since power output is proportional to the square of the velocity, considerable excitation power is generated, even at relatively low values of magnetic field.

Figure II-A3 indicates that the field falls off slowly after reaching the design value. This is due to coil heating. (R_m in Eq. (1) is not a constant.) The magnet, in dissipating the excitation power, heats up, since, in the design of the Mark V, the magnet is uncooled in the interest of simplicity and low cost. The heating effect could be eliminated by water cooling, cooling with a liquid oxidizer, or by use of a superconducting coil.

In actual practice, however, the Mark V field does not vary as rapidly as indicated in Figure II-A3, nor does field variation of the magnitude we expect have a large influence on the net output of the generator. In the actual design, the excitation section is capable of approximately 25% greater output than that required to provide excitation at room temperature and indeed provides nearly full excitation at the end of a run. Also, even if the field does drop slightly during a run, the output is not greatly affected. This occurs because reduced field means lower output current, and hence less pressure drop in the gas. Therefore, as the field drops, the gas speeds up and the velocity increase in the output section largely compensates for any decrease in magnetic field.

2. Principle of Excitation Operation

The schematic of the electrical circuitry of the Mark V generator is shown in Figure II-A4.

The sequence of operation is as follows: the generator requires an initial low value of magnetic field of approximately 3 kilogauss, which is secured by connecting a battery (B) to the magnet by a switch (S). The gas flow is then started and the emf of the generator builds up. When the emf of the generator has reached a value equal to the battery voltage, the generator starts to supply power to the magnet in parallel with the battery. The battery current decreases as the generator voltage increases and becomes zero when the generator voltage equals the emf of the battery. At this time the switch (S) is opened and the generator becomes self-excited. When the generator is shut down, the magnet becomes a voltage source due to the collapsing field, but of reversed polarity. Because of the reversed polarity, the rectifier in the short circuiting loop conducts, permitting the energy stored in the magnetic field to be dissipated in an orderly fashion.

The battery bank is designed to give a maximum initial field of ten kilogauss which corresponds to approximately 6000 amperes current flow in the magnet. If the battery bank is disconnected from the magnet before the generator voltage output is equal to the battery open circuit voltage, a sudden drop in generator output occurs. By having the generator working in parallel with the magnet, a faster excitation can be achieved and also a smoother transition.

3. Generator Design Parameters

The parameters of the operating conditions are given below:

Mass flow	60 Kg/sec
Fuel	Ethyl alcohol
Oxidizer	Gaseous oxygen
Fuel flow	19.1 Kg/sec
Oxidizer flow	39.8 Kg/sec
Seed	1% KOH by volume
Seed flow	1.1 Kg/sec KOH
Duct cross section	Inlet - rectangular; Outlet - square
Combustion pressure	8 atmospheres absolute
Exit static pressure	0.9 atmospheres absolute
Magnetic field	Inlet - 35,000 gauss; Outlet - 30,000 gauss
Magnet configuration	Uncooled copper (heat sink during 3-minute run)
Magnet excitation	Self-excitation by generator output, with small external excitation for start-up

These were the parameters utilized to perform the detailed design of magnet, burner, channel and auxiliary systems for the Mark V generator. These designs are described below.

A more complete discussion of Mark V Generator design can be found in the Final Technical Report, "Design, Development, and Test of a Prototype, Self-Excited MHD Generator," Contract No. AF 33(657)-8380, April 1964.

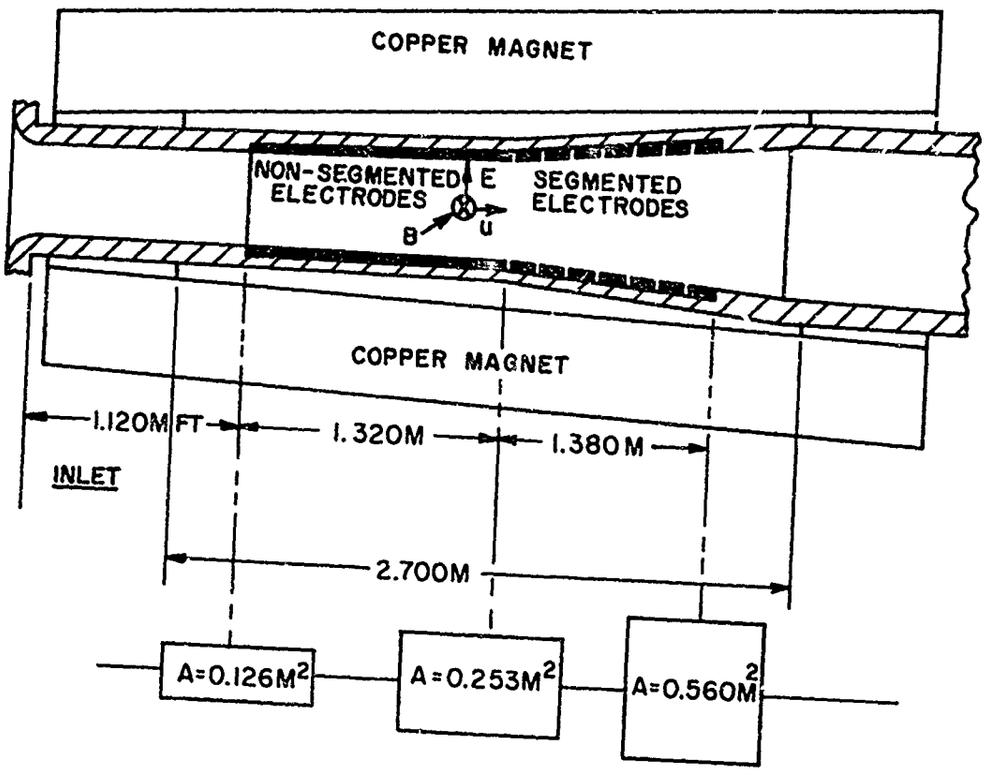

Figure II-A1 Channel Layout of Mark V Generator

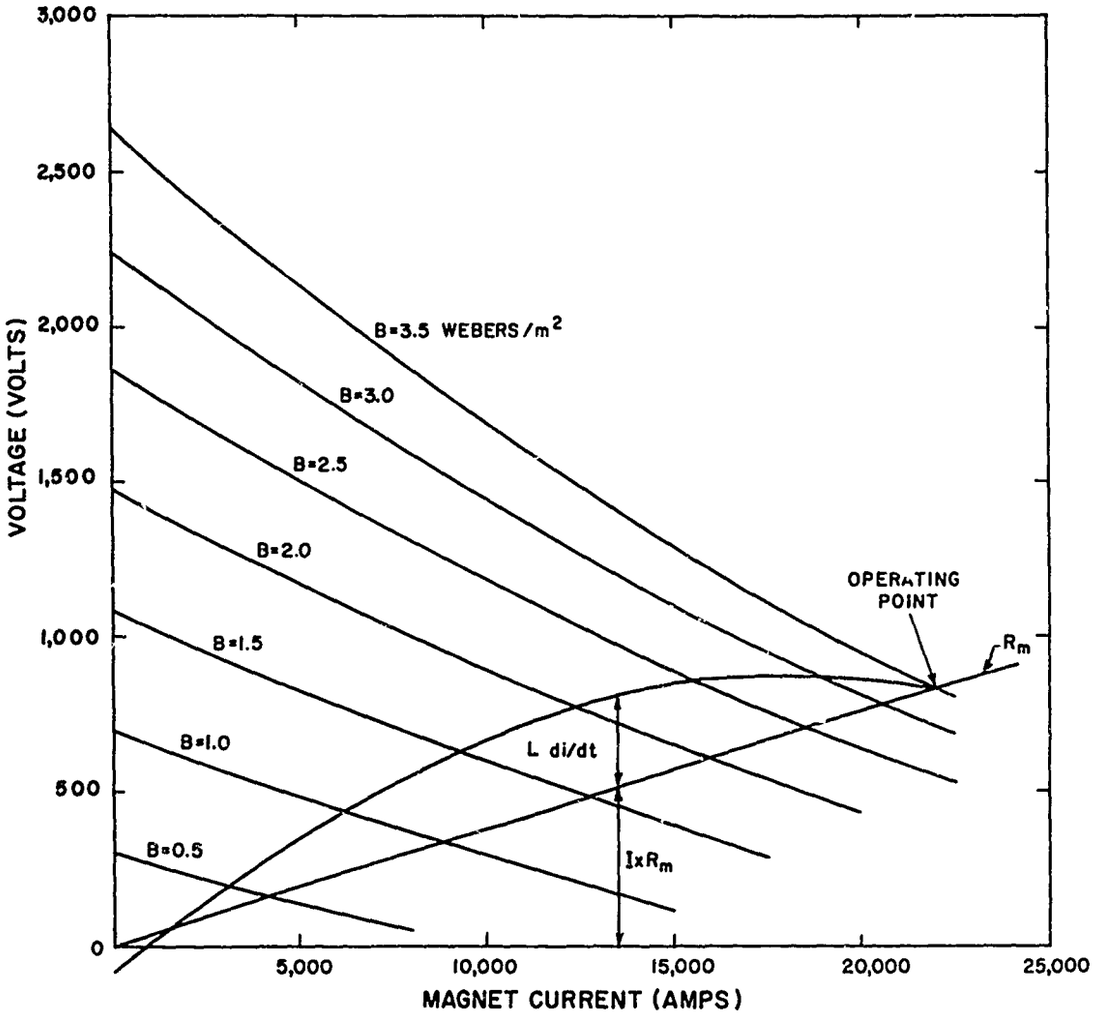

Figure II-A2 V-I Characteristic of the Mark V Self-Excitation Section for Various Values of Magnetic Field

8863

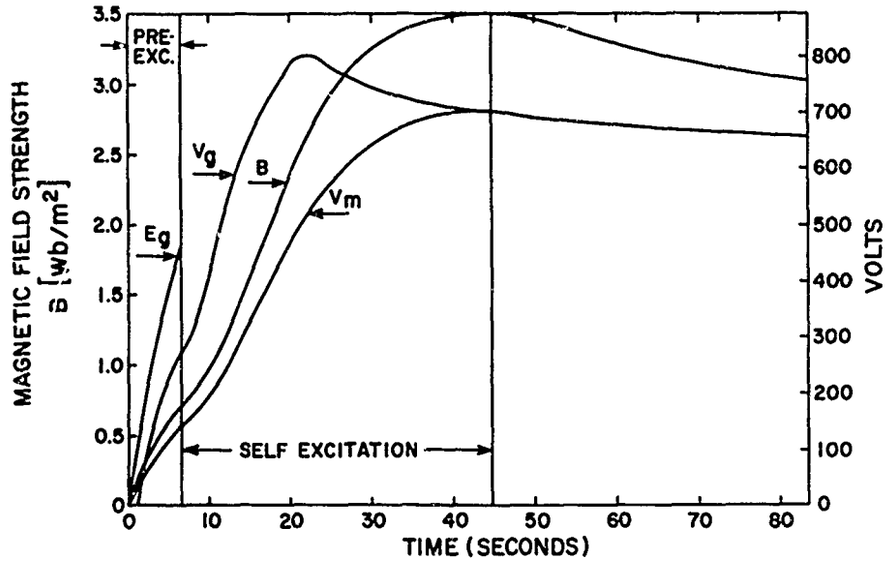

Figure II-A3 Typical Field Time Characteristic for the Mark V Generator During Excitation

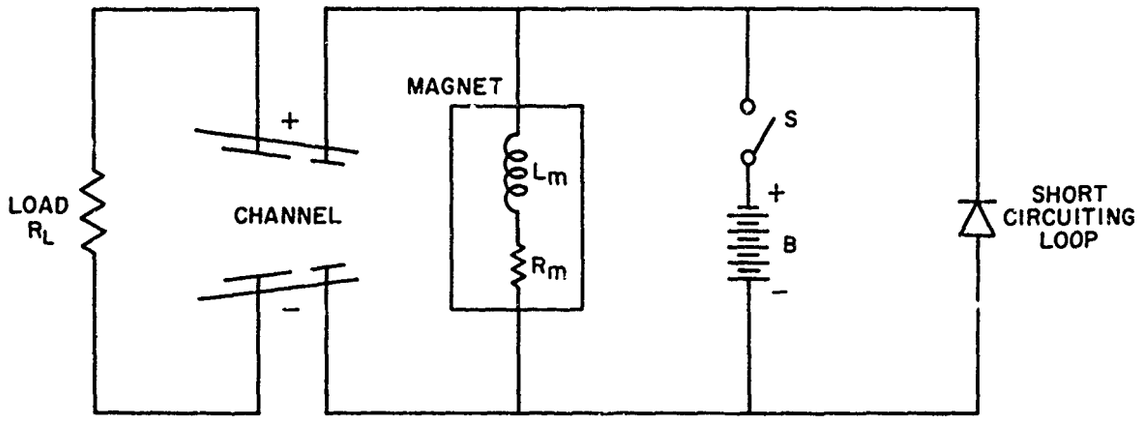

Figure II-A4 Schematic of the Electrical Circuit for the Mark V Generator

A2210

B. BURNER DESIGN

1. Design Requirements and Operating Conditions

The burner is designed for a normal flow of 60 Kg/sec. This flow is composed of 39.8 Kg/sec gaseous oxygen, 19.1 Kg/sec ethyl alcohol, and 1.1 Kg/sec potassium hydroxide (1 mole % K in total flow). The normal chamber pressure is 8 atm. In addition, the mass flow can be varied over the range from 25 to 120% of the design mass flow by changing fuel injectors and by making appropriate changes in the fuel and oxygen injection pressures.

The burner water cooling and structural design are suitable for operation at a flow rate exceeding the design flow by 20%. The structural design is expected to give a life of the hot parts, which is commensurate with the running time required for the test program. The total running time and number of operating cycles is much larger than is required for flight weight rocket engines.

Heat transfer rates were estimated from rocket engine practice and by extrapolation of data obtained from previous experience. The rates for the nozzle and chamber are reliable and conservative values. The heat transfer rate to the injector plate depends on an unpredictable recirculation of hot gas, but the design value is conservative. The estimated heat transfer rates are as follows: nozzle, 1255 watts/cm^2; chamber, 904 watts/cm^2; injector, 574 watts/cm^2. The water passages were designed for nucleate boiling heat transfer with a reasonable safety factor to burn out.

The design of the fuel injection system is based largely on Avco-Everett Research Laboratory experience. Fuel and oxygen are injected with large pressure drops so as to virtually eliminate the possibility of low frequency instability. The oxygen pressure drop is large enough to produce sonic flow from the oxygen nozzles and the oxygen stream impinges on the injected fuel to promote good atomization and mixing.

Previous experience indicated that the nozzle would be most difficult to design because of the high heat transfer rate combined with a complex shape (round to rectangular transition combined with contraction). Accordingly, the nozzle design was carefully examined for adequate cooling.

A continuously operating pilot burner is used to insure prompt ignition in the main burner during operation.

2. Description of Burner

The burner is shown on Figures II-B1 and II-B2.

The nozzle, shown on Figure II-B1, is composed of two inner pieces and an outer jacket. The inner portion was made in two pieces to simplify machining and to reduce the size of the forging required. The cooling is by a system of closely spaced drilled holes with particular emphasis on minimizing the wall thickness to reduce metal temperature and thermal stresses. Due to the massive construction of the nozzle the direct stresses due to water and gas pressures are quite low.

The burner chamber, also shown on Figure II-B1, consists of an inner liner and an outer jacket with a cooling water passage in between. The inner liner is subject to external water pressure, and to prevent failure [illegible] is reinforced with several rings. To provide a reasonably high [illegible] cooling water velocity, the spaces between reinforcing rings [illegible] by filler rings. The inner liner is fixed at the nozzle end and free [illegible] and axially at the backplate end, an "O" ring seal being provided at this point.

Because this burner is operated inside a building, elementary safety considerations dictated that the outer shell of all portions of the burner should be amply strong. The outer jacket of the chamber section, for instance, has a theoretical bursting pressure of 185 atm, which gives a safety factor over normal chamber pressure of 22.

The injector assembly is shown on Figure II-B2. The injector assembly is divided by a series of plates or diaphragms to provide passages for cooling water, oxygen, and fuel. Starting from the left side of the figure, first is a thin plate which forms the back wall of the combustion chamber. Behind this plate is a cooling water passage. The second plate contains the oxygen injectors. The third plate closes the oxygen passage and contains the fuel injectors. The fourth plate closes the fuel passage. The oxygen injectors have a rounded entrance for smooth flow and are sized to produce sonic velocity at the throat.

The fuel injectors are concentric with the oxygen injectors, but the fuel jets are at a 45° angle to the oxygen stream. There are a total of 60 injectors arranged in four concentric circles. The effectiveness of this injector system was checked by flow and combustion tests with a single injector.

In the center of the injector assembly is the pilot burner. The pilot burner is intended to run continuously so as to provide a constant source of ignition in the main burner. The pilot is started by a very small igniter burner, which is not shown on the drawing. Both the pilot and igniter burners use gaseous ethane as fuel and gaseous oxygen. The all-gas system provides simple and reliable operation. The pilot burner will operate at a chamber pressure of 13.5 atm and a mass flow of 0.1 Kg/sec.

During assembly of the burner, some delays were encountered because of problems in fabrication. The injector design which evolved is, in retrospect, much more suitable for flight weight hardware and quantity production than for use in the MHD generator. Success with the all-welded structure is greatly dependent on the skill of the welder. The selected hot face material, Inconel X-750, requires meticulous care during welding and heat treating to secure a sound structure and suitable mechanical properties.

The sequence of events with the injector plate was as follows: The first attempt at fabrication resulted in failure when the piece was only partially finished. At this time a fairly simple and effective repair cycle was evolved which should have produced a satisfactory piece. At the conclusion of welding and heat treating, the injector was found to have many cracked welds with cracks in some cases running into the base metal. Figure II-B3 shows an oxygen nozzle welded into place with typical cracked welds. The failure was attributed to lack of proper cleanliness in making the welds and failure of the heat treater to follow instructions regarding heating rate.

At the conclusion of the repair cycle the injector assembly was carefully inspected by both X-ray and dye penetrant methods. As a result of this inspection, a second repair cycle appeared feasible which would cut out all weld metal and replace those parts which showed cracks. About eight out of sixty oxygen nozzles were replaced and a new injector face plate was made. At the conclusion of welding and heat treating, the welds were all sound, but some of the oxygen nozzles had developed cracks. The cracks in the nozzles had possible developed from small undetected cracks which were present after the first rework, or from some metallurgical deterioration of the material.

Since the Inconel X-750 injector assembly was not suitable for operation at full mass flow, the construction of a second injector assembly was started. A material change to Type 347 stainless steel was made to reduce the likelihood of defective welds and to eliminate heat treatment. As in regard to material properties, there is a considerable loss of yield strength, but a gain in ductility as compared to Inconel X-750. Since this piece operates in a low cycle fatigue regime, the net loss in life appears to be small.

In the design of the cooling passages in the injector plate, it was anticipated that some flow guides might be required to assure good cooling at all locations. Specifically, the water flow is perpendicular to the cylindrical exterior of the oxygen nozzles and a stagnant wake was expected behind each oxygen nozzle. To locate the stagnant areas, a transparent plastic window was attached to the injector plate in place of the face plate. Water flow was then established through the cooling passage and flow guide wires were determined in this manner. A photograph of this test setup is shown in Figure II-B4.

Careful analysis of the cooling system in the pilot burner as designed indicates that the safety factor on burnout was rather small. Dependable operation of the pilot burner is considered an essential safety feature for our application. Various ways of increasing the burnout safety factor were considered, and the most satisfactory appeared to be by nitrogen dilution. Diluting the oxygen flow with nitrogen reduced the combustion gas enthalpy and the gas-to-wall heat transfer rates. A nitrogen-oxygen ratio of one was selected, which increased the safety factor on burnout by approximately a factor of two.

A modification of the original pilot burner control system permits controlled nitrogen dilution. This modification will be described under Auxiliary Systems.

The pilot burner is started by means of a small igniter burner which need operate for only a few seconds. Figure II-B5 shows a cross section of this burner. Oxygen and ethane are injected as shown and ignited by a sparkplug. The design injector pressures are 34 atm and the desired chamber pressure is 17 atm. The burner is water-cooled, but due to the construction of the pilot burner, it is impossible to properly cool all of the throat section. Because of the partial cooling of the throat, the running time must be limited to a few seconds at the beginning of a generator run.

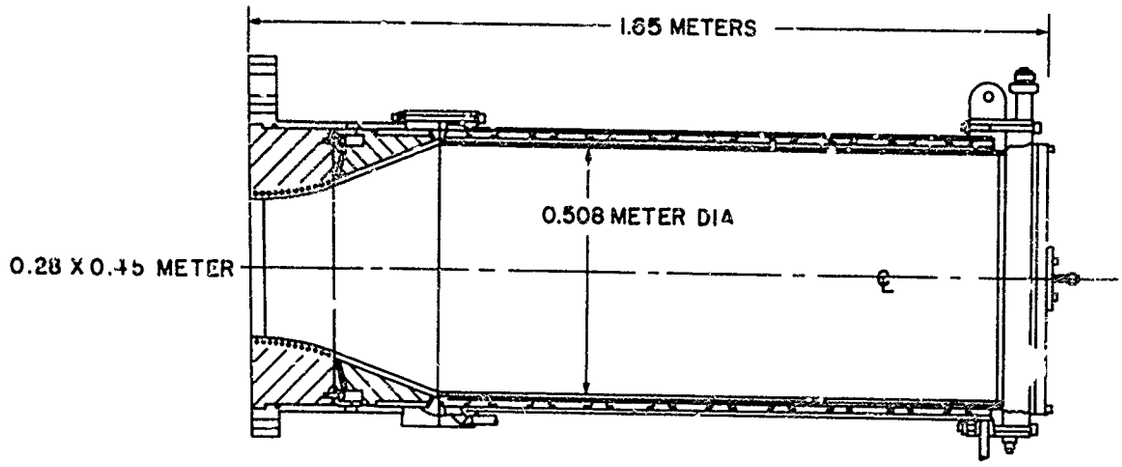

Figure II-B1 Burner Assembly

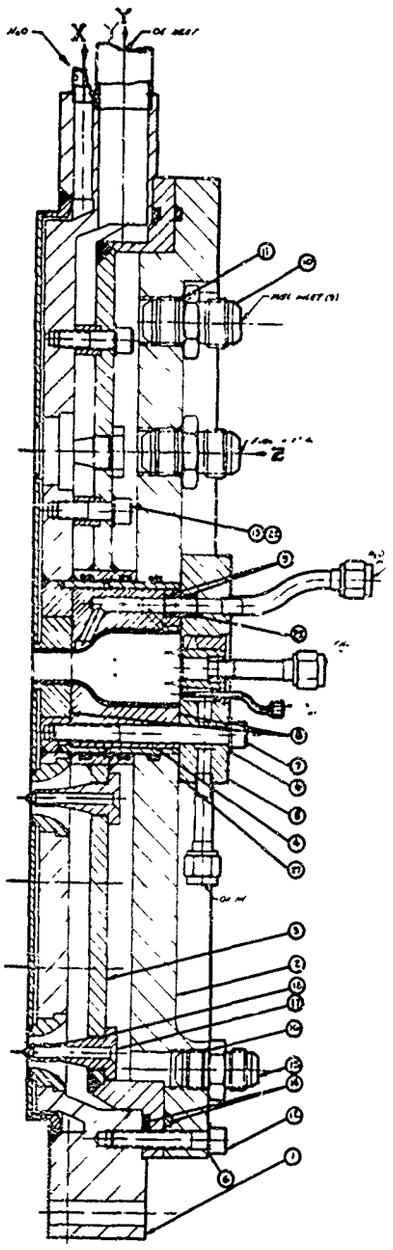

X - WATER INLET
Y - OXYGEN INLET
Z - FUEL

1. INJECTOR PLATE
2. FUEL CLOSURE PLATE
3. OXYGEN PLATE
4. PILOT LINER
5. PILOT BURNER CAP
6. WASHER
7. CAP SCREW
8. "O" RING
9. "O" RING
10. FUEL INLET FITTING
11. "O" RING
12. CAP SCREW
13. SEALING WASHER
14. "O" RING
15. FUEL MANIFOLD DRAIN
16. "O" RING
17. FUEL INJECTOR
18. "O" RING
22. CAP SCREW
25. CONNECTOR, COOLING WATER
27. SHIM

Figure II-B2 Injector Assembly

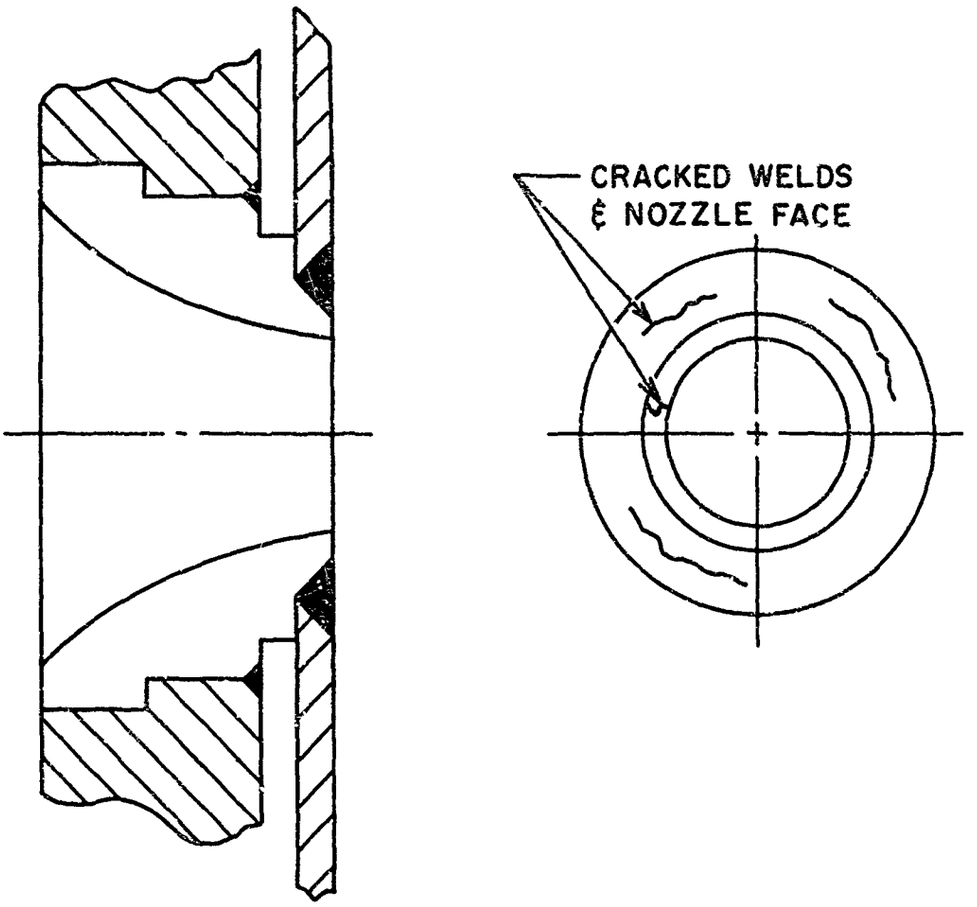

Figure II-B3 Oxygen Nozzle Showing Defective Welds

A1403

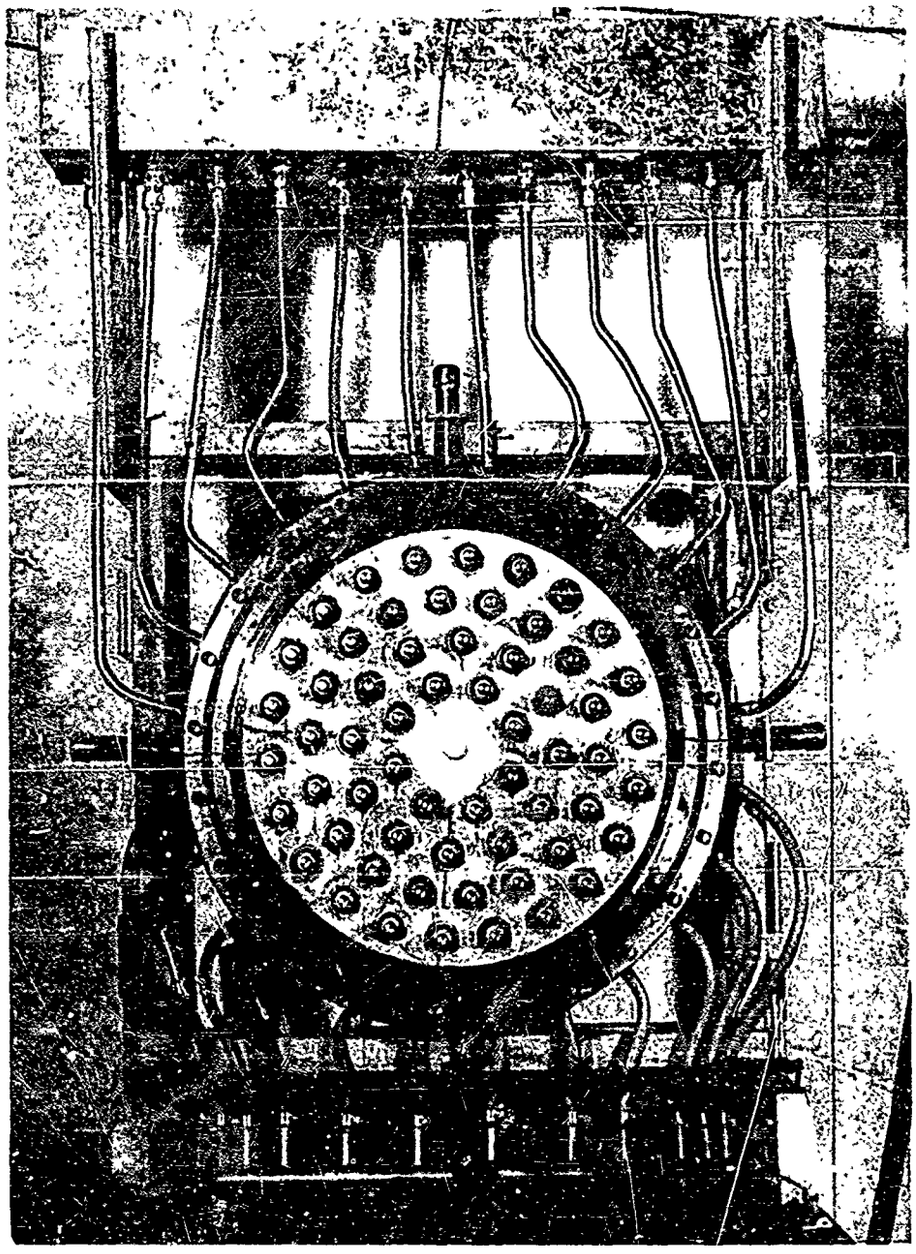

Figure II-B4 Burner Injector Plate Setup for Cooling Water Flow Tests

A1083

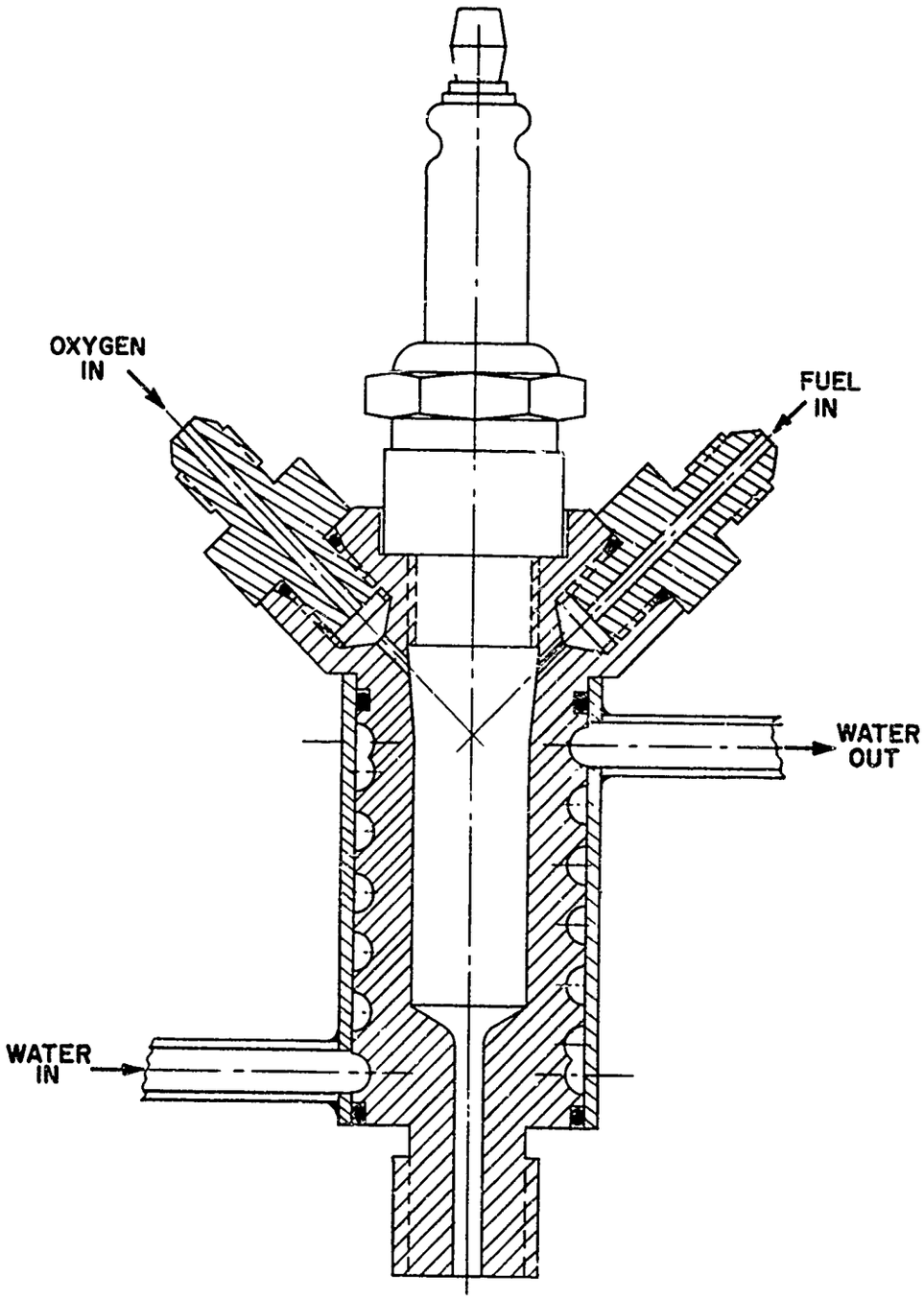

Figure II-B5 Cross Section of Igniter Burner

A7403

C. MAGNET DESIGN

A general analysis of the performance of an MHD generator indicates the desirability of operating with a high magnetic field strength. As the field strength is increased, the power density in the channel is increased, and for a given output the size of the machine is reduced. Reduction in size gives a corresponding reduction in heat loss to the channel walls. Desirable field strengths run from 30 to 50 kilogauss or higher. Since the saturation field strength of iron is approximately 20 kilogauss, conventional iron core magnets are not useful. Aircore solenoids can be made to produce the required fields provided sufficient power is available to drive them.

An MHD generator with linear channel geometry requires a field magnet of approximately rectangular shape. The calculation for the field strength of such a magnet gives the field between a pair of infinitely long parallel rectangular conductors:

$$B = G \left(\frac{P\sigma\lambda}{L} \right)^{1/2}$$

B = field, gauss
G = Geometrical factor
P = Power dissipation, watts
σ = electrical conductivity mhos/cm
λ = Space factor of winding
L = length, cm

In a real magnet it is assumed that the ends compensate for the fact that the sides are not infinitely long. This assumption is quite accurate if the length to width ratio of the magnet is greater than about five.

The basic conductor configuration, along with the coordinate system, is shown in Figure II-C1. The two conductors extend to infinity in both directions; they carry current in opposite directions with current density $j \frac{\text{amps}}{\text{m}^2}$ so that their fields reinforce in the gap. The coordinate system is as shown.

Plots of $G(\alpha, \beta)$ vs α and β are shown in Figure II-C2. G is constant along each contour line. Minimum weight occurs when β times $(\alpha - 1)$ is a minimum. Actually, however, the weight is not sensitive to moderate departures from the minimum weight curve. The final design points for the Mark V generator magnet are shown in Figure II-C2.

A hybrid magnet may be made by adding iron pole pieces to an aircore solenoid, thereby increasing the field strength at a given power level. At higher field strengths the contribution of the iron becomes less significant.

The large power dissipation in an aircore magnet introduces some thermal problems. For continuous operation some form of cooling is essential. For short duration tests the conductor material may be used as a heat sink. In a heat sink magnet there is an undesirable increase in magnet resistance as the conductor heats up and a limiting temperature dependent on the materials of construction.

Mechanical problems consist of fabrication techniques and structural reinforcement to contain the large forces developed on the conductors.

In designing an aircore magnet with a complex shape, the construction of a scale model can be very useful. By using a suitable fluxmeter, the field can be surveyed to determine nonuniformities in the working area and for calculating forces on the conductors. The model may be operated at low power levels and field strength and the results extrapolated using the relation $B \approx P^{1/2}$. However, if iron pole pieces are used, it will be necessary to run at full field strength because of the nonlinearity of the iron.

1. Detail Design

a. Preliminary Calculations

Based on early estimates of generator channel dimensions, several heat sink magnets were calculated using different copper geometries and with temperature limits corresponding to AIEE class B and H insulation. The magnets were tapered to conform to the channel dimensions. In all cases the calculations were based on the following figures:

Run duration	= 3 min.
Field at inlet end	= 35,000 gauss
Field at outlet end	= 30-31,000 determined by geometry
Inlet opening width	≃ 0.7 meter
Outlet opening width	≃ 1.0 meter
Inside length	≃ 3.0 meter
Space factor, λ	= .95
Conductor material	= copper

Estimated copper weights varied from 50,000 to 80,000 Kg.

Estimated power requirements varied from 14 to 18 megawatts.

At the same time some thought was devoted to construction techniques and estimates of the loads which the reinforcing structure must carry.

b. Evaluation of Heat Sink vs Water-Cooled Design

As run duration is increased, more copper must be added to a heat sink magnet in order to limit the maximum temperature. At some running time it becomes more economical to build a water-cooled magnet. For the Mark V generator it was estimated that a practical water-cooled magnet could be built with about 45,500 Kg of copper. The saving of 15,900 Kg of copper would not have paid for the more complex magnet construction, pumps, and piping required for a water-cooled magnet. For a run duration of 5 minutes a heat sink magnet would weigh over 91,000 Kg and a water-cooled magnet would clearly be more economical.

c. Evaluation of the Use of Iron

It is estimated that by using iron pole pieces with a total weight of about 60 tons the magnet power input could be reduced by about 30% and the copper weight reduced by a similar amount. However, experience indicates that the iron tends to spoil the field distribution. In addition, the use of iron would have made the model magnet work far more complicated and costly. Hence, the decision was made to use an aircore magnet.

d. Model Magnet

Two model magnets were built and tested with the following objectives:

1) Verification of the calculated centerline field strength in a magnet of small length to width ratio.

2) Determination of field strength variations within the generating channel.

3) Measurement of external field strength, this information being useful for the design of the reinforcing structure and for estimating magnetic forces on adjacent equipment.

The first model was based on early estimates of the channel dimensions and preliminary magnet design calculations. This model was

thoroughly tested and produced information for the design of the second model and the full sized magnet. At the completion of testing of the first model the channel gas flow calculations and wall design had progressed to the point where final internal magnet dimensions were fixed. Channel dimensions had changed appreciably from original estimates and this fact, coupled with the desire to minimize copper content and cost of the final magnet, prompted the construction of a second model magnet. The second model is virtually identical to the full sized magnet.

Both models were of the same general design and construction and the same testing equipment was used for both. The models are built to a 1/16 scale, are composed of 24 turns of 1 6 mm sheet copper. Each turn was cut from copper sheet and the ends bent 90° to form the opening for the channel. The turns were cut at a convenient location to form an open loop. The ends of the loops were then sprung slightly to permit butt brazing to adjacent loops, thereby forming a helical circuit. The space between the turns permitted the use of a forced air cooling system which in turn allowed operation at reasonably and constant temperature for reasonably high current and field strength. A photograph of the first model magnet is shown in Figure II-C3.

In the model testing program the first objective was the verification of the calculated field strength. Reference to the design equation will show that all factors can be scaled or accounted for except the quantity "G," the geometry factor. Careful measurement of field strength, power input, conductivity (copper temperature) and space factor will give actual values of "G." The models showed that the actual value of "G" is 5% higher than computed values due to the contribution of the end turns to the total field. The second and third test objectives of finding field variations within and outside the magnet became a matter of careful surveying. Excessive variation inside the generating channel would require redesign of the magnet.

The model magnets were excited by means of a welding generator at a current of 200 amps. The field strength was measured with a rotating coil type gaussmeter having 1% accuracy and .1% sensitivity. Maximum field values of about 380 gauss were produced or slightly over 1% of the design value for the generator magnet. Figure II-C4 shows a longitudinal centerline survey with full scale dimensions and shows the locations of the excitation and power sections of the generator channel. Figure II-C5 is a transverse field distribution, measured in the horizontal central plane of the magnet and at approximately the junction of excitation and power sections. To obtain this survey the 12th and 13th plate of the model were separated to allow the insertion of the 6.3 mm diameter gaussmeter probe between the turns. The value of the average field strength within the copper conductors is essential for calculating the forces on the conductors. Figure II-C6 is a composite of the field strength inside the generator channel compared to the centerline field strength. It will be seen that in the excitation section and the upstream end of the power section, the field strength variations are moderate, but near the outlet of the power section, due to the rapid

divergence of the channel, the variations are becoming rather large. Although a more uniform field would be desirable from the standpoint of channel performance, it could be obtained only at a considerable increase in copper weight because the present magnet geometry is near optimum for minimum copper weight.

The presentation of the work with model magnets has been presented in considerable detail because it is believed that a considerable saving in time and cost has been achieved as compared to a technically feasible but cumbersome computation program. In addition, the need for a large scale testing program for the full sized magnet is virtually eliminated, since the required information can be reliably extrapolated from the model tests.

e. Magnet Inductance

The rapidity with which the generator builds up to full output is dependent, in part, on the magnet inductance. The inductance may be estimated using handbook formulas for rectangular coils. However, the unusual configuration of the ends of the generator magnet causes some uncertainty as to the accuracy of the computed figure. The magnet inductance may also be determined by measuring the inductance of the model magnet experimentally and scaling the result to the full sized magnet. Using a battery to drive the model magnet the circuit time constant and total resistance may be determined. The model magnet inductance was thus found to be 1.08×10^{-4} henries. The inductance of the full sized magnet is then:

$$L_F = L_M \frac{1}{S} \left(\frac{N_F}{N_M} \right)^2$$

where

L_F and L_M = inductance of full size and model magnet, respectively

N_F and N_M = number of turns of full size and model magnet, respectively

S = scale factor of model

The estimated inductance of the full sized magnet is about .27 henries. Although no direct measurements have been made it appears that the actual inductance is fairly close to this value.

In making calculations of generator excitation and buildup time, the conservative value of .3 henries was used for magnet inductance. This value corresponds closely with the actual figure.

f. Final Design

With finalized channel dimensions and the results of the model testing program, the final magnet design calculations could be made. The following procedure was used. The allowable temperature rise in the copper conductor is limited by the properties of the insulation. An investigation of various types of insulating materials led to the choice of Mylar film. Mylar has good strength at elevated temperatures and is fairly inexpensive and easy to work with. Previous experience indicated the desirability of a fairly heavy film to resist mechanical damage such as puncture by small chips or burrs. A 0.25 mm thickness was selected. A maximum temperature of 175°C is possible with Mylar, but a 15° allowance for current concentration in the corners plus a 15°C allowance for plate thickness tolerance brought the maximum average temperature to 145°C. Starting at room temperature (25°C), the magnet would heat to 145°C in a full-power full-duration (3 min) run. A current density of 1190 amps/cm^2 was calculated to obtain the required design field strength. Using corrected values of the geometry factor as determined by model tests a conductor cross section can be computed along with the total power input and total weight. The conductor dimensions may be optimized for minimum copper weight and this was done but with a slight bias toward extra height to improve field distribution. The number of turns required can be computed, based on the supply voltage or output of the excitation section, and the required power input. Layout of the copper plates can then be made and final construction details completed. The specifications of the magnet are as follows:

Field strength	35,000 gauss inlet; 30,000 gauss outlet
Width of openings	0.81 meter inlet; 1.16 meter outlet
Active length	3.18 meter
Overall length	4.52 meter
Power requirement	16-20 Mw
Current	22,000 amps
Resistance	0.0318 ohms
Inductance	0.27 henries
Weight of copper	61,000 Kg
Number of turns	316
Conductor dimensions	0.00368 x 0.496 meter
Insulation	Mylar

g. Reinforcement

The high values of field strength and current in the generator magnet produce large forces on the conductors. The magnitude of these forces at any point is equal to the factor product j x B. These forces are far too large to be contained by the mechanical strength of the conductors and therefore a reinforcement system is necessary. The magnet may be envisioned as a pressure vessel with an internal pressure of 61 atm. The total of all forces absorbed by the reinforcing system is of the order of 4.5×10^6 Kg.

The reinforcement system was designed to be built quickly and cheaply with little regard for space or weight. Accordingly, standard structural shapes were used as much as possible. The primary reinforcement consists of 0.6-meter I-beams arranged in pairs along the sides of the magnet and connected by tie rods. Support for the ends is provided by rectangular I-beam structures joined by longitudinal tie rods. To prevent buckling of the plates under compressive loading, a top structure is provided which clamps the stack of conductors to the magnet base. Any portion of the structure which forms an electrical loop and which intercepts an appreciable amount of flux could be subjected to additional forces during magnet buildup or shutdown. To prevent such forces from developing, the structure is provided with insulation to break the loop. A cross section of the magnet at the exit end is shown in Figure II-C7.

The copper conductors must, of course, be insulated from the reinforcing structure and on flat surfaces this was done with sheets of polyester-fiberglass material. Along the sides of the magnet the surfaces were too irregular to permit the use of sheet insulation. On the sides a small space was left between the conductors and the steel beams. This space was filled with an epoxy potting mixture. The inside of the magnet was coated with a similar epoxy mixture but thickened with a flow control agent to a putty-like consistency. The inside coating is intended to prevent accidental short circuiting of the power connections to the channel and to provide some short-term protection for the magnet in the event of a bad hot gas leak in the channel wall.

2. Construction

a. Methods

During the designing of the magnet, considerable time was directed to exploring construction methods. Essentially, there are three problems; the effect of copper sheet size and grade upon price; the method of building and connecting turns; and the problem of dimensional tolerances

and allowances. In the construction finally adopted, the ends are cut and formed from moderate size plates and the sides consist of comparatively narrow plates. The joints are welded by a tungsten arc inert gas shielded process. Figure II-C8 is a photograph showing the copper portion of the magnet and Figure II-C9 shows the magnet completely assembled.

Ordinarily, welding of copper is considered practical only for the oxygen-free grades. However, the higher price of oxygen-free copper encouraged an investigation into the feasibility of welding tough pitch copper which has an appreciable oxygen content. Two potential copper suppliers made some samples in tough pitch copper which had very satisfactory mechanical and electrical properties. Accordingly, the tough pitch copper was ordered and a welding fixture was designed.

The use of the shielded tungsten arc to weld copper is not unusual, but this particular application presented several new problems which took a considerable time to solve. The most important of these was the design of a portable but rigid, semi-automatic welding fixture and the necessity of producing welds with a flush underside to eliminate the dressing and cleaning of the weld at a location difficult to reach and to keep clean.

b. The Welding Fixture

A cross section of the welding fixture may be seen in Figure II-C10. The fixture is constructed almost entirely of aluminum. It consists of an aluminum base (1) with supports bolted to each end. These supports hold guide bars (2) and a driving lead screw (3) which run parallel to the direction of the weld. The screw is driven by a small AC motor and gear box. The speed of feed can be changed by moving the drive belt to different steps on the pulleys. The clamping bars (4) are designed in two sections connected by springs (5). As the top bar is bolted down on the ends, the springs transfer the load to the bottom clamp bar to hold the copper (6) firmly in position. A flat carbon bar (7) is inserted into the water cooled aluminum base as a backing for the weld. The welding torch (8) is a standard inert gas shielded tungsten arc machine holder. The welding head is supported by a ring clamp (10) attached to a plate which is mounted on the guide bars and driven by the screw.

c. Development of Welding Technique

To obtain a satisfactory welding technique required the making of many test welds in which approximately a dozen parameters were varied. Some of the difficulties which had to be overcome were: the elimination of arc blow due to location of ground leads and external fields, the lack of complete weld penetration, embrittlement and porosity because of current,

speed, type of carbon backing, type and diameter of electrode, shape of electrode point, gas flow, condition of plates, and direction of feed. The final technique arrived at gives ductile welds on both top and root, complete penetration, elimination of arc blow, a flat back, and no porosity.

The technique consists of the following conditions which must be kept constant:

1) A welding current of 405 to 415 amps

2) A welding speed of 0.25 meters per minute

3) A 4.75-mm diameter 2% thoriated tungsten welding electrode

4) A helium flow of 0.15 Kg/hr

5) A pure carbon backing material

6) Spring loaded aluminum clamping bar tightened to a specific load

7) A specific shape of electrode tip (see Detail A of Figure II-C8)

8) The electrode tip located 1.9 mm above the filler material (see Detail A of Figure II-C10)

9) Top edges of plates radiused along the weld

10) All edges and surfaces of the plates around the weld must be perfectly clean

11) The electrical ground leads fastened to the copper plates and located such that the weld is always made toward the grounding point

12) The fixture located so that the direction of the arc feed is always from the inside of the magnet towards the outside with the motor end of the fixture always on the outside of the base.

Methods were also developed to remove a bad weld in the event a weld made on the magnet was not of good quality.

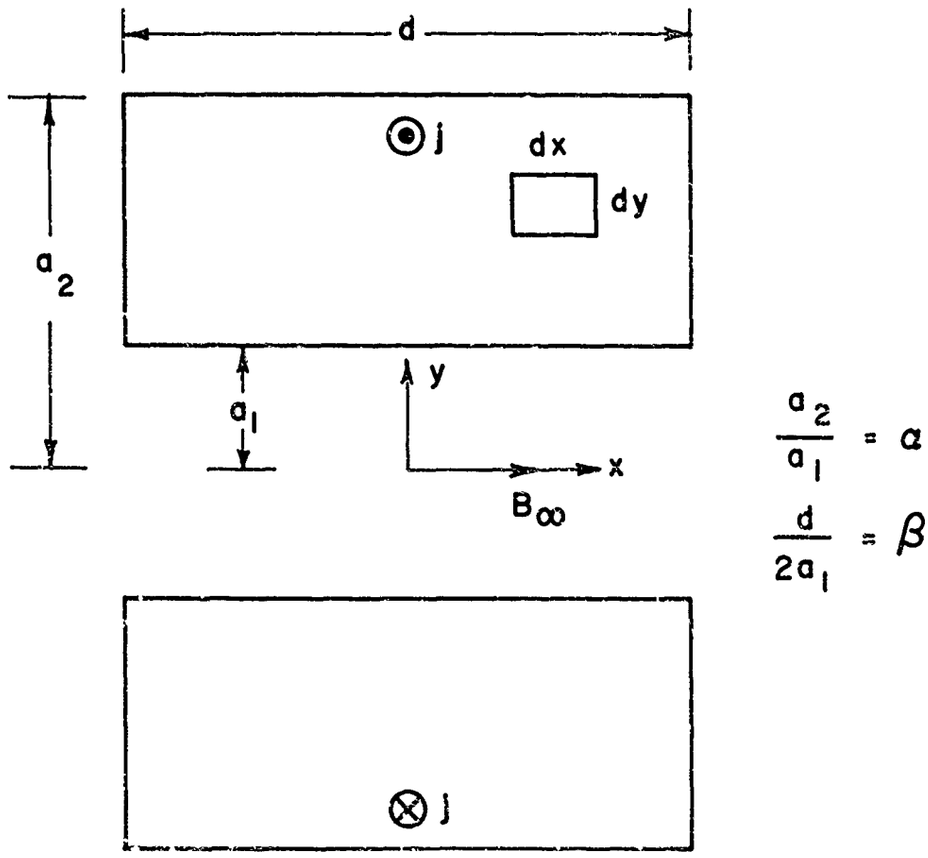

Figure II-C1 Configuration for Calculation of Magnetic Field Due to Infinite Straight Conductors

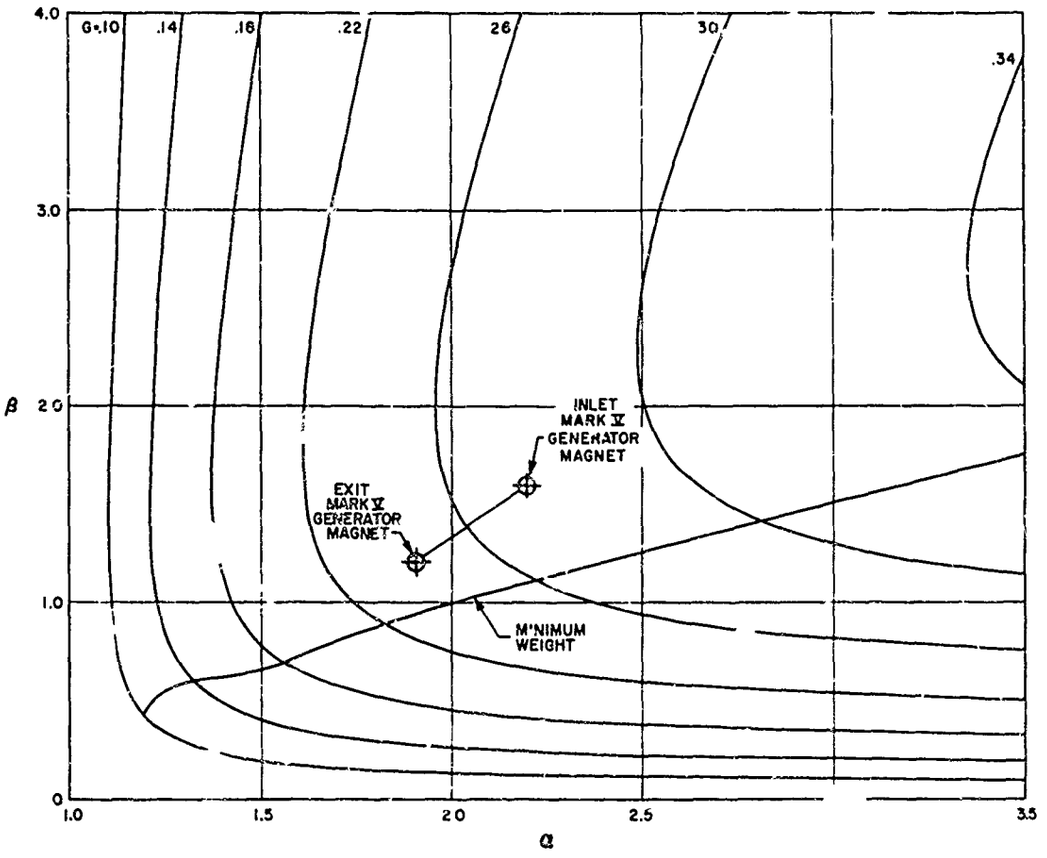

Figure II-C2 Plots of G (α, β) vs α and β with the Curve of Minimum Magnet Weight and the Mark V Magnet Shown

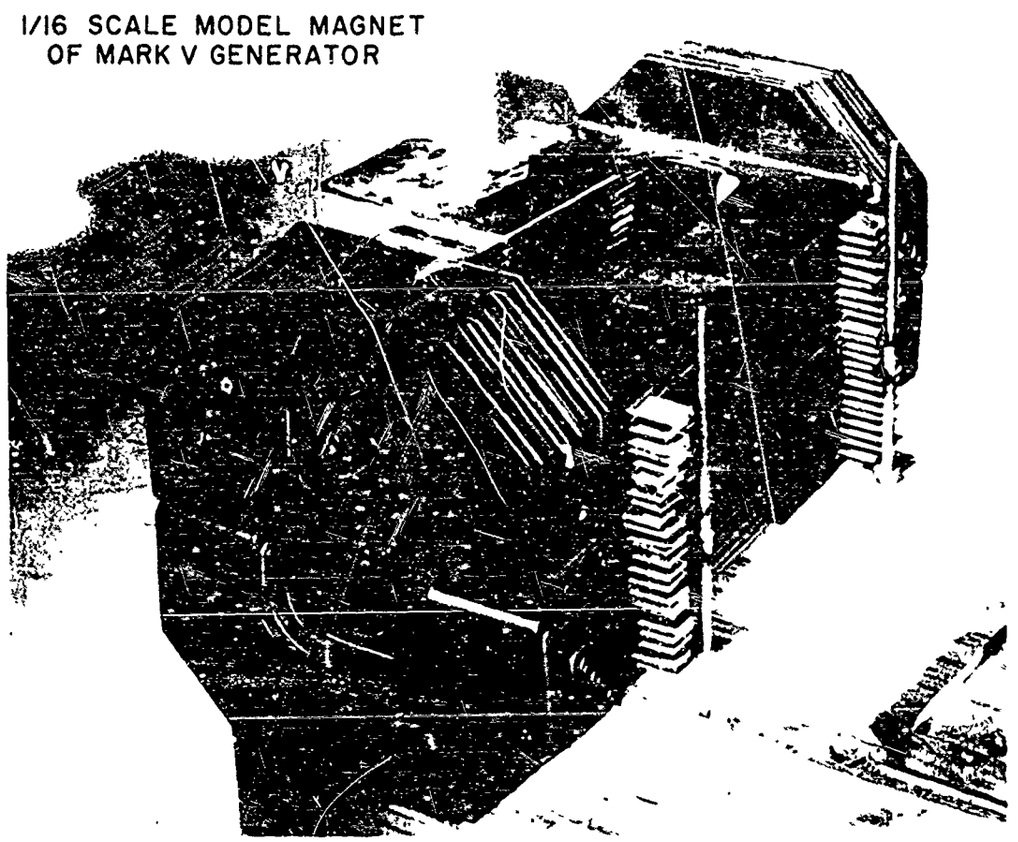

Figure II-C3 1/16 Scale Model Magnet of Mark V Generator

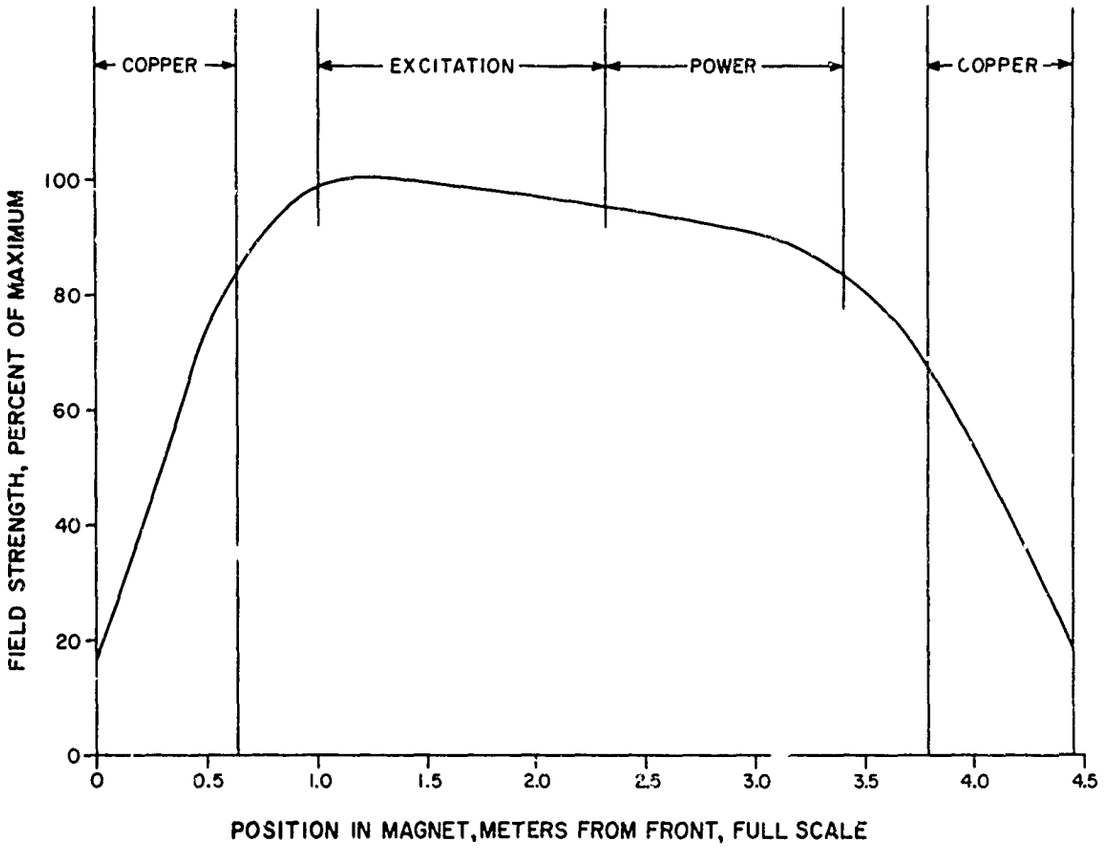

Figure II-C4 Field Distribution Taken on the Longitudinal Centerline of the Model Magnet

8868

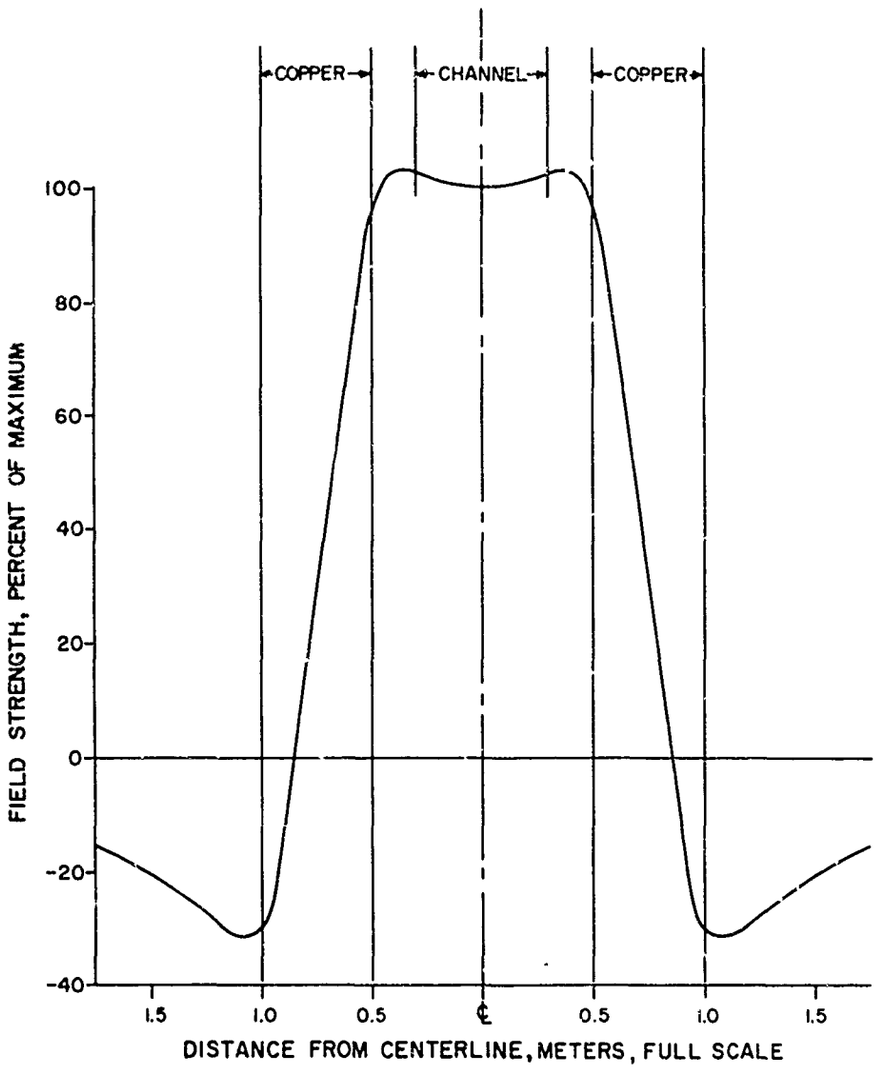

Figure II-C5 A Transverse Field Distribution in the Model Magnet for the Mark V Generator

3869

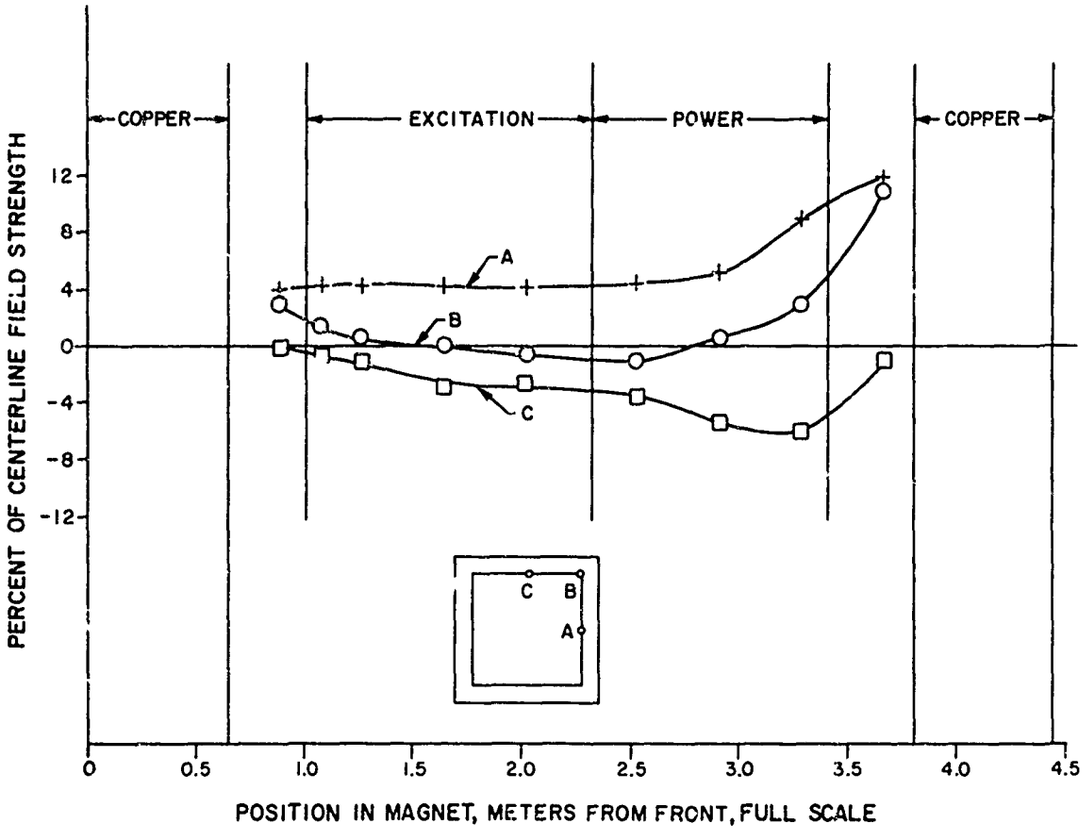

Figure II-C6 Variation of the Field Strength Along the Channel Walls in the Flow Direction Taken in the Model Magnet

8870

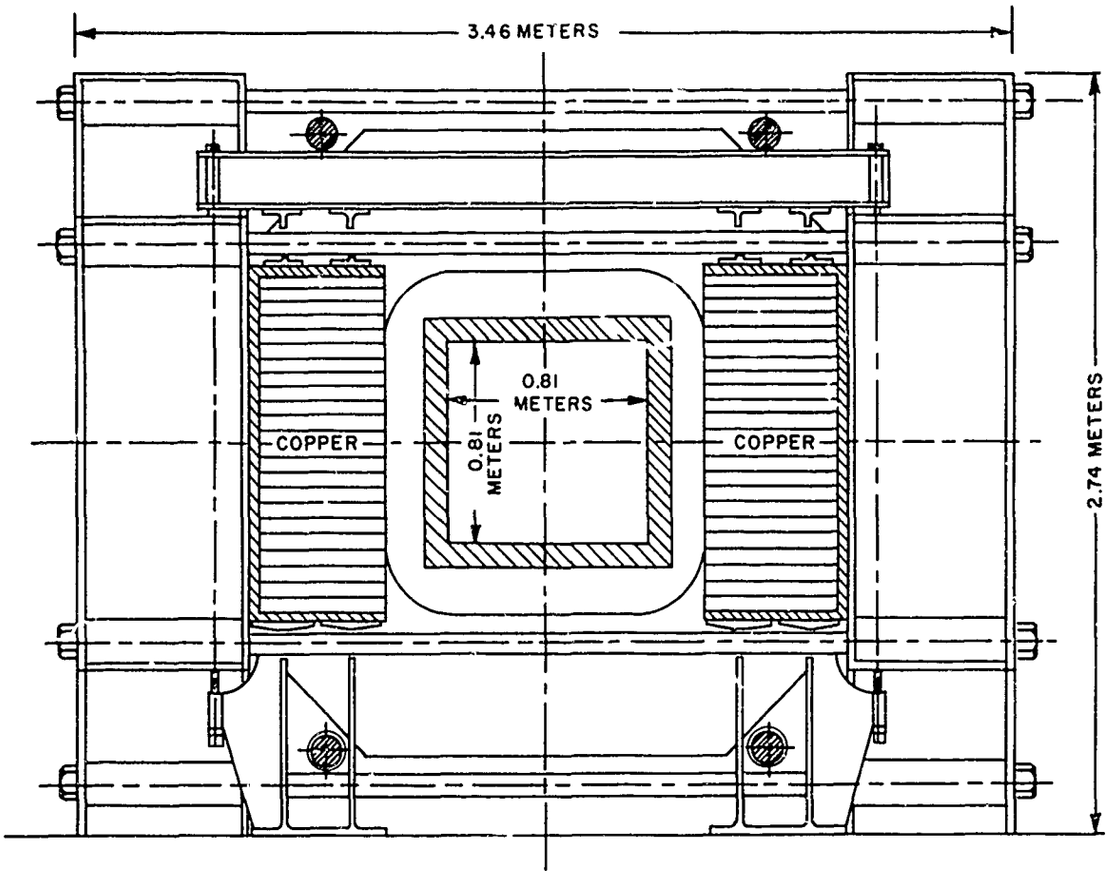

Figure II-C7 Cross-Section of Copper Magnet and Reinforcement Structure

8871

Figure II-C8 A Photograph Showing the Copper Portion of the Magnet

Figure II-C9 A Photograph Showing the Magnet Completely Assembled

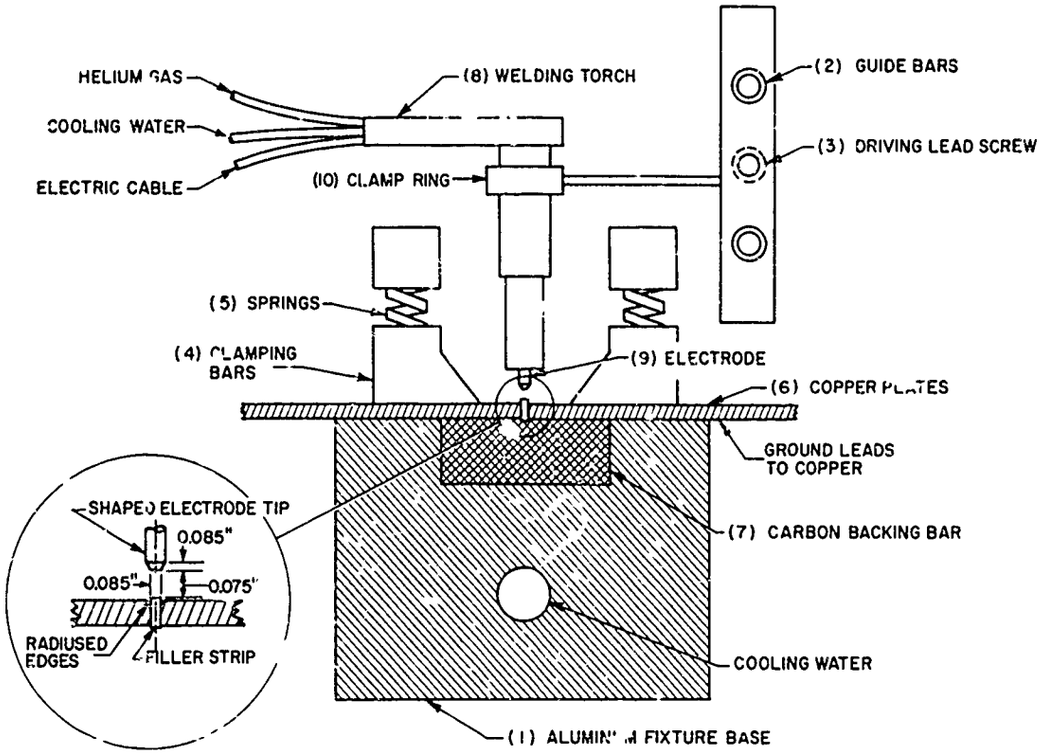

Figure II-C10 Sketch of the Welding Apparatus Used in Building the Mark V Generator Magnet

D. CHANNEL DESIGN

The channel configuration is shown in Figure II-D1. The channel is divided into four sections; inlet, excitation, power, and outlet. The inlet section guides the flow from the burner nozzle, through the magnet end, into the excitation section. It also serves as an electrical insulator between the combustion chamber nozzle and the excitation section which starts at the point of maximum field strength. Figure II-D1 shows the length and cross sections for the channel as well as the arrangement and numbering of electrodes. The nine electrodes in the downstream end of the inlet section are segmented and numbered 1I through 9I. The electrodes in the excitation section are mounted on a continuous slab, with the exception of the downstream end which has nine segmented electrodes numbered 1S through 8S and 9sx. Electrode 9sx is located in the junction between the excitation and net power sections. The electrodes in the net power section are numbered 1 through 50. In the exit section are non-working copper slabs with the same general arrangement as electrodes. These slabs are numbered 51 through 53 and EX1 through EX18.

The excitation section is that part of the MHD channel from which the power, required to energize the magnet, is extracted from the working fluid. For reasons to be described below, a single, continuous (non-segmented) electrode pair is used in the excitation section. This section has a power output of 18 Mw at full field strength, and starts with a rectangular cross section of 0.126 square meters and diverges to a square cross section of 0.253 square meters. Most of this area increase is attained by diverging the two insulating walls which connect the electrode walls. The electrode distance along this part of the channel is therefore nearly constant, which together with the magnetic field and gas velocity variation along the excitation section, makes it possible to maintain a constant output voltage.

By accomplishing this, it becomes possible to utilize the total current flow in the excitation section of the channel (22,000 amps) to energize the magnet. Since the magnetic field strength, for a conductor of given geometry, is proportional to the number of ampere turns, the use of the total current through this part of the generator gives the smallest number of turns in the magnet and therefore a magnet of simplified construction. However, one disadvantage was that a reduction in the power output per unit volume of the gas flow is experienced by using a non-segmented electrode pair, because the Hall potential is allowed to short out. The fact that the values of $\omega\tau$ are low in the first part of the channel makes it feasible to use this design and locate the excitation section in the high pressure (low $\omega\tau$) inlet section of the channel.

The power section starts from the exit of the excitation section, and diverges in both directions to a square cross section of 0.56 square meters in a length of 1.38 meters. The power section of the channel ends at a point where the magnetic field strength on the centerline of the gas flow is 30 kG.

The power section utilizes segmented electrodes and therefore gives a higher efficiency than the excitation section due to the increased gas conductivity. Fifty electrode pairs are used, with each pair having a power output of approximately 0.40 Mw. Each electrode pair is connected to its individual load resistor which is made of water cooled stainless steel tubes.

The outlet section serves the same purpose as the inlet section by being an electrical insulator and a flow passage through the hole in the end of the magnet into the exhaust duct.

Also included as a portion of the channel design was a dummy channel to be used as a part of the burner test program, a wooden mock-up of the actual channel to check dimensions and fix the centerline of the generator, and a channel extension pipe and exhaust duct for conveying the generator exhaust gases and cooling water from the test cell.

A sketch, schematically illustrating the electrode and insulating walls can be seen in Figure II-D2. Voltages at various important junctions along the length of the channel are also shown in the sketch.

The channel wall materials have to withstand relatively high temperatures, high local gas velocities, the chemical action of a corrosive and oxidizing atmosphere, and high thermal and mechanical stresses. Since the rate of energy release is high, the walls have to withstand an initial thermal shock and permit high heat transfer rates and thermal expansion.

The requisite properties of a channel are that it must be an effective electrical insulator in the plane of the wall and either conduct heat normal to itself or operate with its surface temperature very nearly equal to the temperature of the gas. Since MHD generator technology is such that the lowest gas temperature in the generator is approximately equal to the maximum temperatures which can be tolerated by refractory materials, a wall whose surface was entirely refractory would have to be subjected to long warm-up and cool-down periods to prevent destructive thermal shock. This could have important consequences when quick and repeated operation is required. On the other hand, if the wall temperature is reduced below that of the gas, there is appreciable heat transfer and the wall must be a good thermal conductor in order to transfer the heat to a coolant.

1. Channel

a. Segmentation

In each section of the channel there are two vertical electrode walls and two horizontal insulating walls. The design of both the insulating and electrode walls utilizes water-cooled metal segments previously used

in other Avco MHD generator designs. The metal segments are separated by thin sections of refractory material to stand off the electric field potential. The principle of operation for this type of construction is illustrated in Figure II-D3. The metallic segments conduct the heat transferred from the gas into a coolant which can be circulated through the elements. The refractory provides a high temperature electrical insulation between the metallic elements. The refractory is in fact a poor thermal conductor and may be used only where its surface temperature can be held to a tolerable value by the use of thin sections. The pitch, d, between the metallic pegs is determined by the value of the local electric field, E. together with the value of an arc burning voltage, V_o, typical of the working gas, and the metallic elements which can be considered to have properties similar to cold electrodes. E, B, and U are the electric and velocity, respectively. As long as the product of E and d is less than V_o, there will be no breakdown to the metallic elements, and the current will flow in the gas.

A total Hall potential of 1750 volts was obtained in the flow calculations over the length of the net power output section. Based on earlier experience, a voltage difference between electrodes of 40 volts was proven satisfactory; therefore, 50 electrode pairs were chosen for the net power output section, giving an average voltage between adjacent electrodes of 35 volts.

In the electrode wall, segments are used in the inlet section to insulate the self-excitation section from the burner which is grounded. In the self-excitation section, a single continuous electrode is used for providing electrical power to the magnet; however, provisions have been made to utilize the exit part of this section for additional net power output in the event that power required for magnet energization can be successfully attained with less than the entire section. For this purpose, segmented electrodes have been included in the design, which can be uncoupled from the magnet and connected to individual load resistors. In the power output section, segmented electrodes are used, each electrode being connected to an individual load resistor. In the outlet section, segmented slabs are used to isolate the power output section from a metal exhaust tube used to discharge the gases to the atmosphere.

In the insulating wall, the inlet section consists of a continuous slab and then successive rows of pegs to insulate the self-excitation section from the burner, and to insulate against the transverse field. Figure II-D4 shows a section of the insulating wall being assembled. In the self-excitation section, axial tubes are used to provide transverse insulation, axial segmentation not being required since there is no axial field. At the exit of the self-excitation section, there is a provision for both axial and transverse insulation, which will be required in the event that any of the segmented electrodes in this section are used for net power output. In the power output section, insulation exists both axially and transversely. In the outlet section axial segmentation is used to insulate from the exhaust duct, and transverse segments to stand off the transverse voltage differential.

b. Heat Transfer

The channel insulating and electrode walls have been designed to withstand heat transfer rates 20 percent above those expected at the rated gas flow condition. The maximum heat transfer rate at this condition occurs at the channel inlet section, where the heat transfer rate from the gas to the metal surface is estimated at 1100 watts/cm^2. Because of the high heat transfer rates, copper, with its high thermal conductivity is used for the metallic segments. The maximum metal surface temperature occurs at the inlet section and is approximately 425°C. Copper was also selected for all gas side metal elements because of its high heat transfer rates and past experience in channel design dictates its advantages. The variation of calculated heat flux, and copper surface temperatures, along the length of the insulating wall, may be seen in Figure II-D5. The electrode walls have also been designed to withstand heat transfer rates equivalent to that of the insulating walls.

The cumulative heat loss along the length of the channel walls is shown in Figure II-D6. Separate curves are drawn for both the insulating and electrode walls, the heat loss being 9.4 Mw for one insulating wall and 7.7 Mw for one electrode wall. The total heat loss to all four walls is therefore 34.2 Mw.

The water flow rate requirement was determined by selecting a safe permissible water bulk temperature rise and then calculating the quantity of water necessary to maintain that rise. Figure II-D7 indicates the cumulative bulk rise along the channel length is 44°C at a flow of 3000 liters/min for the insulating wall, and 64°C at 1700 liters/min for the electrode wall. The total channel cooling water flow rate is thus 9400 liters/min. To maintain a simple design of the water cooling system, water flows through the channel in a single pass, with water entering at the inlet section and leaving at the exit section, where it is further utilized to quench the exhaust gas discharging from the generator. The total water pressure drop through the channel walls is approximately 13.6 atm.

c Electrode Design

The functions of the electrodes in an MHD generator serve the same purpose as the brushes in a conventional generator: to provide a good connection between the generator armature and its load circuit. As in the conventional generator, losses are associated with this function. In an MHD generator, however, the problems are more severe because the electrodes have to provide a good contact between a moving gas which is a relatively poor electrical conductor and the external electrical load circuit. Due to the nature of this problem, the losses associated with this function in an MHD generator have more influence on the generator output (performance) than do the brush losses in the conventional generator. The direct

electrical losses occurring in the immediate vicinity of the electrode surface defines the electrode drop. These losses are of two natures; one is the loss associated with charge transfer at the electrode surface, and the second with joule loss due to the current passage through a thin aerodynamic boundary layer existing over the electrodes, as well as joule dissipation in the electrode itself.

To secure thermionic emission from the electrodes, they must be heated to a high temperature. The desired electrode surface temperature can be obtained by convective heat transfer from the gas if the dimensions of the electrode material are well chosen. Another important factor in the design of the electrodes is that the electrodes have to reach emission temperature within a few seconds. In a self-excited generator this time is adequate since the generator operates in parallel with the battery bank for a few seconds immediately after the burner is fired.

The surface temperature of the electrodes also determines the thermal gradient within the boundary layer for a given flow condition. The temperature gradient within the boundary layer results in a large variations of conductivity within it and therefore large joule losses.

From the above mentioned facts, the conclusion can be drawn that it is desirable to have as high an electrode surface temperature as possible. However, the mechanical and thermal properties of the electrode materials limit the temperature. The original plan was to utilize a replaceable carbon or graphite electrode which would be consumed during testing. Results of tests performed outside the original contract indicated that a semi-permanent copper-zircoa electrode would be more suitable than a consumable electrode for the Mark V generator.

Experience with stabilized zirconia has shown that the required emission is obtained at temperatures of between 2000 and 2500°K, and that the joule losses in the boundary layer as well as the internal joule dissipation, become small at these temperatures. However, it lacks sufficient mechanical properties, which necessitated the use of copper as the retainer.

Zirconia shows quite an important drop in its mechanical strength, but retains enough strength for the groove design. In this design, the shear stresses are taken by a high strength, low temperature metal which also acts as a low electrical resistance path. Zirconia has a small coefficient of thermal expansion and has demonstrated good resistance to thermal shock.

With the anisotropic groove design as originally used, zirconia was found to have a good resistance to erosion. Further, zirconia bears the thermal stresses better than most ceramics and the groove design reinforces this resistance. The corrosive action is not a problem in the Mark V generator due to the three-minute duration of the runs.

The electrode design essentially consisted of a water-cooled copper bar with two milled grooves to retain the zircoa. This design provides cold edges between adjacent electrodes which helps prevent electrical breakdown. The groove dimensions were varied to maintain a constant but sufficient electrode surface temperature throughout the channel. Figure II-D8 shows a section of the electrode wall being assembled.

d. Structure and Materials

The channel insulating walls are made up of the individual copper segments which are mounted to plastic plates composed of a glass epoxy laminate. This plastic material was selected because of its relatively high strength, fairly high temperature resistance, and good electrical insulation qualities. Plastic, however, has a low modulus of elasticity, and hence it was necessary that the plates be reinforced to limit the deflection resulting from the high pressures of the generator working fluid. The reinforcement is provided by stainless steel ribs, located at specific intervals along the channel to limit the wall deflection. The structural ribs insure not only the structural integrity of the channel, but they also maintain an alignment of the various components which is well within the limits successfully encountered in previous channel designs.

The structural reinforcement of the electrode walls is considerably varied from that of the insulating walls. Each individual segmented electrode is supported by its own stainless steel bar. This bar is sandwiched between the electrode and a plastic plate, which is of the same material used in the insulating walls. The stainless support bars are exactly the same width as the electrodes and vary in thickness as the wall loading varies. These bars in the electrode wall add to the structural integrity of the channel, since the plastic on the insulating wall bolts to these bars accepting some of the load from the insulating walls. A picture of the completed channel is shown in Figure II-D9.

Figure II-D10 shows the variation in channel wall deflection with channel length for both the insulating wall reinforcing ribs and the electrode reinforcements. The gas pressures used in these calculations are also shown in this figure.

The material used for electrical insulation between the metallic segments is an alumina castable with a calcium aluminate cement binder. This material has been proven to be the most satisfactory yet discovered in the various channel and electrode tests conducted at the Avco-Everett Research Laboratory, as its resistance remains relatively satisfactory to very high temperatures.

The entire channel assembly is mounted directly and permanently to a stainless steel chassis. The chassis is designed with a longitudinal angle iron section, having the proper angles to accept the channel

w ls. The base of these sections is a solid stainless steel bar into which are mounted ball bearing rollers on which the channel will be moved. The two sections are connected together transversely by angle struts which are insulated such that no electrical circuits can exist from one longitudinal section to the other. The channel is also insulated electrically from the chassis.

The channel roll out stand is a structural steel truck mounted on three sets of casters. A set of rails is located on the top to accept the rollers of the channel chassis. The roll-out stand was used for an assembly table for the channel and a stand onto which the channel can be removed directly from the generator magnet for maintenance purposes.

A rail system on the test cell floor allows the roll-out stand to be moved aside from the generator when tests are conducted.

2. Dummy Channel

To provide a method for in-place burner testing before receipt of the final channel, a dummy channel was constructed. This channel consists of an inlet flange used to connect the channel with the burner. The channel is then made of two concentric steel pipes which form an annulus for cooling water flow. The pipes are connected together structurally at strategic points along the channel length to prevent buckling of the internal pipe when water pressure is applied. A cooling water flow of 9400 liters/min passes through the annulus, and is discharged through fixed orifices at the end of the pipe directly into the exhaust duct.

Another 5700 liters/min of water is injected through orifices at the inlet flange to partially quench the hot gas on the inside surface of the pipe. This injection is required to reduce thermal stresses on the inside pipe to a tolerable level. The dummy channel is mounted on rollers so it can be moved on the same rails, inside the magnet, which support the real channel. A photograph of the completed dummy channel may be seen in Figure II-D11.

3. Channel Extension and Exhaust Duct

The channel extension is a 1.2-meter diameter steel pipe which is 0.79 meters long, with a 6.35 mm wall thickness. The function of this part is to extend the channel through the steel framework forming the magnet support structure and conduct the working fluid into the exhaust duct. This section is film cooled by water injected tangentially at two points and by the cooling water ejected from the channel.

The exhaust duct is used to conduct the generator gases from the channel, out of the test cell, and into the atmosphere. The duct is 2.44 meters in diameter, 10.7 meters long, and is made of low carbon steel (Figure II-D12). It is designed with three sets of casters so that it may be rolled away from the generator. The purpose of this is to allow room for extraction of the channel from the magnet. The water used to cool the load resistors is injected into the gas stream at the inlet of the duct, where it quenches the exhaust gases.

The duct is completely insulated from ground by insulating the casters and cooling water inlet flange. There is also an air gap between the channel extension piece and exhaust duct, so there is no direct connection to the channel.

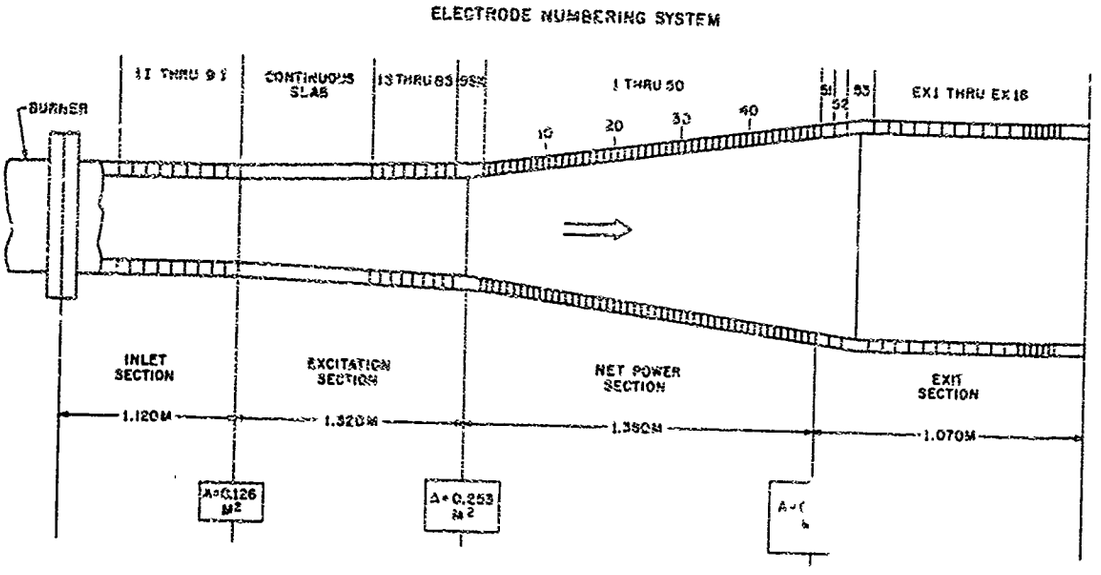

Figure II-D1 Layout and Electrode Arrangement of the Mark V Generator Channel

A8937

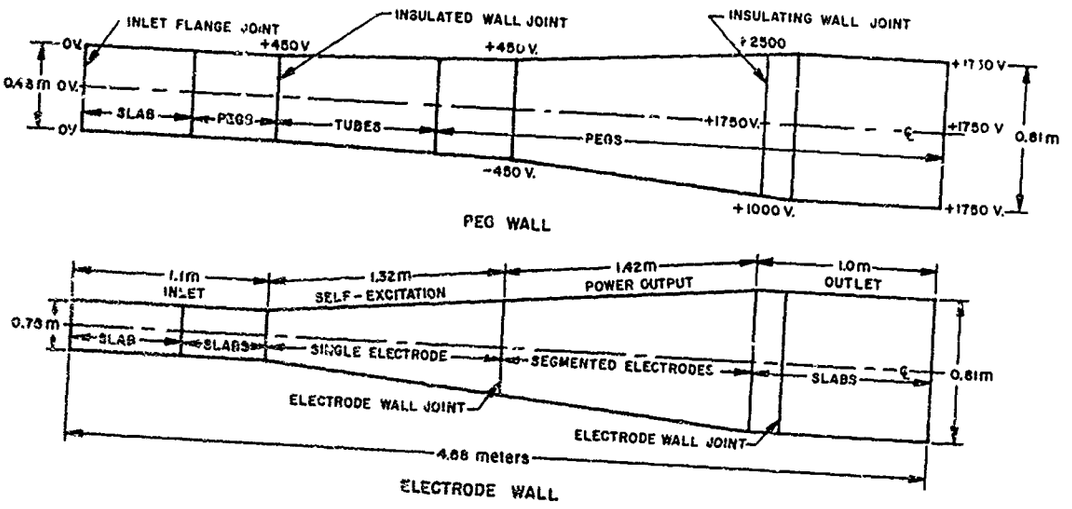

Figure II-D2 Sketch Illustrating the Electrode and Insulating Walls of the Channel

9752

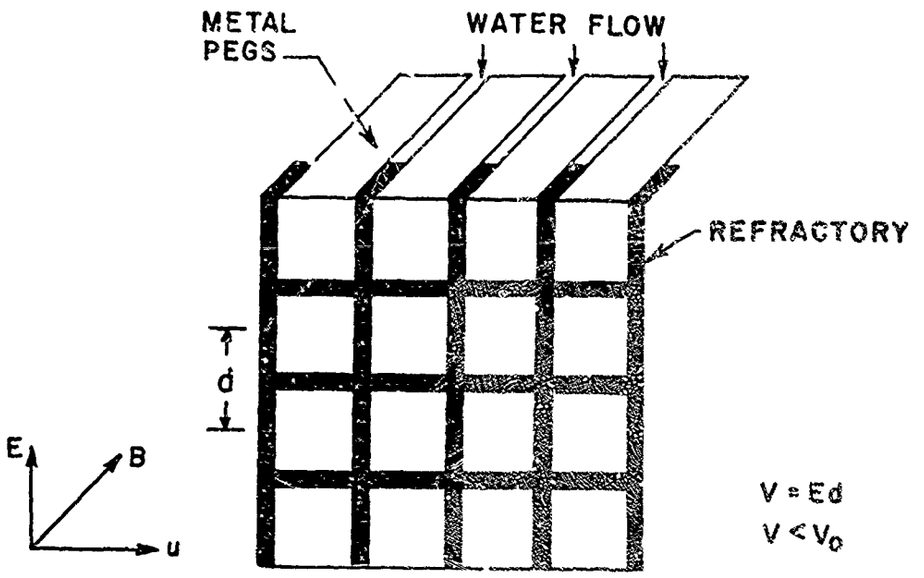

Figure II-D3 Principle of Water Cooled Wall

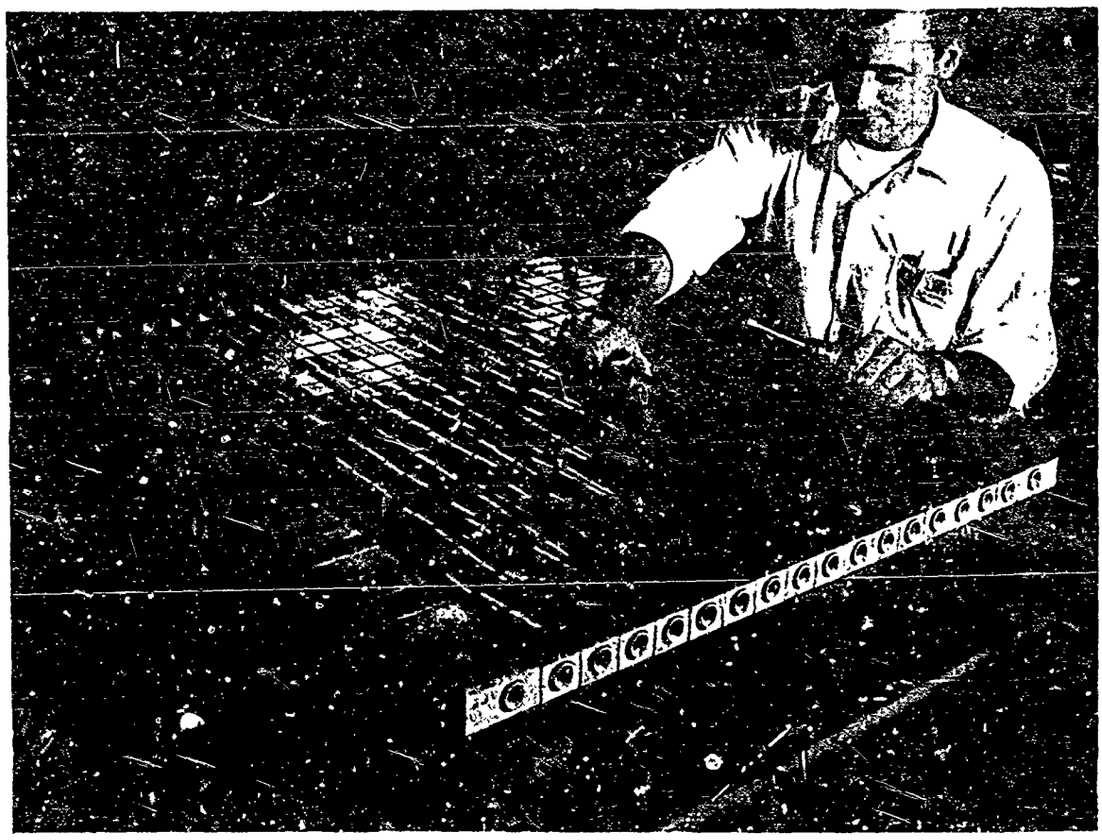

Figure II-D4 Section of the Insulating Wall Being Assembled

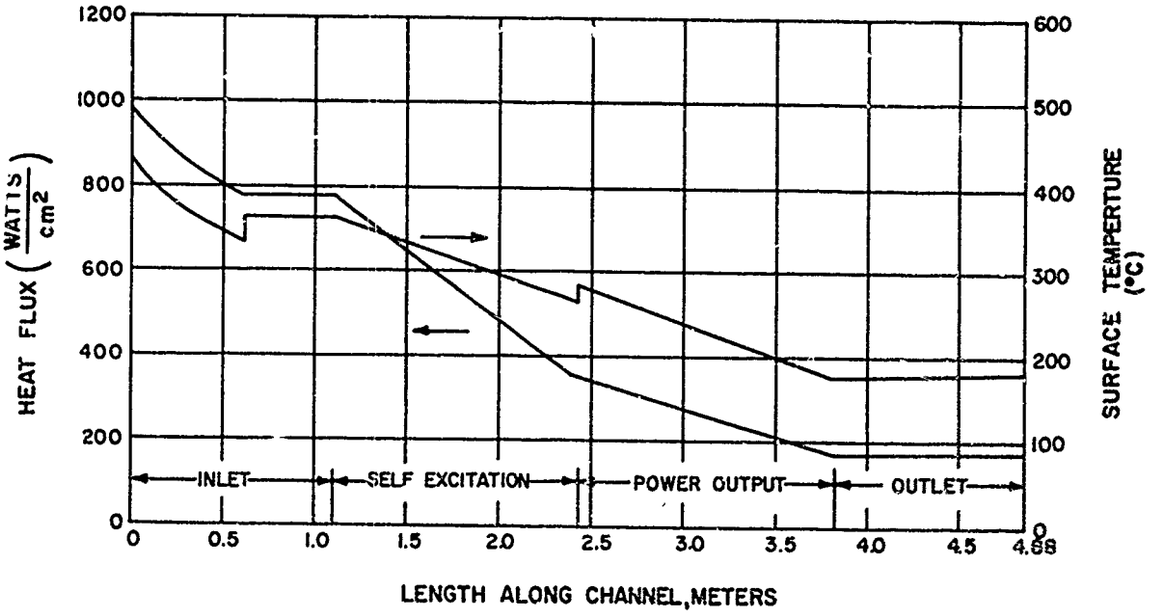

Figure II-D5 Heat Transfer and Surface Temperature for Insulating Walls

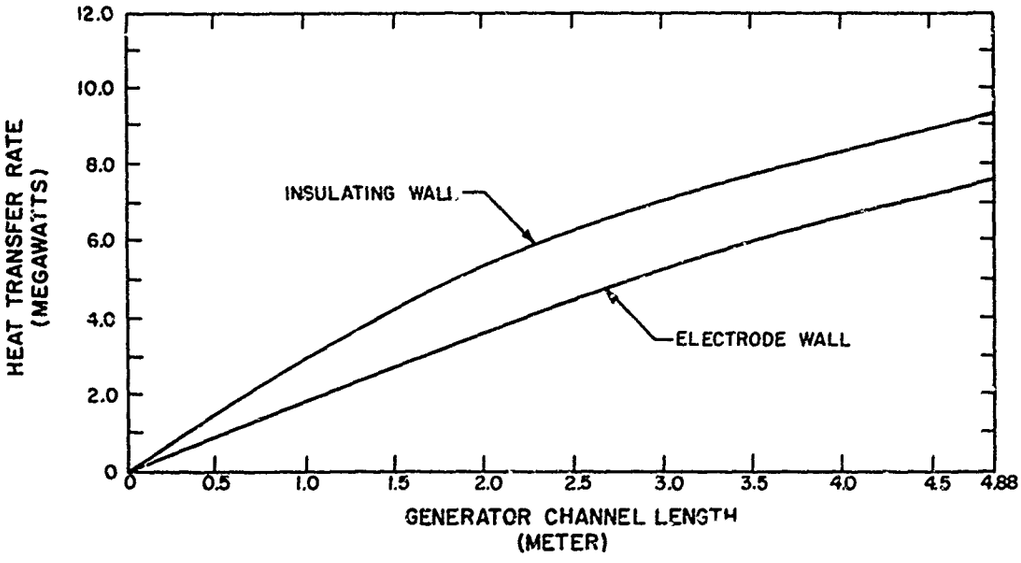

Figure II-D6 Cumulative Heat Losses to Channel Walls

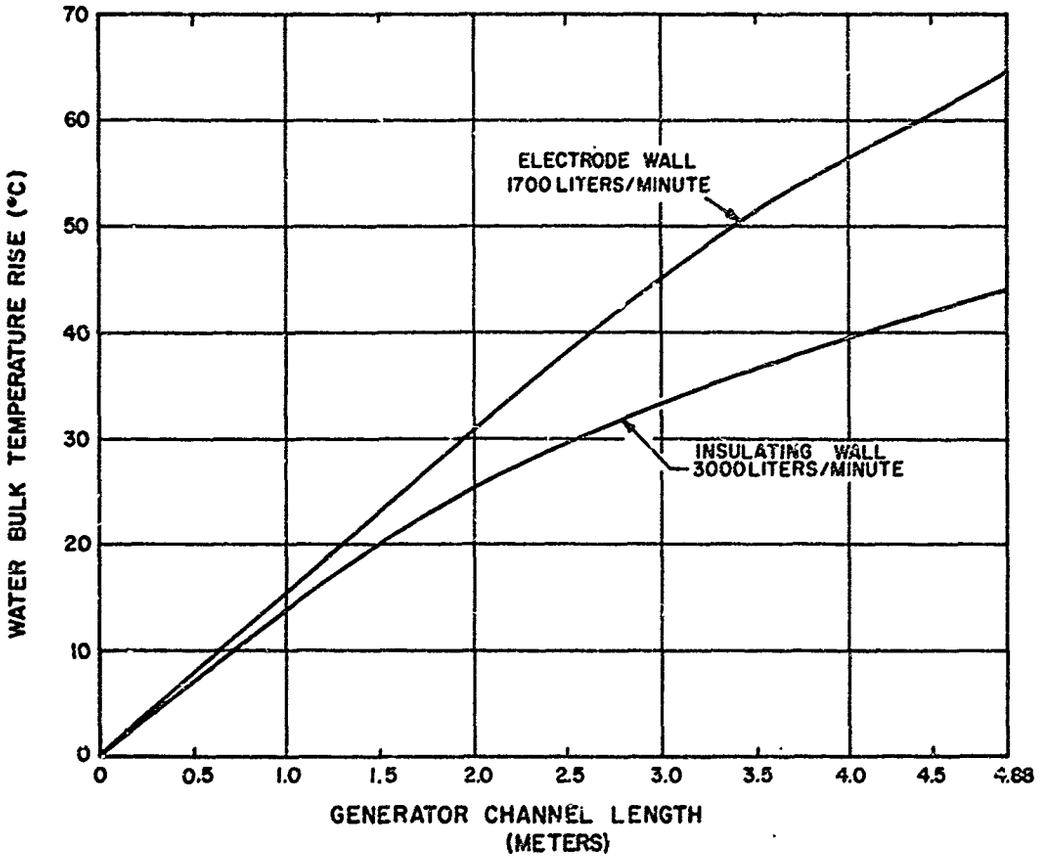

Figure II-D7 Cooling Water Bulk Temperature Rise in the Channel Walls

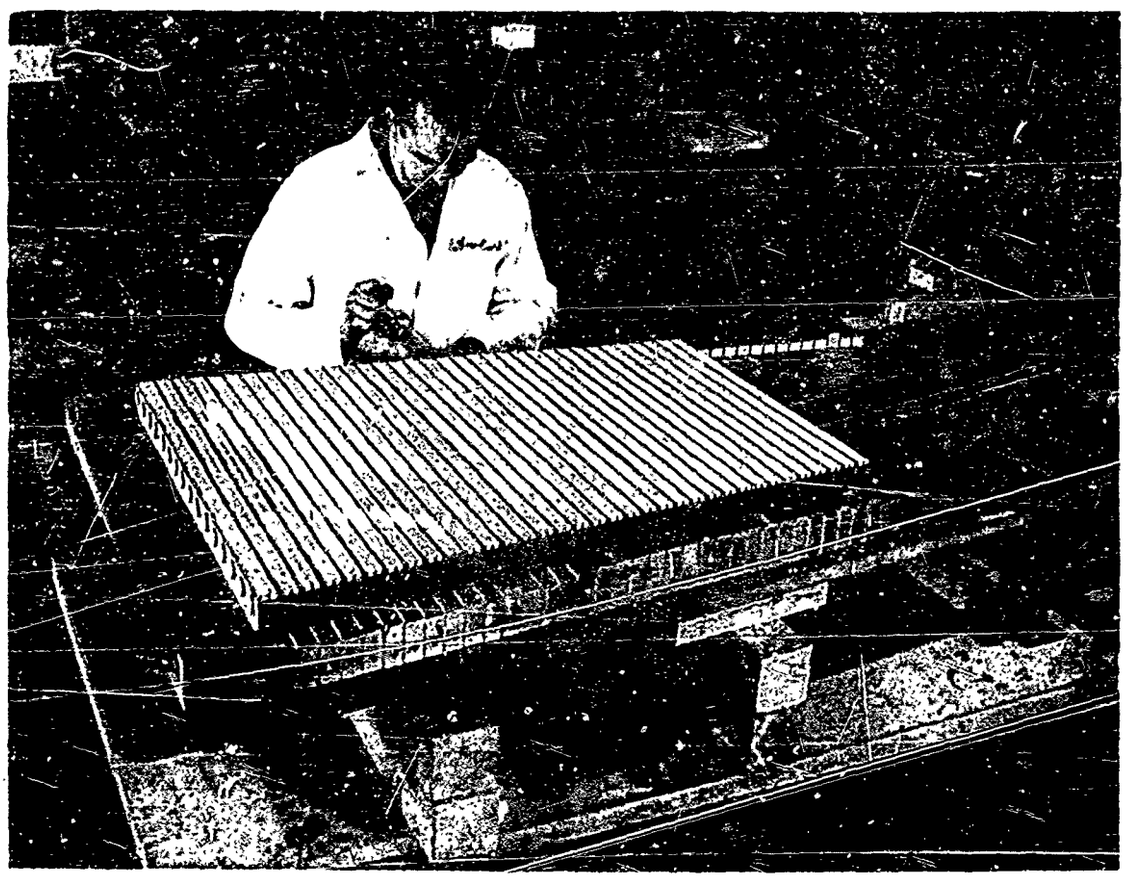

Figure II-D8 Section of the Electrode Wall Being Assembled

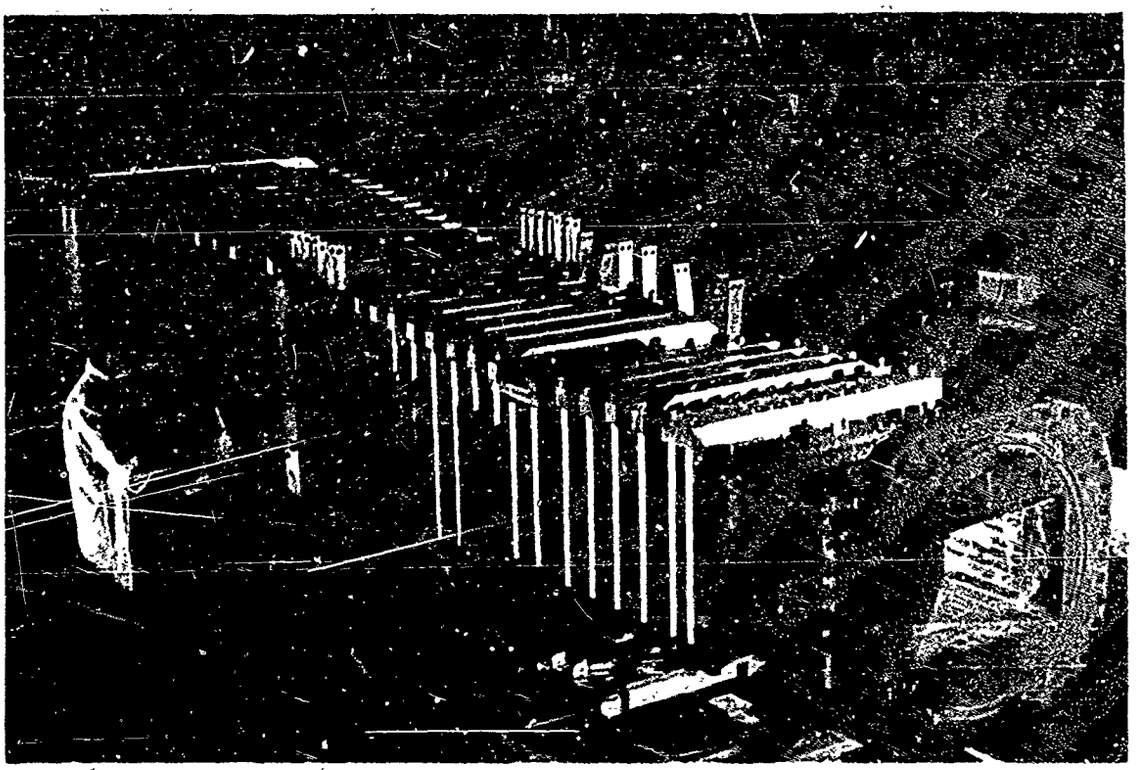

Figure II-D9 Completed Channel

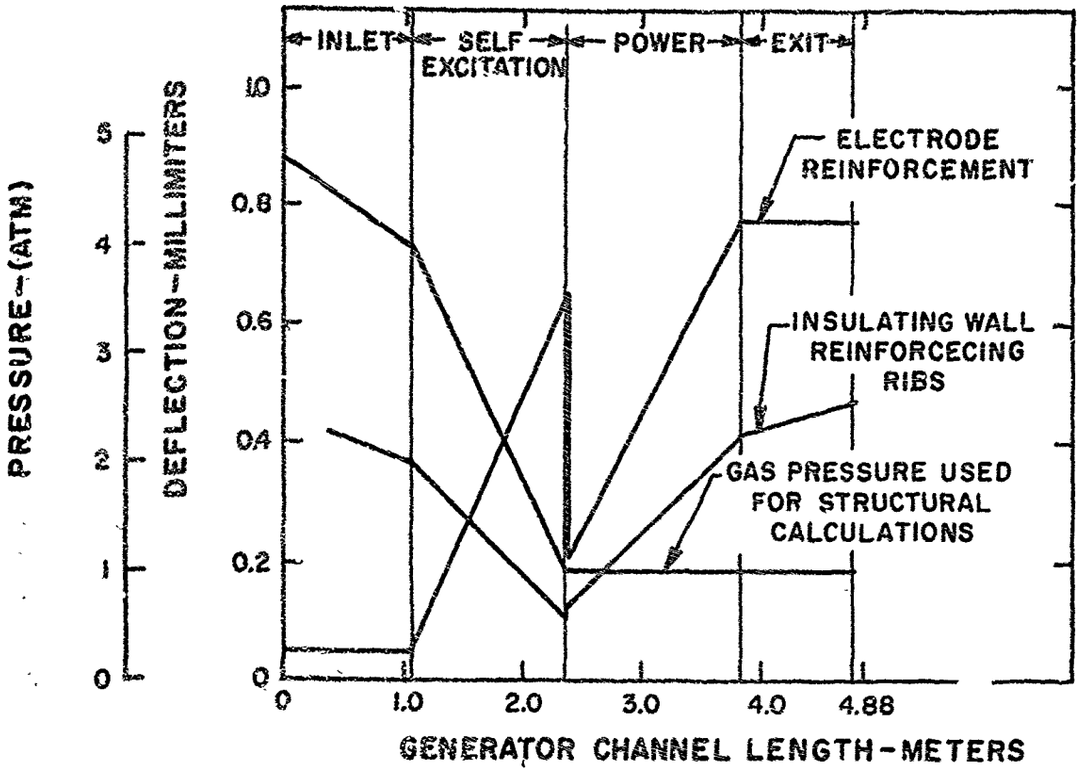

Figure II-D10 Channel Wall Deflections

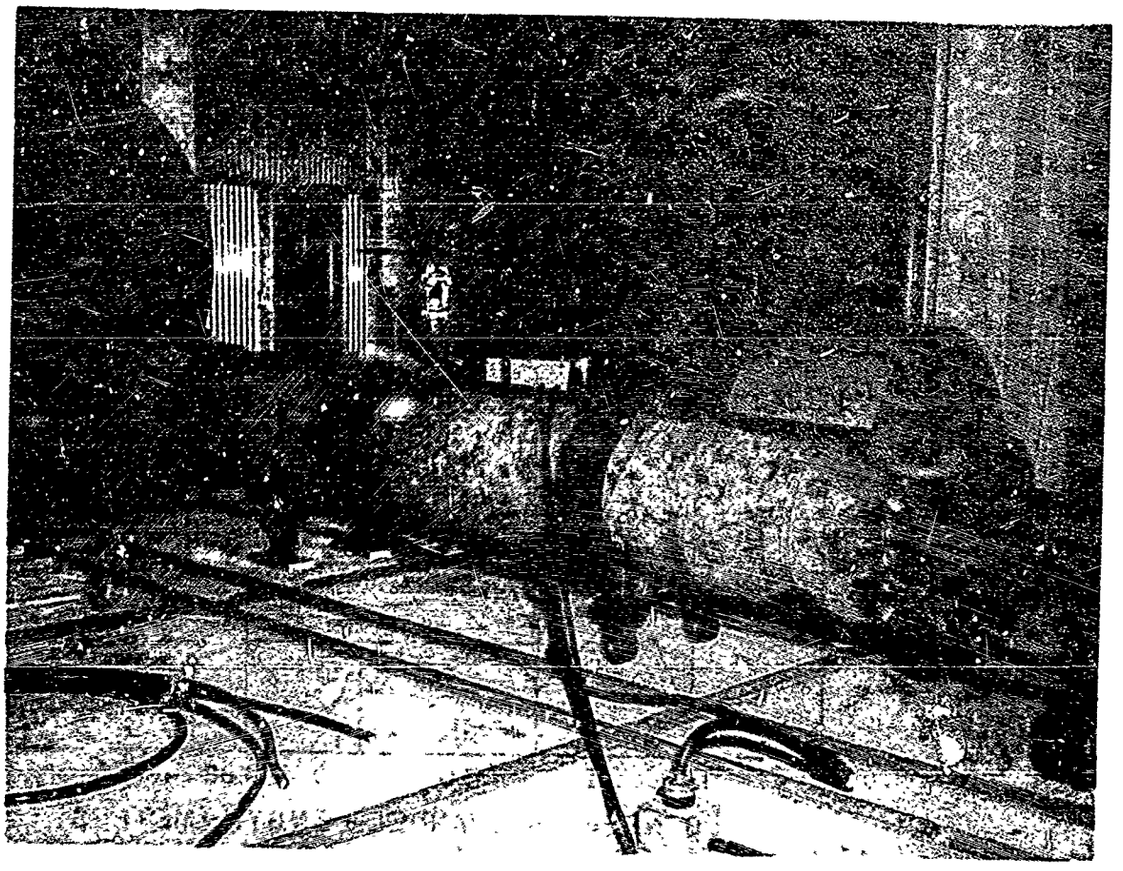

Figure II-D11 Dummy Channel

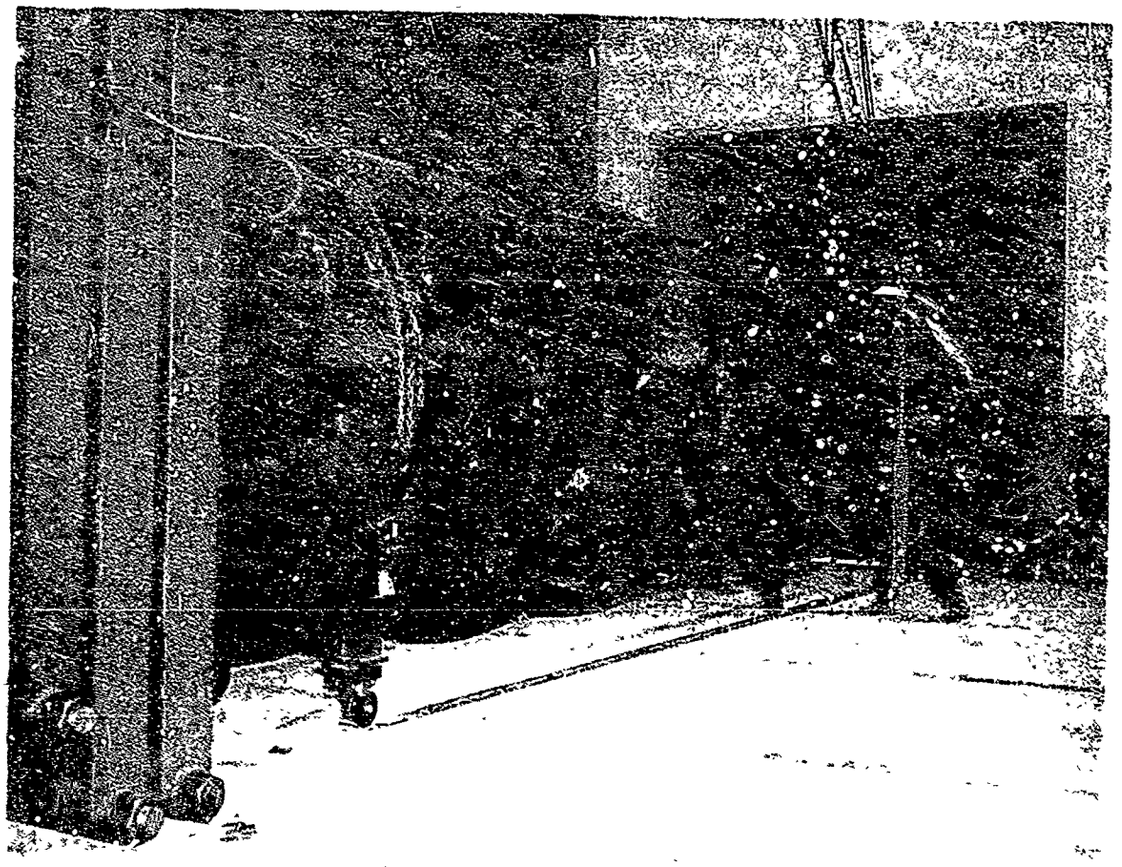

Figure II-D12 Exhaust Duct

E. AUXILIARY SYSTEMS DESIGN

1. General Arrangement

The generator itself consists of three essential items: burner, magnet and channel, which require the use of auxiliary systems to provide the necessary cooling water, fuels, and generator controls. The general arrangement of the equipment and systems may be seen in Figure II-E1.

The final design of these components is based on the parameters resulting from the design analysis and an intimate knowledge of the generator component requirements. These systems are, for the most part, designed to be as simple and inexpensive as possible and are fabricated from off-the-shelf items.

Their existence may be considered secondary to the major generator components; however, the opposite is true, as they are required to operate in such a manner as to insure proper operation of the generator, since the failure of these systems to perform their functions properly could result in serious damage to one or more of the major components. For this reason, they were designed with great care and special attention was paid to the effect of failure of one or more of these systems on the overall generator.

2. Burner Systems and Controls

Each auxiliary system basically consists of a storage and a control system. Bulk storage facilities for oxygen, fuel and water are located outside of and away from the test cell.

A suitable control system, consisting of regulating and shut-off valves, is employed to control the flow of each system and to permit orderly starting and stopping of combustion. A nitrogen system is utilized for the purpose of purging the burner and channel of combustibles, immediately before and after operation of the burner.

The design of the control system has been performed with certain basic principles in mind: the fuel and oxygen flow to the main burner must be accurately measured, since any variation in the total mass flow or fuel oxidizer ratio has an important effect on generator performance. The shut-off valves which control the flows to the burner must be located as close to the burner as possible, so as to minimize the volumes to be purged. These valves are remote controlled from the control room. The flow of gaseous fuel and oxidizers to the igniter and pilot burner is calibrated and set prior to operation.

The starting and stopping sequence used in all burners is based on AERL's experience with similar burners. The general description of the design and arrangement of each individual system and its control is as follows:

a. Water System

The water to be used for cooling purposes is stored in a 150,000-gallon concrete tank. It flows from the tank to a water pump. Then it is pumped at 10,000 gpm and 250 psig into the test cell. A schematic of the cooling water system may be seen in Figure II-E2. The flow is divided and 5000 gpm is allowed to cool the stainless steel tubes used as load resistors. The remaining 5000 gpm flows to the burner and channel where 2000 gpm are allowed for the burner and nozzle and 3000 gpm are allowed for the channel (2500 gpm design). All water is then discharged into the exhaust duct where some will be converted to steam and go off into the atmosphere and the rest will drain out of the duct to a drain basin outside the building.

b. Oxygen System

The gaseous oxygen storage consists of high pressure gas cylinders which are mounted in racks and manifolded together. The storage is designed for 430,000 scf at a pressure of 2200 psig.

During burner operation, oxygen from the outdoor storage enters the building as indicated in the Oxygen System Schematic shown in Figure II-E3. Oxygen for the main burner is throttled by valve 1 to about 100 to 400 psi depending on required mass flow. The flow rate is measured by the venturi, 4, and the valve, 1, is regulated from the control room to maintain the desired flow. A nitrogen purge connection, valve 3, permits purging the oxygen line, burner, and generator channel. Oxygen for the pilot and igniter flows through a branch line and manual shut-off valves 2 and 5 to a regulator, 6, which reduces the pressure to 500 psi. From the regulator, oxygen flows through the manual back-up valves, 7 and 9, through the solenoid valves, 8 and 10, to the igniter and pilot burners.

The oxygen venturi is designed to operate with critical flow (sonic velocity in the throat). Critical flow operation simplifies the instrumentation because it is only necessary to measure initial pressure and temperature. However, the oxygen storage system is small in relation to the quantity of gas removed during a full duration run, and a considerable drop in temperature occurs. In addition, a further temperature drop occurs at the throttle valve. In the worst case the oxygen temperature at the venturi throat can be as low as 112°K. At this temperature and at the pressures corresponding to 40 Kg/sec, there is considerable departure from ideal gas

laws. The oxygen venturi flow chart shown in Figure II-E4 was constructed from information obtained from a Bureau of Standards publication.

c. Nitrogen System

The gaseous nitrogen storage also consists of high pressure gas cylinders, mounted and manifolded in a similar manner as the oxygen. This storage is designed for 60,000 scf at a pressure of 2200 psig.

Nitrogen from the outdoor storage enters the building as shown in Figure II-E5 (a schematic of the nitrogen system), and flows through a main shut-off valve, 11, then to the main burner through valves 12 and 13. Valve 12 is a throttle for regulating nitrogen flow. Valve 13 is a fast-acting remote control valve which works simultaneously with a similar valve in the fuel line to switch from "purge" to "fuel" or vice versa. Nitrogen for purging fuel injectors of the igniter and pilot burners flows through valve 14 and regulator 15 to solenoid valves 17 and 19 at the burners. Valves 16 and 18 are manual back-up valves to be used in the event that a solenoid valve fails to operate. Valve 3 connects to the main oxygen line for purging of the main burner oxygen injectors.

d. Fuel System

The main ethyl alcohol storage has a capacity of 7500 gals. The alcohol is transferred from this tank to a 1500-gal. mixing tank located in a fuel room. The potassium hydroxide is added to the alcohol in the tank and the mixture is agitated by a propeller-type mixer until the potassium hydroxide is dissolved in the alcohol. The fuel is then pumped to the burner by an 8-stage centrifugal pump.

The fuel system is shown schematically in Figure II-E6. A three-way remote control valve, 7, is used to direct fuel flow either to the calibrating loop or the burner. The calibrating loop contains an orifice, 8, with hydraulic impedance equivalent to the burner fuel injectors. The sequence for starting the burner is to start the main fuel pump, 5, with the valve open to the calibrating loop, then adjust the bypass valve, 9, to produce the desired flow as indicated by the venturi, 6, and then divert the fuel flow by means of the three-way valve, 7, from the calibrating loop to the burner. If the calibrating orifice is truly equivalent to the burner injectors, the fuel flow to the burner should be correct.

In order to assure proper operation of the fuel system over the required flow range three sets of fuel injectors, fuel venturies and calibrating orifices are required. In sizing the fuel injectors, a minimum safe injection pressure drop was selected, and the injectors were sized for the required flow at this pressure. The maximum flow for any injector set is

limited by the pump pressure at that flow. Figure II-E7 is a fuel system performance curve which illustrates the flow characteristics of each injector set. The following example will illustrate the working of this chart. Suppose a flow of 250 gpm is required. The 250-gpm line intersects the medium size injector characteristic curve. Using the medium size injectors, the 250-gpm line intersects the dotted curve at 325 psig, which is the fuel injection pressure drop. The 250-gpm line intersects the solid curve at 410 psig, which will be the pump discharge pressure. At 410 psig, the total output of the pump is 525 gpm, of which 250 gpm will go to the burner and 275 gpm will be bypassed back to the fuel tank. If the oxygen-fuel mixture is stoichiometric, the corresponding burner chamber pressure will be 60 psig.

e. Pilot Burner

The fuel selected for use in the igniter and pilot burners is gaseous ethane which is stored in bottles as a liquid. The vapor pressure of ethane at room temperature is 525 psi and is suitable for direct injection into the igniter and pilot burners without the use of a pressure regulator. A schematic of the fuel system to the igniter and pilot burners is shown in Figure II-E8. Ethane therefore flows directly to solenoid valves 29 and 31 which operate in conjunction with nitrogen purge valves 17 and 19 to permit switching from "purge" to "fuel" or vice versa. Valves 28 and 30 are manual back-up valves in the control room to be used in the event of solenoid valve failure.

During operation 0.91 Kg/min of ethane must be evaporated in the bottles. The latent heat of vaporization is supplied by the heat capacity of the liquid ethane and the material in the bottle walls. To prevent an excessive drop in the temperature and the corresponding vapor pressure during a run, a minimum of 100 lbs. of ethane must be in the storage system.

Before burner testing was started, the need for nitrogen dilution in the pilot burner became apparent, and therefore a revised pilot burner control was designed. The modified control is shown in Figure II-E9. The two additional elements are the nitrogen solenoid valve, Item 2, and the mixing venturi, Item 4. The nitrogen valve, 2, opens simultaneously with the oxygen valve, 1. The mixing venturi proportions the nitrogen and oxygen flows. The mixing venturi contains two concentric entrance cones, one for each gas, and a single diffuser. The inner, or oxygen, cone is adjustable axially to permit varying the area of the outer, or nitrogen, cone. By suitable adjustment the desired degree of nitrogen dilution may be obtained.

A simplified pilot burner electrical circuit is shown in Figure II-E10. The igniter burner is an uncooled heat sink design with a running time of six seconds. The electrical circuit is designed to shut off the igniter combustion in six seconds and to shut off the pilot burner fuel and

oxygen valves if the pilot burner does not ignite within this time period. However, if the pilot burner is properly ignited, it will keep operating, and, due to its interlock with the main burner control, permit starting the main burner. Safety interlocks are provided as follows: the main burner shuts off if the pilot burner goes out or if the magnet current becomes excessive. Both pilot and main burners are shut down if the discharge pressure of the cooling water pump drops to a minimum allowable value.

In addition, pressure switches in the various burner cooling circuits cause the burner to shut off if the flow in any individual circuit becomes too low. An interconnection to the magnet battery circuit turns off the batteries in the event they are still connected when the burner is shut off.

The operating sequence is as follows: Assuming all pumps are started and proper pressures have been established to the control valves on the burner cart, the starting of the water pump closes PS3 supplying power to the whole circuit. The switches S_1 and S_2 are closed, which closes the contacts in the time delay relay and energizes T_1, C_1, C_2 and C_3. Of these solenoids the nitrogen valve is normally open and the fuel and oxygen valves are normally closed. Energizing these solenoids shuts off the nitrogen purge and turns on the fuel and oxygen. When the igniter chamber pressure builds up, the pressure switch PS1 closes, energizing the solenoids C_4, C_5 and C_6, thereby shutting off the nitrogen purge and starting oxygen and fuel flow in the pilot burner. When the pilot burner chamber pressure builds up, the pressure switch PS2 closes and the pilot burner solenoids remain energized. After five seconds, the time delay relay contacts open which stop the igniter burner and also switch the pilot burner valves to purge if the pilot burner has not started. In normal operation the closing of PS2 permits the starting of the main burner by means of C_7 and C_8 which are the solenoid valves which control the air actuators for the main burner nitrogen and fuel valves. Ordinarily, the solenoids C_7 and C_8 would not be energized until oxygen flow to the main burner had been established, as explained previously.

Safety interlocks operate in the following manner; low water pressure opens PS3 which shuts off all burners. Loss of pilot chamber pressure or overexcitation of the magnet shuts off the main burner by opening PS2 or R2, respectively.

f. Burner Control System

All of the remote control valves and pressure switches for the burner control are mounted on a heavy steel plate on the back of the burner cart as shown in Figure II-E11. This picture was taken before all tube and pipe connections were completed, but is reproduced here to show more clearly the construction. On the right is the oxygen pipe. The two large valves in the center are the fuel 3-way valve and the nitrogen purge valve.

The panel below these valves has all the solenoid valves and pressure switches. The panel was made deliberately heavy to provide some degree of magnetic shielding for the solenoid valves. The one solenoid valve which must function reliably at maximum field strength is the valve which controls the fuel valve air cylinder. An air operated override device has been made which will actuate this valve even if the solenoid fails.

The generator is operated from the control room by four people at individual panels as shown in Figure II-E12. Starting from the right, the first panel contains the pump controls, the fuel bypass valve and gauges indicating fuel and water pressures. The next panel contains regulators, valves, switches and gauges for operating the pilot burner. The third panel contains controls for the magnet circuit and main burner operation. The panel on the left is for measuring and controlling oxygen flow to the main burner.

Figure II-E13 shows the main oxygen control valve. The requirements for this valve are most stringent since it must maintain a desired flow rate without fluctuations, with a large but varying pressure differential and also provide a tight shutoff. The large air operated toggle actuator is controlled by a loading regulator in the control room. The loading pressure is controlled manually to maintain an oxygen flow as indicated by the oxygen venturi.

3. Magnet Control

Initial excitation of the magnet is provided by a battery bank which consists of 180 storage batteries. The battery bank, when fully connected, is capable of producing 1.1 Mw for a period of 45 seconds. The batteries are arranged in six parallel strings of 30 batteries in series. This array will produce 360 volts open circuit and 6000 amps at matched impedance. In addition, 10 batteries of each string may be disconnected, reducing the open circuit voltage to 240. The strings are connected through switches and shunts to bus bars. A 20 kw motor generator set with suitable circuitry is provided to recharge the batteries. Power from the batteries to the magnet is controlled by a circuit breaker which may be actuated from the generator control room. During normal startups, the breaker is opened by a low current detector when the generator excitation section is powering the magnet. In the connection between the generator channel and the magnet, there is a shunt to measure current and to actuate the over-excitation relay to stop the burner before the magnet becomes damaged from excessive field strength. The magnet shorting loop, which protects the magnet from excessive voltage during shut down, contains 88 silicon rectifiers, arranged such that there are 44 parallel circuits of two rectifiers in series, to provide a peak inverse voltage rating of 1200. Parallel bleed resistors and series resistors provide for proper distribution of voltage and current, respectively, between the 88 rectifiers. Figure II-E14 shows a schematic circuit diagram of the magnet control and exciter.

In practice the initial excitation current can be set between 2500 and 6000 amps by selecting the appropriate number of strings and voltages. The circuit breaker can safely interrupt the maximum current of 6000 amps because the rectifier circuit prevents the buildup of high voltages.

4. Load Resistors

Sizing of the load resistors was performed using the voltage-power characteristics obtained from the final generator design program. As previously reported, the number of electrode pairs is 50 in the net power output section. These, together with the possible nine additional electrode pairs in the end of the self-excitation section, require 59 separate load resistors. Due to the required flexibility of the loading while performing the test program for the Mark V generator, the load resistors have been designed to dissipate as much as 35 Mw.

The final load resistor design consists of 1000 stainless steel tubes requiring a total cooling water flow of 5000 gpm for the maximum power dissipation. The load resistors are water-cooled stainless steel tubes. The material for all tubes was fixed as Type 316 S.S., as this material has the highest resistivity of any standard commercially available material, giving the highest resistance and shortest length of tube for any fixed diameter and wall thickness. Needless to say, it is impossible that the requirements for any two sets of load resistors be exactly the same. To not end up with 59 completely different sets of resistors and flow controls for these resistors, it was attempted to standardize the system as much as possible. Having fixed the material, it was then possible to fix the tube diameter into various sizes for certain groups of load resistors. Through a process of elimination, it was then possible to fix the tube size to three different diameters and one standard length.

To provide the simplest design for the lowest costs, many items were standardized. The tubes were standardized by making them all 5.12 meters long. The tube outside diameters are 7.95 mm (500 tubes), 9.55 mm (485 tubes) and 15.9 mm (15 tubes for special load in section of channel where divergence changes). Cooling water flow control was simplified by designing the cooling requirements such that the tubes are grouped in four sets of cooling water manifolds with 250 tubes between each set and one valve controlling the water flow through each set of 250 tubes. The stainless steel resistor tubes are assembled vertically with a water inlet manifold on the bottom and a water outlet manifold on the top.

The tubes are connected to the inlet and outlet manifolds by a standard short length of electrically non-conductive hose. The pressure seal for the hose is affected by use of a standard hose adapter on the manifolds and standard hose clamps on the tubes. The flow control valves are located on the discharge end of the outlet manifolds. The water flow through the tubes is in parallel; the electrical current flow through the tubes is in

series. By having the distance between each tube constant it was possible to design a standard electrical jumper clamp. With this arrangement each tube in a set of 250 receives approximately the same water flow and therefore the flow through each tube has approximately the same pressure drop. This design is made possible only through a sacrifice in the overall efficiency of the heat transfer capabilities for the tubes. The results of bulk temperature rise calculations show differences of as much as 22.2°C from tubes receiving the same water flow.

Due to the voltage distribution in net power output section and the associated Hall potential, a total potential difference in the load resistor bank of approximately 3000 volts exists, as can be seen in Figure II-E1. It was therefore necessary to electrically insulate each cooling water inlet and outlet manifold from one another and from ground. The insulation is furnished by the electrically non-conductive hose and phenolic insulation as indicated in Figure II-E15.

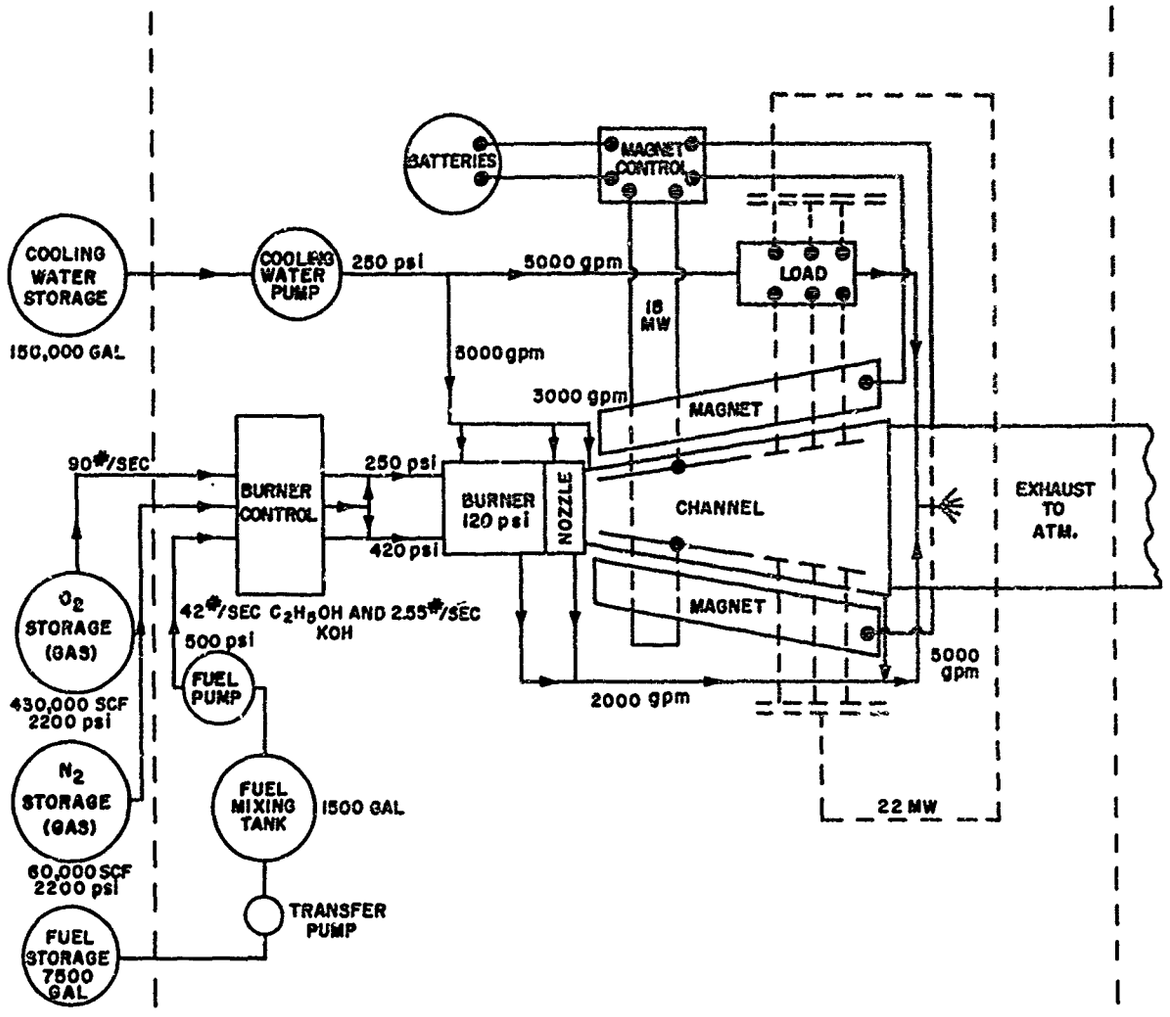

Figure II-E1 General Arrangement of Equipment and Systems for Mark V Generator

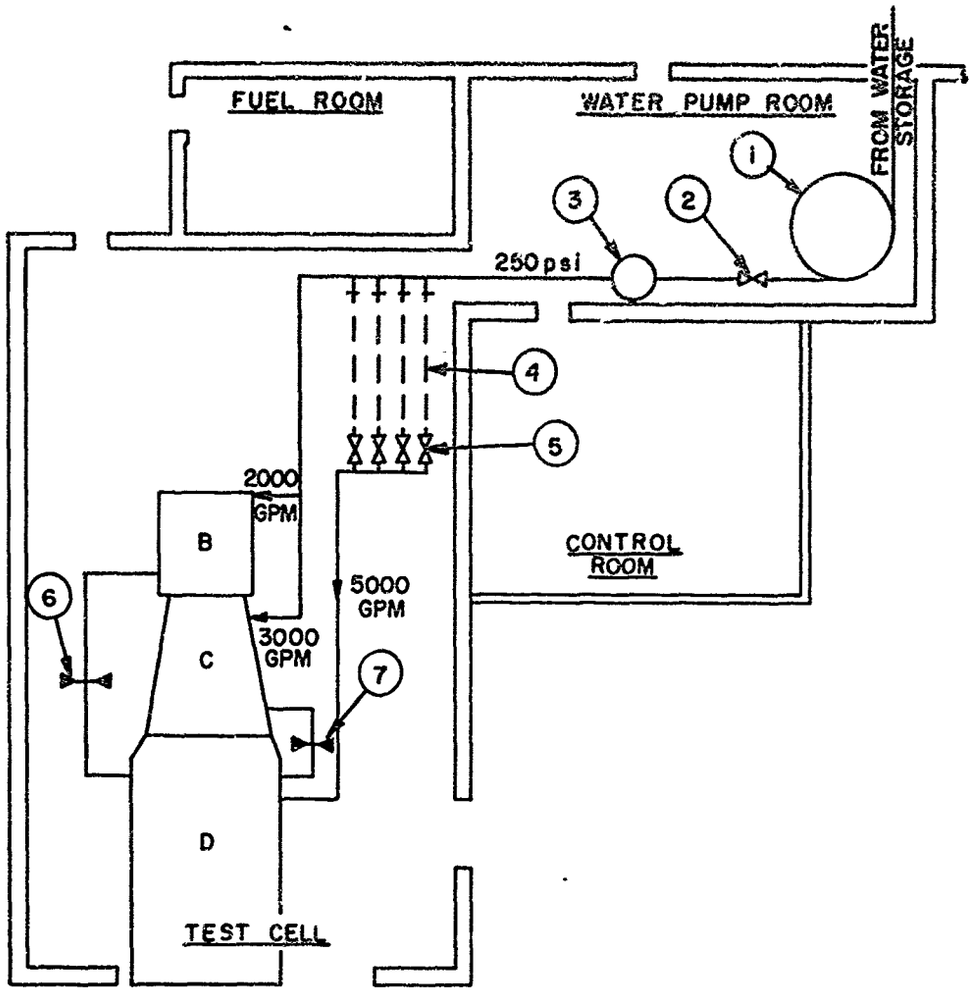

B = Burner

C = Channel

D = Exhaust Duct

1 Cooling water pump

2 Main cooling water shut-off valve

3 Strainer

4 Load resistors

5 Control valves for load resistor cooling water

6 Burner cooling water restriction orifices

7 Channel cooling water restriction orifices

Figure II-E2 Cooling Water System Schematic for Mark V Generator

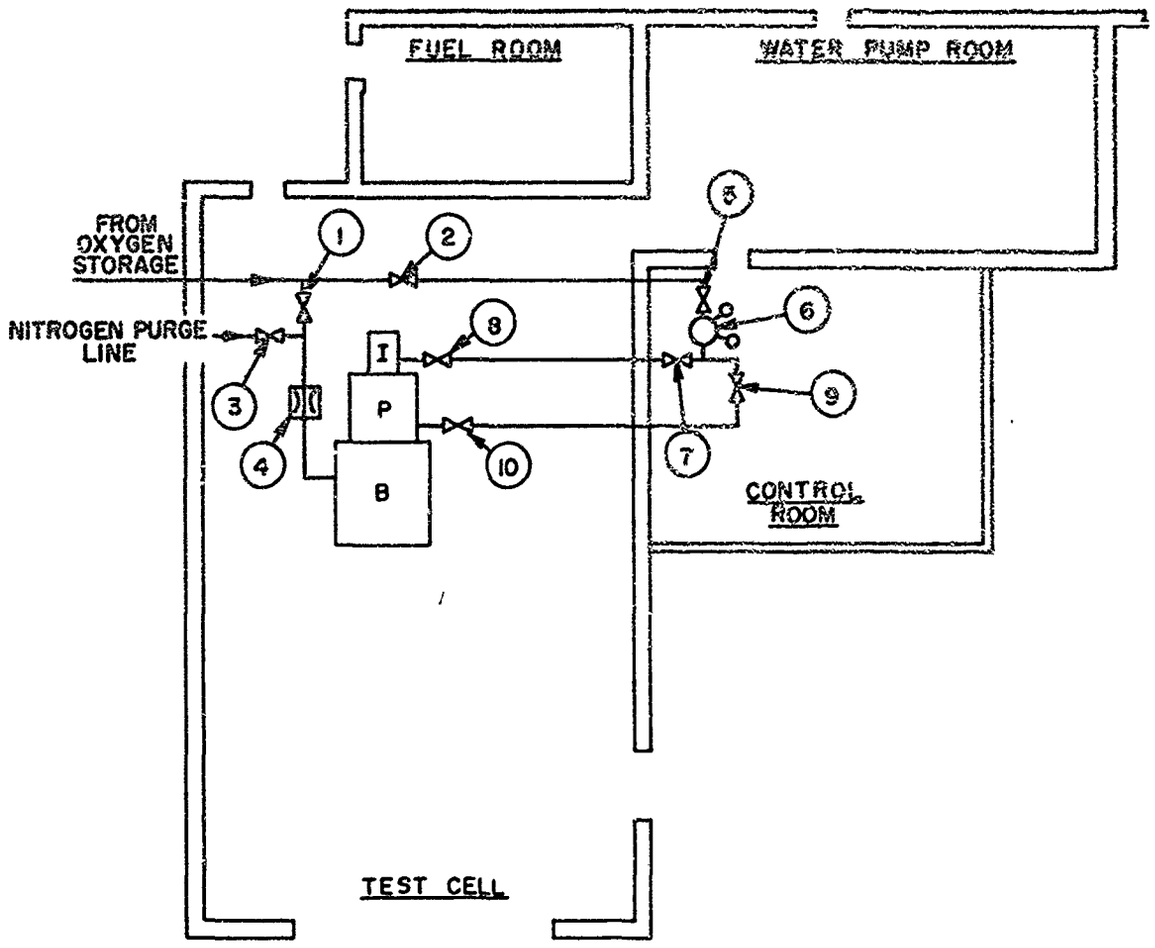

I = Igniter Burner

P = Pilot Burner

B = Main Burner

1 Main oxygen control valve and shut-off (remote controlled)

2 Auxiliary oxygen shut-off valve

3 Nitrogen purge valve for oxygen line, burner, channel, and exhaust stack (manual control)

4 Oxygen venturi

5 Main oxygen shut-off for igniter and pilot burners (manual control)

6 Oxygen regulator for pilot and igniter burners

7 Oxygen shut-off valve for igniter burner (manual control)

8 Oxygen valve for igniter burner (remote controlled)

9 Oxygen shut-off valve for pilot burner (manual control)

10 Oxygen valve for pilot burner (remote controlled)

Figure II-E3 Oxygen System Schematic for Mark V Generator

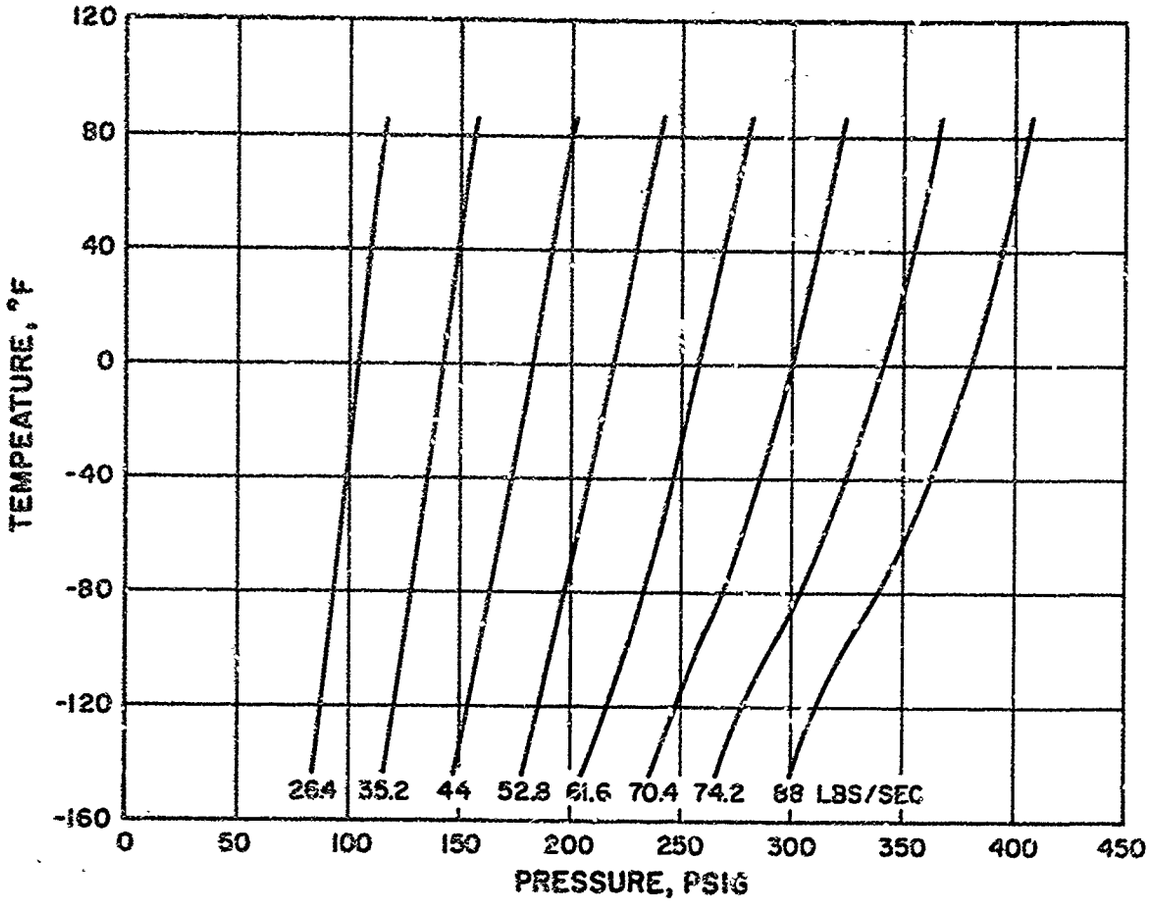

Figure II-E4 Oxygen Venturi Flow Versus P_1 and T_1

A1408

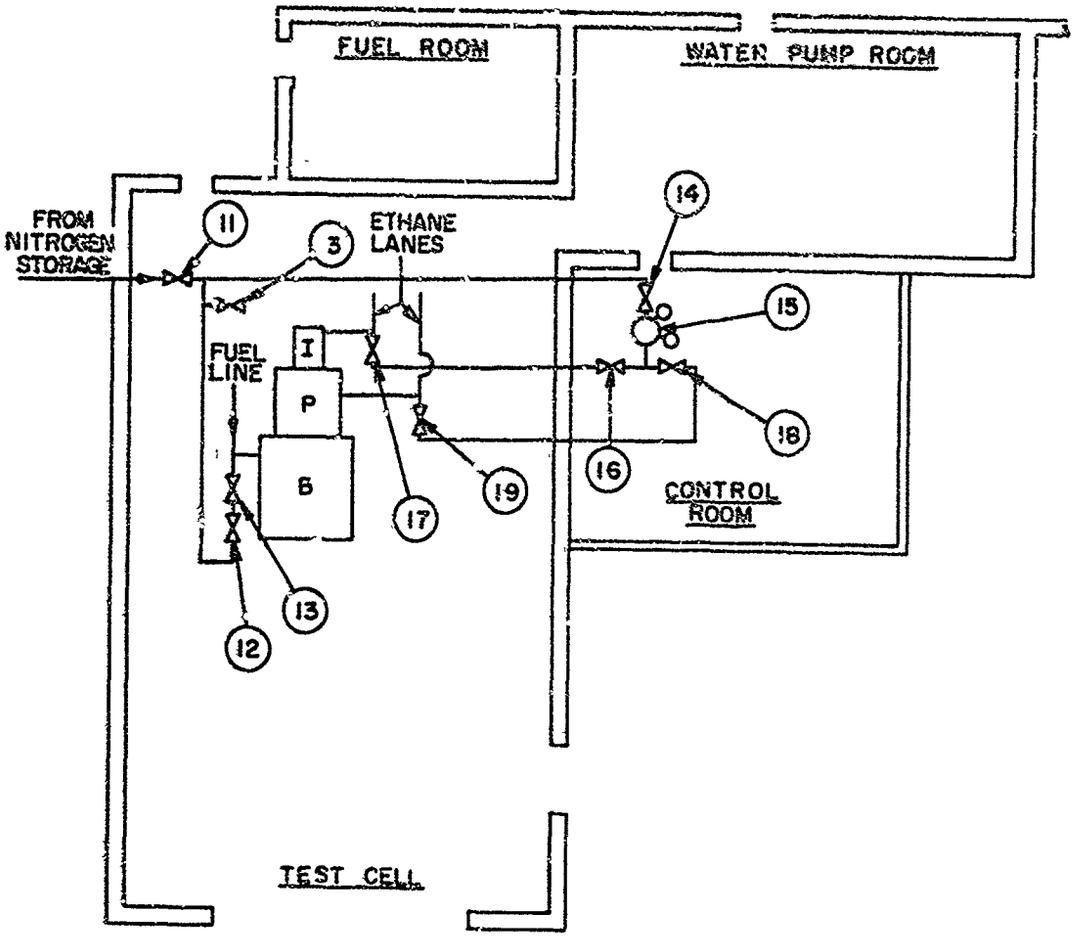

I = Igniter Burner

P = Pilot Burner

B = Main Burner

3 Nitrogen purge valve for oxygen line, burner, channel, and exhaust stack (manual control)

11 Main nitrogen shut-off valve (manual control)

12 Nitrogen throttle valve for main fuel system purge (manual control)

13 Nitrogen purge valve for main fuel system (remote controlled)

14 Nitrogen purge shut-off valve for igniter and pilot burners (manual control)

15 Nitrogen regulator for igniter and pilot burners

16 Nitrogen shut-off valve for igniter burner (manual control)

17 Nitrogen purge valve for igniter burner (remote controlled)

18 Nitrogen shut-off valve for pilot burner (manual control)

19 Nitrogen purge valve for pilot burner (remote controlled)

Figure II-E5 Nitrogen System Schematic for Mark V Generator

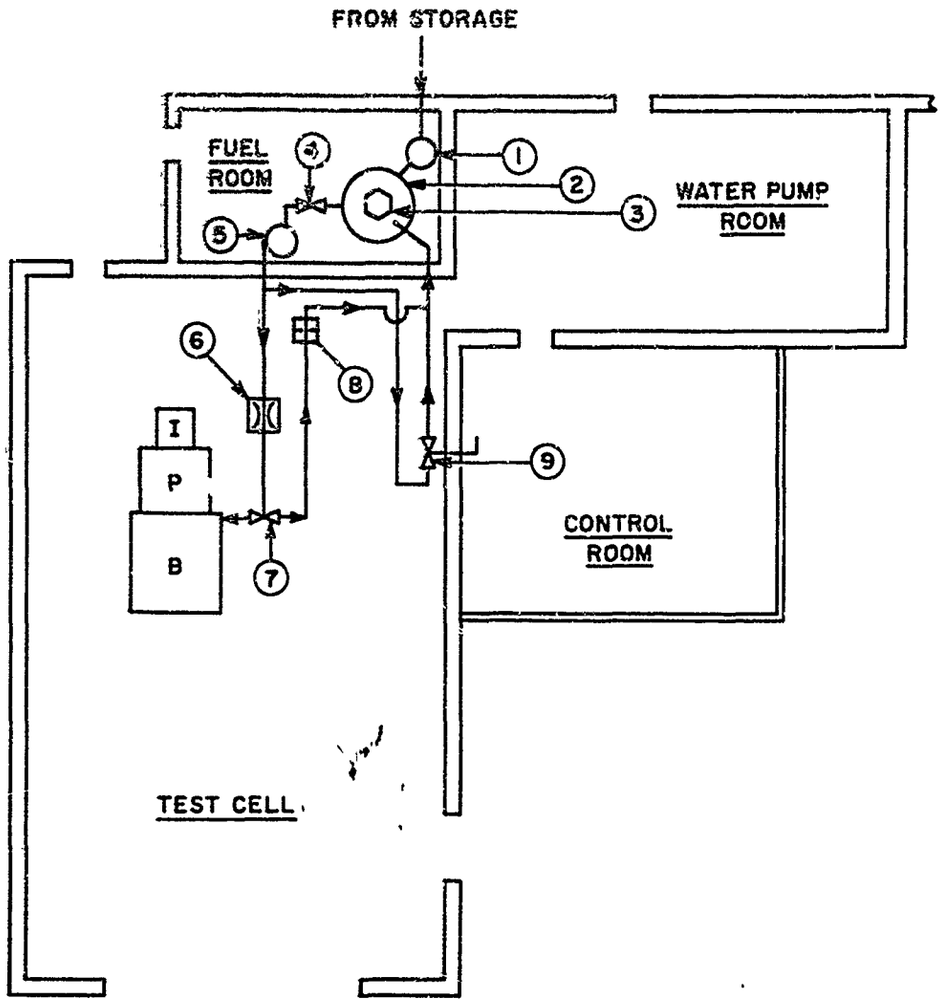

1 Transfer Pump
2 Fuel Tank
3 Mixer
4 Main Fuel Shut-off Valve (manual control)
5 Fuel Pump
6 Fuel Venturi
7 Three-Way Fuel Valve (remote control)
8 Restriction Orifice
9 Fuel By-Pass Valve (manual control)

Figure II-E6 Main Fuel System Schematic

A1604

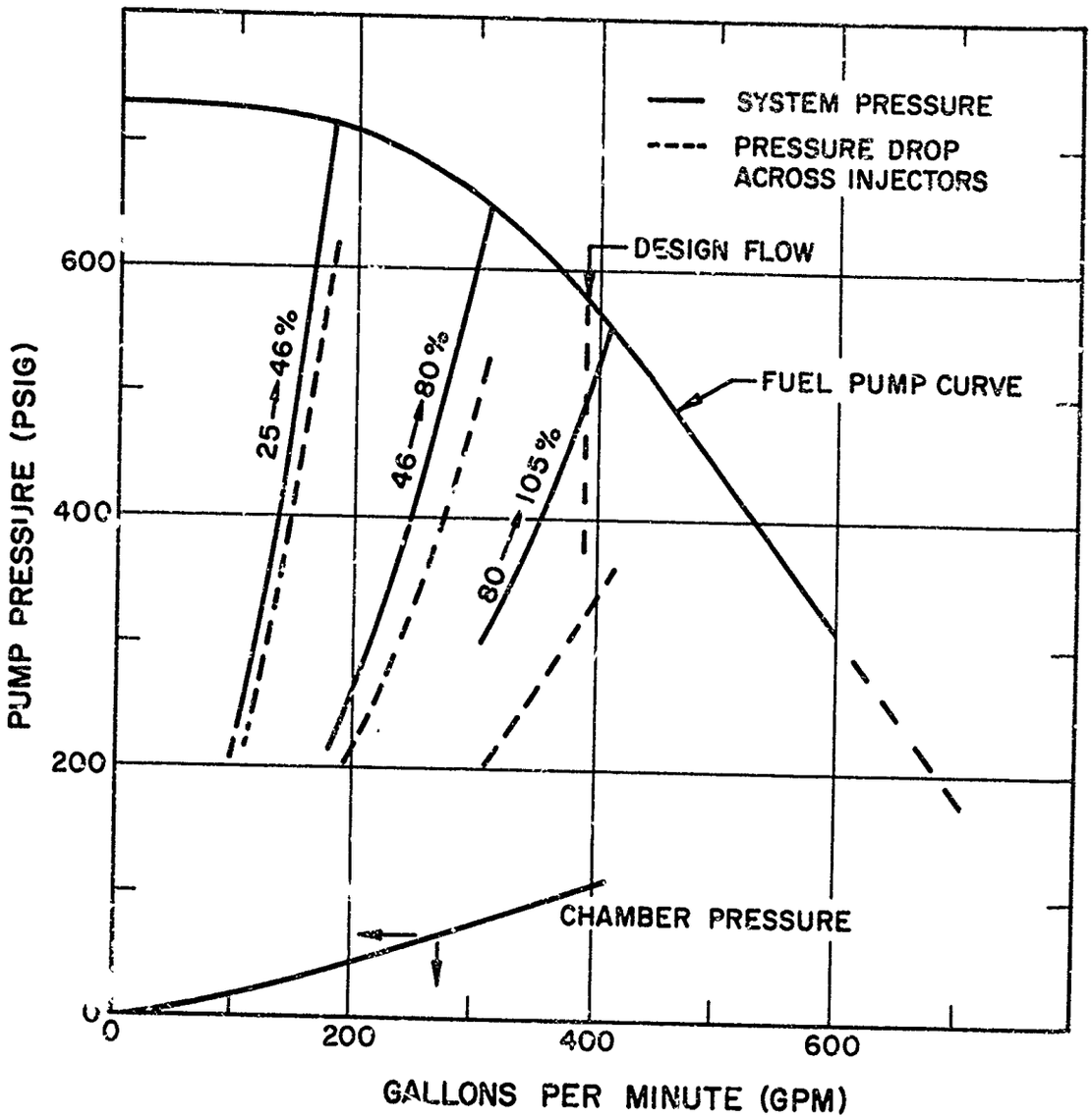

Figure II-E7 Fuel System Characteristics for the Mark V Generator

A1455

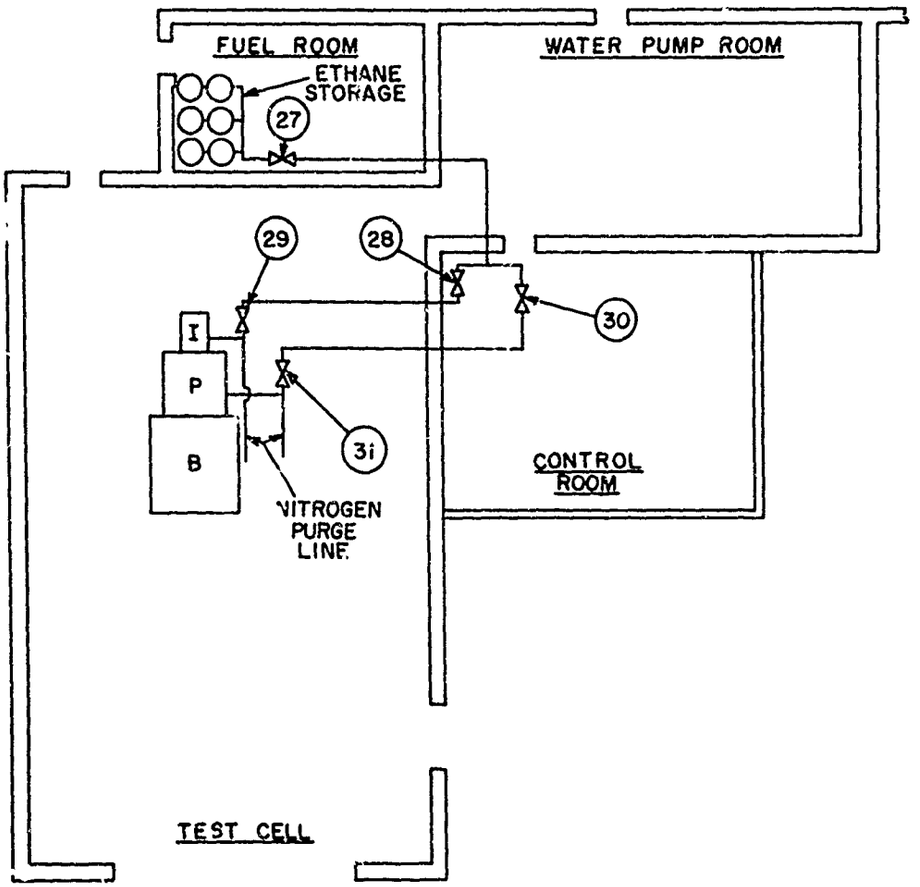

I = Igniter Burner

P = Pilot Burner

B = Main Burner

27 Main ethane shut-off valve (manual control)

28 Ethane shut-off valve for igniter burner (manual control)

29 Ethane valve for igniter burner (remote controlled)

30 Ethane shut-off valve for pilot burner (manual control)

31 Ethane valve for pilot burner (remote controlled)

Figure II-E8 Fuel System Schematic of Igniter and Pilot Burners

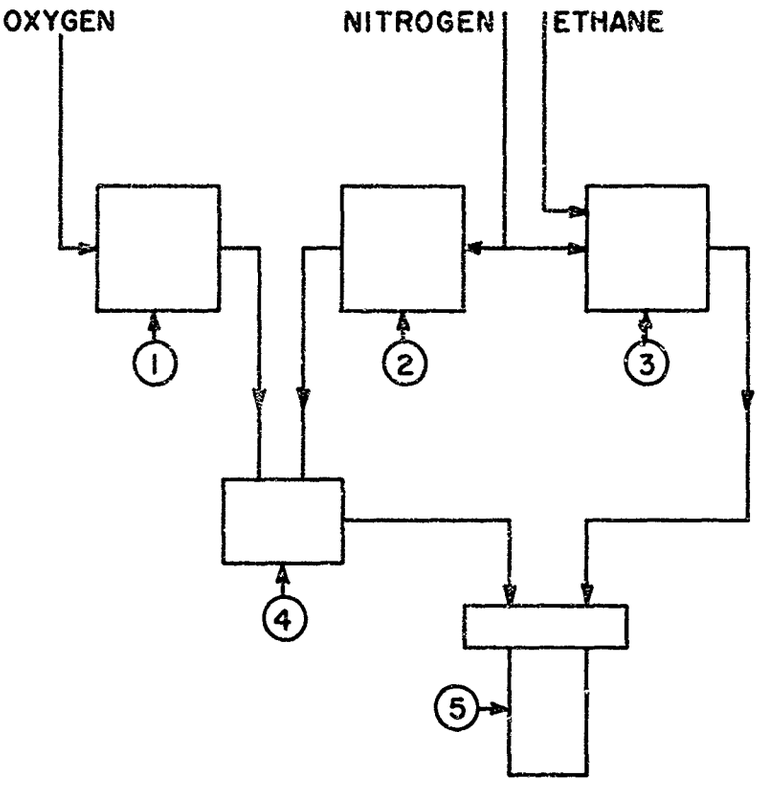

1. OXYGEN SOLENOID VALVE
2. NITROGEN SOLENOID VALVE
3. NITROGEN-ETHANE THREE-WAY SOLENOID VALVE
4. MIXING VENTURI
5. PILOT BURNER

Figure II-E9 Revised Pilot Burner Control System

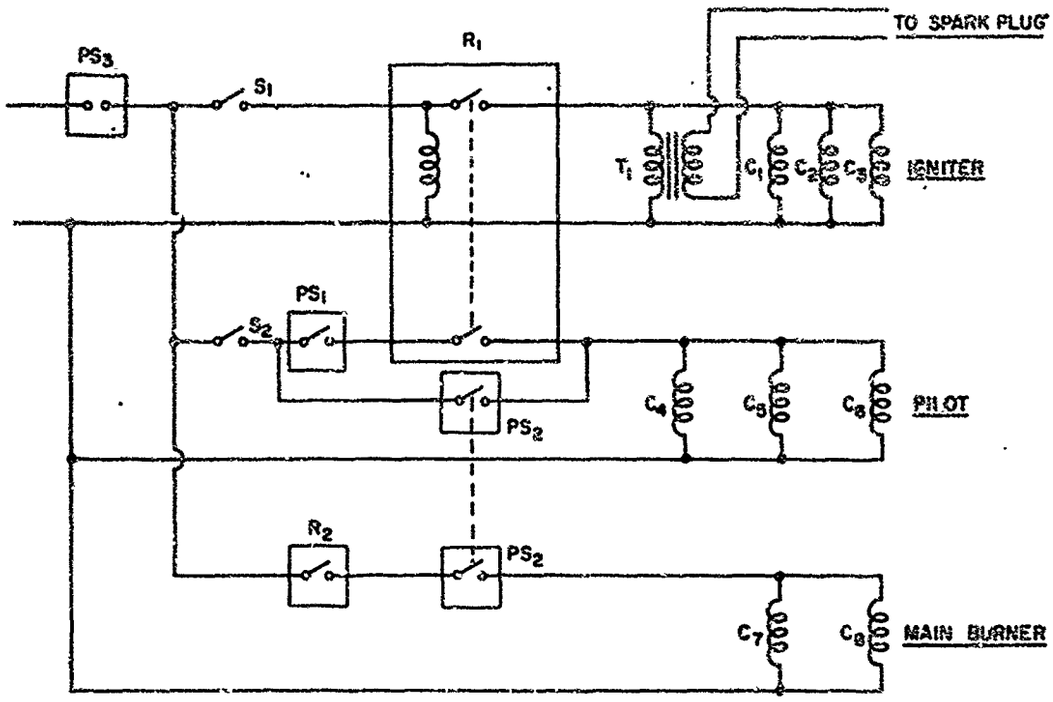

S_1	Igniter manual switch
S_2	Pilot manual switch
R_1	Time delay relay
R_2	Magnet overexcitation cut-off relay
PS_1	Pressure switch, Igniter chamber
PS_2	Pressure switch, Pilot chamber
PS_3	Pressure switch, low water pressure cut-off
T_1	Ignition transformer
C_1, C_2, C_3	Solenoid valves for Igniter, N_2, O_2 and Ethane
C_4, C_5, C_6	Solenoid valves for Pilot, N_2, O_2 and Ethane
C_7, C_8	Solenoid valves for air operated valves, Main Burner, N_2 and alcohol

Figure II-E10 Pilot Burner Control, Electrical Layout

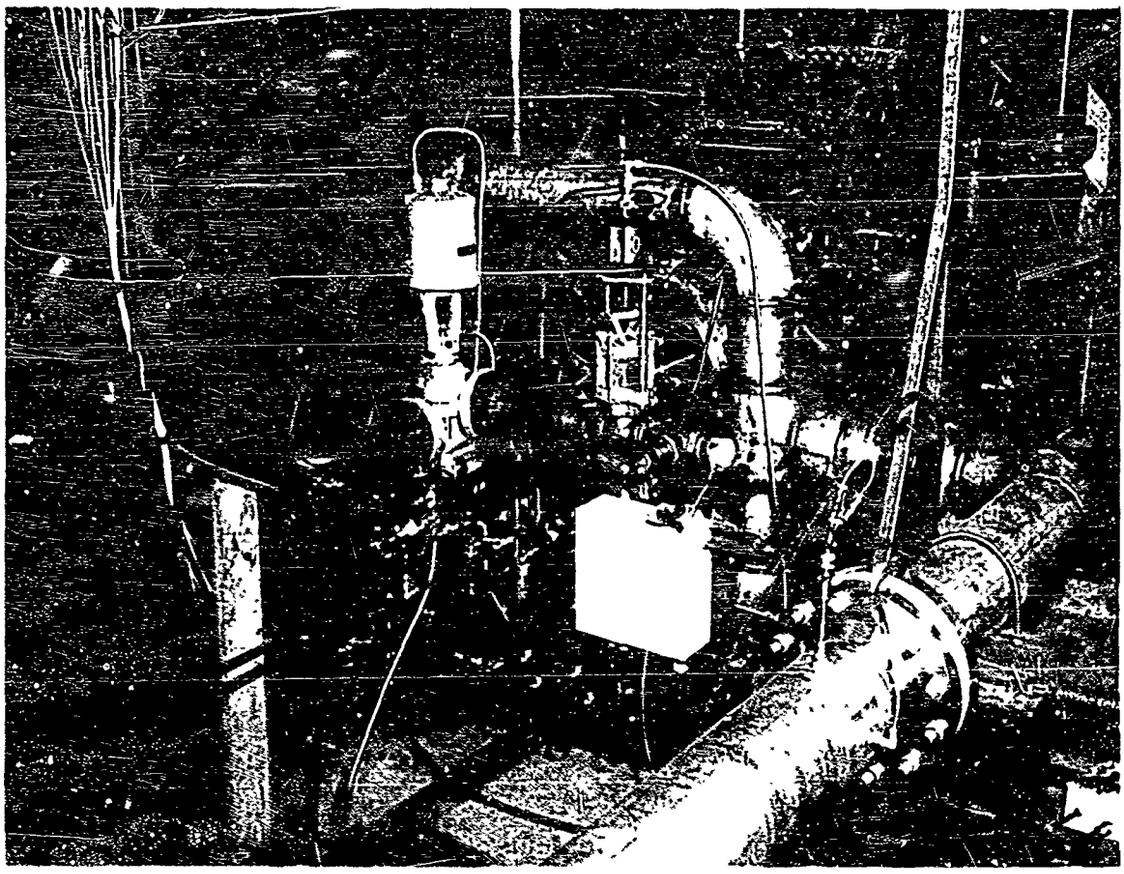

Figure II-E11 Remote Control Valves and Pressure Switches for Burner Control

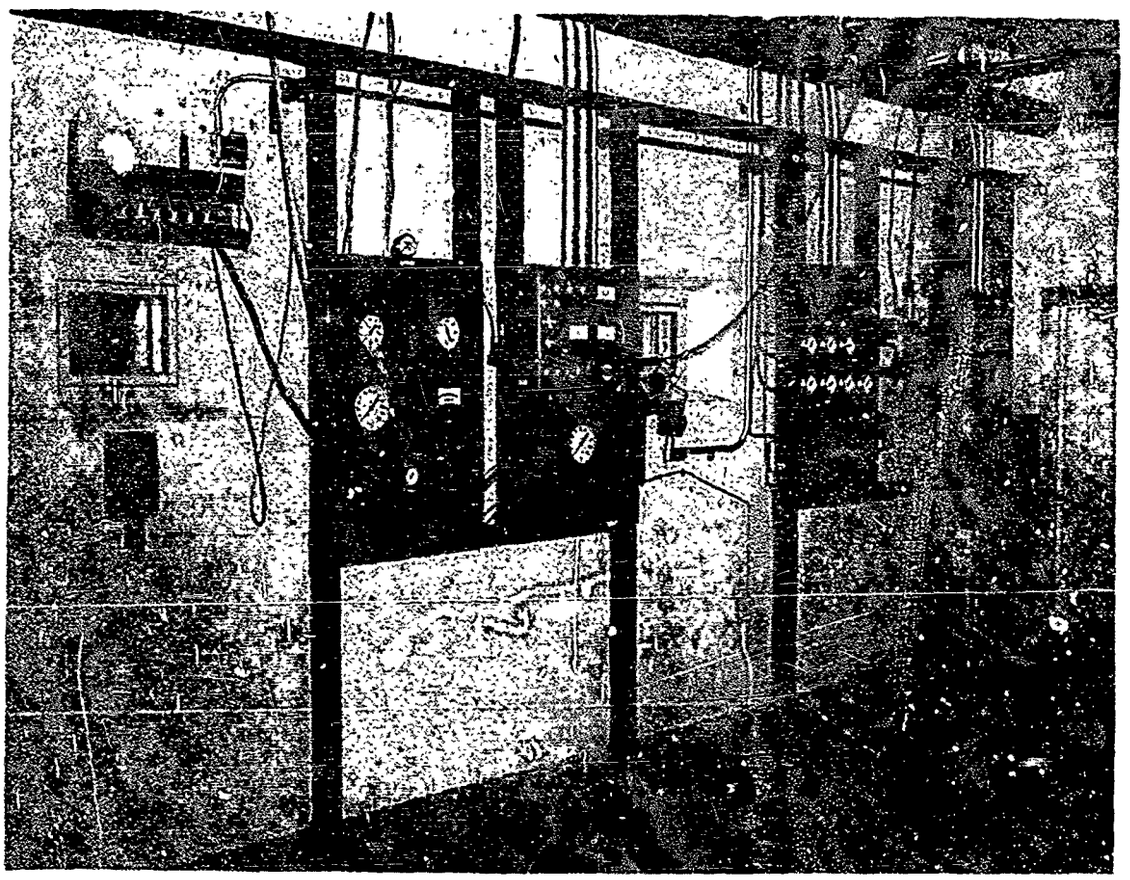

Figure II-E12 Completed Mark V Generator Control Panels

A1417X

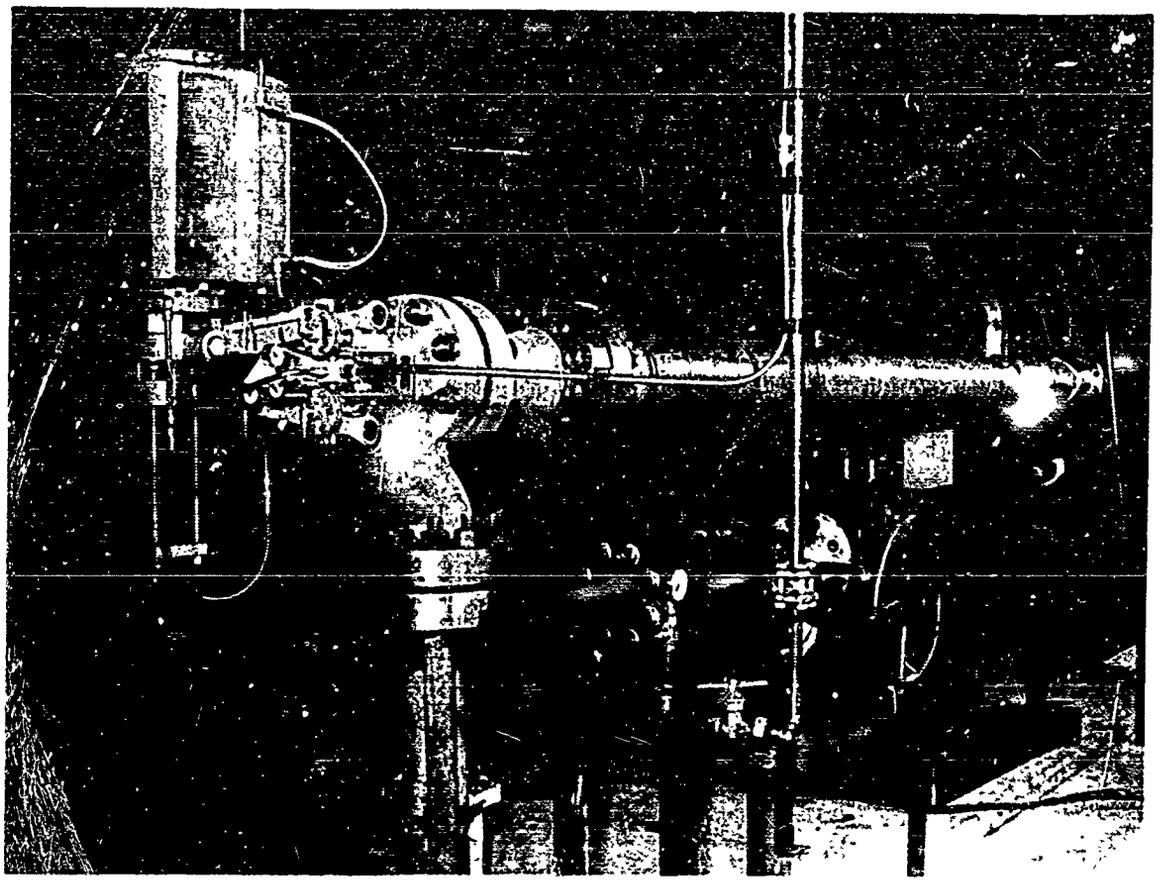

Figure II-E13 Main Oxygen and Nitrogen Control Valves

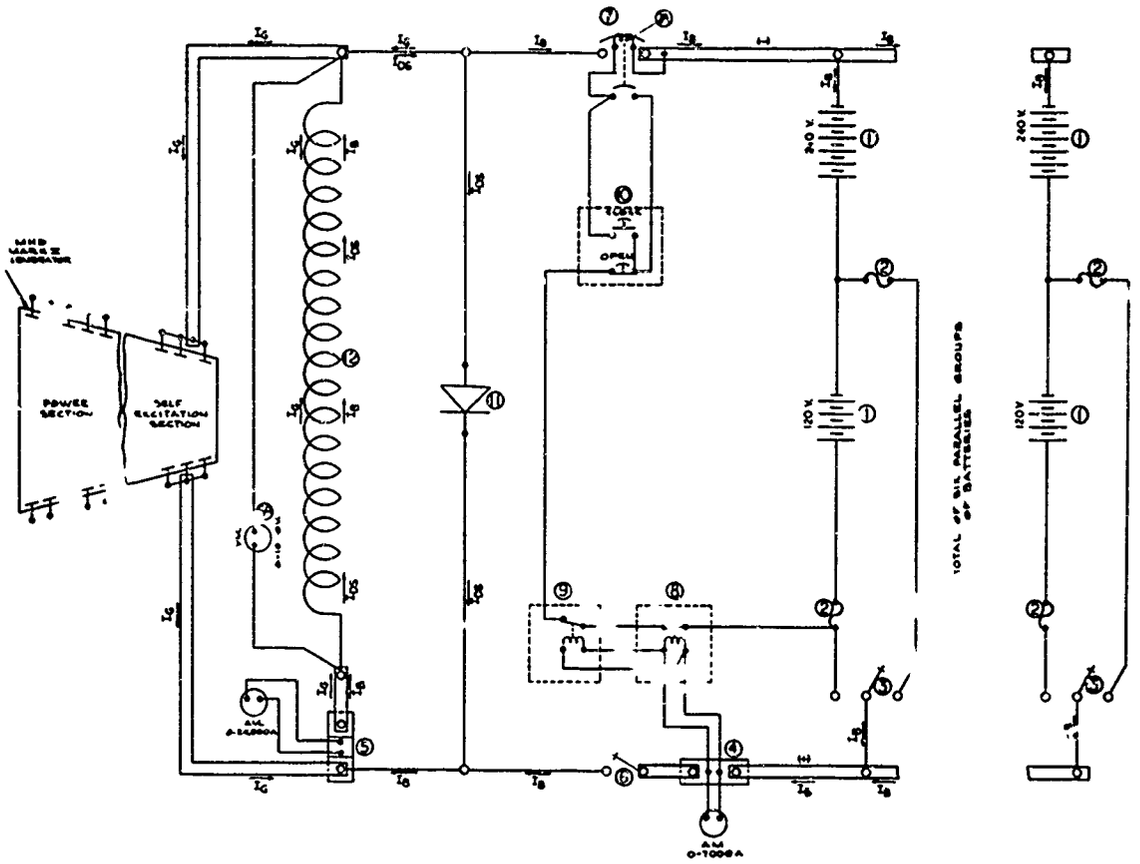

1. D.C BATTERY POWER SUPPLY FOR SEPERATE EXCITATION OF FIELD MAGNET, TO GIVE INITIAL GENERATOR OUTPUT TO SUSTAIN SELF EXCITATION OF GENERATOR.
   (FIELD MAGNET HAS NOT ENOUGH RESIDUAL MAGNETISM TO SUSTAIN SELF EXCITATION)
2. FUSES FOR SHORT CIRCUIT AND REVERSE CURRENT PROTECTION OF D.C BATTERY POWER SUPPLY.
3. BATTERY VOLTAGE SELECTOR SWITCHES FOR SEPERATE EXCITATION.
4. D.C SHUNT FOR MEASURING BATTERY OUTPUT CURRENT.
5. D.C SHUNT FOR MEASURING INPUT CURRENT TO FIELD MAGNET FROM EITHER THE BATTERY CIRCUIT OR GENERATOR CIRCUIT.
5A. D.C VOLTMETER FOR MEASURING FIELD MAGNET VOLTAGE.
6. KNIFE SWITCH FOR ISOLATING BATTERY CIRCUIT FROM FIELD MAGNET.
7. D.C CIRCUIT BREAKER.
7A. D.C CIRCUIT BREAKER REVERSE CURRENT TRIP COIL (OPENS CIRCUIT BREAKER ON 500 AMPS OF REVERSE CURRENT).
8. CURRENT SENSING SAFETY DEVICE FOR AUTOMATICALLY OPENING CIRCUIT BREAKER AT SELF EXCITATION TAKE OVER POINT (OPERATES ON LOW FORWARD CURRENT, ADJUSTABLE FROM 100 A TO 1,000 A).
9. CURRENT SENSING SAFETY DEVICE FOR AUTOMATICALLY OPENING CIRCUIT BREAKER ON REVERSE CURRENT FROM GENERATOR AT SELF EXCITATION TAKE OVER POINT.
   (OPERATES AT 50 AMPS OF REVERSE CURRENT)
10. PUSH BUTTON STATION FOR CONTROL OF BATTERY POWER.
11. FIELD DISCHARGING RECTIFIER (FREE WHEELING) [CONSISTS OF 88 RECTIFIERS IN SERIES AND 44 PARELLEL EACH RATED 250 A@600 V PRV.]
12. FIELD MAGNET.

I_B CURRENT FLOW OF BATTERY POWER SUPPLY
I_G CURRENT FLOW OF GENERATOR
I_{DS} DISCHARGE CURRENT FLOW THROUGH RECTIFIER UPON COLLAPSING OF THE FIELD FOR SELF DISCHARGING.

Figure II-E14 Schematic of Magnet Control and Exciter Circuit

A1413

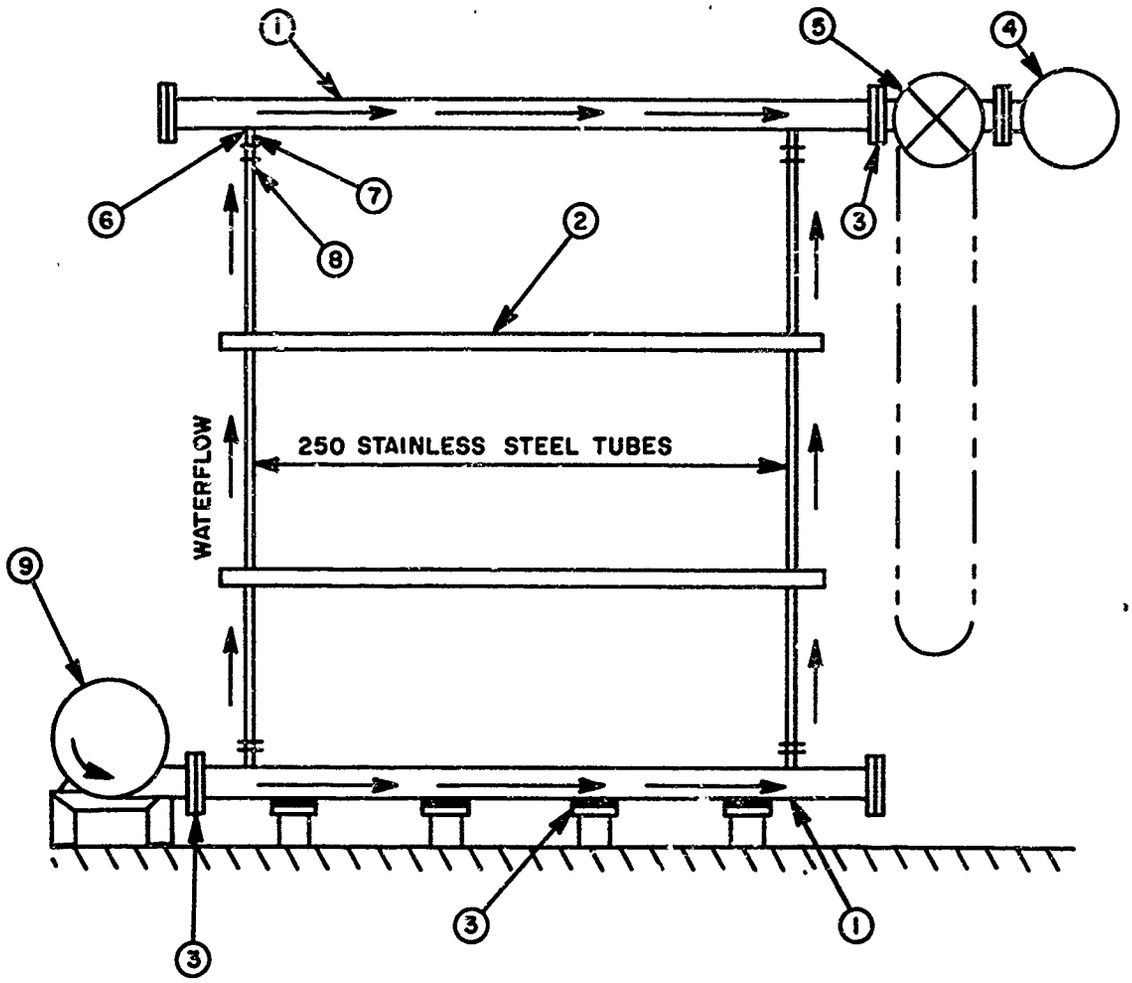

1 Manifold
2 Tube supports
3 Phenolic insulation
4 Discharge header
5 Control valve
6 Hose adapters
7 Insulating hose
8 Hose clamps
9 Inlet header

Figure II-E15 Mark V Generator Load Resistor Schematic

F. INSTRUMENTATION

Instrumentation for the Mark V MHD Generator may be broken down into four sections: Channel monitoring, power monitoring, magnet control and burner operating control instrumentation.

1. Channel Monitoring Instrumentation

Figu[illegible]s a sketch showing the location of the various channel measure[illegible] taken.

Pres[illegible] have been placed to measure both axial and transverse gas pre[illegible]stribution across one insulating wall. Eighteen centerline taps have b[illegible] installed along with four transverse taps located in three positions in the power section of the channel. The four transverse taps, together with a centerline tap, provide a five-point distribution as indicated in Figure II-F1.

Provisions were made to measure the bulk water temperature for a single water passage in one insulating and one electrode wall. Twelve thermocouples are used in each wall, having a distribution as indicated in Figure II-F1. It was later decided, however, that these temperatures would not be measured in the initial phase of the test program. Channel cooling water temperature rise was to be measured only to verify design calculations. Since the channel heat flux is the greatest when operated in the unloaded condition, and since the cooling system was adequate for this situation, it follows that the cooling was satisfactory for power generation runs. Previous experience with MHD generator channels allows extrapolation of heat flux values with a fair degree of accuracy. In addition, thermocouple measurements are difficult to take to any degree of accuracy while a magnetic field is present.

Originally, a transverse voltage distribution was to be taken at three locations in the channel as shown in Figure II-F1. Nine points are taken for each of the three locations. This measurement was later expanded to acquire a more extensive knowledge of electrical phenomena occurring at generator startup.

Six Hall voltages are measured between electrodes as indicated in Figure II-F1. Another Hall voltage is taken from the exhaust duct and two total Hall voltage readings taken, one at the end of the power section and one at the exit of the channel.

Additional instrumentation was used to verify calculated stresses and strains when the channel was subjected to loading. Strain gauges were placed on the plastic walls and steel reinforcing bars, while linear

variable differential transformers were used to measure any outward wall deflections. These readings were taken during static pressure leak checks of the channel.

2. Power Monitoring Instrumentation

To obtain the net power output of the generator, the current flow through 20 sets of load resistors is measured. This is approximately every third electrode in the channel. The current flow through the loads is obtained using a calibrated section of the stainless steel tube in each load as a shunt. The calibrating device was specially designed for the application and is adjustable for a limited shunt range on the tube.

Six electrode pair voltages are measured. These voltage values were not taken on the same electrodes for which the current is measured. This data will be obtained by measuring the total voltage drop across the load resistor set.

The power instrumentation as designed covers approximately one-third of the load resistors. The load resistors are adjustable, and can be set to a value to give a certain generator loading; therefore, the external resistance is known. The bulk temperature rise in the load resistors is measured during operation, and by having this data the actual external resistance during operation is known. By taking the current flow at approximately every third load resistor, the distribution of generator output voltage is, therefore, known, as well as the power output. Since power measurements can be found by using either voltage or current is resistance is known, power will be recorded for a total of twenty-six loads.

3. Magnet Control Instrumentation

The total magnet current and voltage is monitored and recorded as well as the total battery supply output. The magnet current is measured on a shunt connected between the channel self-excitation electrodes and the magnet. The magnet voltage is measured across the full magnet while the battery current is taken from a shunt on the battery switchboard.

The total magnet and battery currents are recorded on a two-channel strip chart recorder and are duplicated on meters for the instrumentation panel.

As a further check on the magnet pre-excitation rise time, there is a time indicator displayed on the instrumentation panel which starts when the exciter circuit switch is closed.

4. Burner Operating Control

To properly evaluate burner operation requires the recording of pressures and temperatures for the burner and auxiliary systems.

Pilot burner operation is evaluated by recording the fuel manifold, oxygen manifold and chamber pressures.

Main burner operation requires a knowledge of the pressures in the fuel manifold, oxygen manifold, and combustion chamber. The bulk temperature rise and cooling water discharge pressure for the burner are monitored at six locations.

The cooling water pump discharge pressure and temperature is recorded as is the temperature and pressure of the main burner oxygen as it flows through the flow control venturi.

The total bulk temperature rise and discharge pressure for each of the four load resistor manifolds is also indicated.

In all, approximately 100 separate measurements are made to evaluate the overall generator performance. To best display, record, and reduce data of such a large volume, it was decided to photograph an instrument panel on which the values could be displayed with fairly inexpensive meters and gauges. To photograph these instruments two surplus K-25 aerial cameras are used.

A power supply was designed to operate the cameras. The power supply makes it possible to operate either or both cameras continuously or the cameras can be timed to pulse separately or individually in combination with continuous operation.

For power testing one camera is operated continuously at a speed of one frame per second to record very closely the magnet pre-excitation, burner startup, and magnet self-excitation. The second camera is pulsed at approximately one frame every four seconds.

The film produces a picture which is 4 in. x 5 in. and sixty frames long. Using adapter lenses for fixed distances, it is possible to record the entire panel with each camera so that all data is on a single roll of film.

A photograph of the completed instrument panel, assembly, cameras and strip chart recorders may be seen in Figure II-F2.

As the testing program was initiated a recording oscillograph was made available to monitor the voltage distribution along the axis of the channel. This recorder is a 15-channel oscillograph which operates on a

galvanometer mirror principle to expose a trace on photographic paper. The data is therefore available for reduction immediately. This instrument required the design and assembly of voltage dividers to protect, calibrate, and properly damp the galvanometers.

Upon initiation of the testing program some problems were encountered in the channel operation which required some revisions to the instrumentation. The most serious problem has been electrical breakdown between electrodes due to excessive voltage difference. The breakdown was localized as discontinuities in channel loading; for instance, between electrodes in the excitation and power sections. The original complement of voltmeters was inadequate for diagnosing the problem and therefore 22 additional meters were installed. The large number of extra voltmeters permitted the taking of voltage distributions both across and along the channel in troublesome regions. The physical layout of instrumentation wiring allows meters to be connected to any electrode pair as desired.

The good sensitivity and frequency response of the recording galvanometer made it a useful instrument for monitoring the self-excitation performance of the generator. Displaying magnet current and voltage on the galvanometer provides a good record of the excitation buildup.

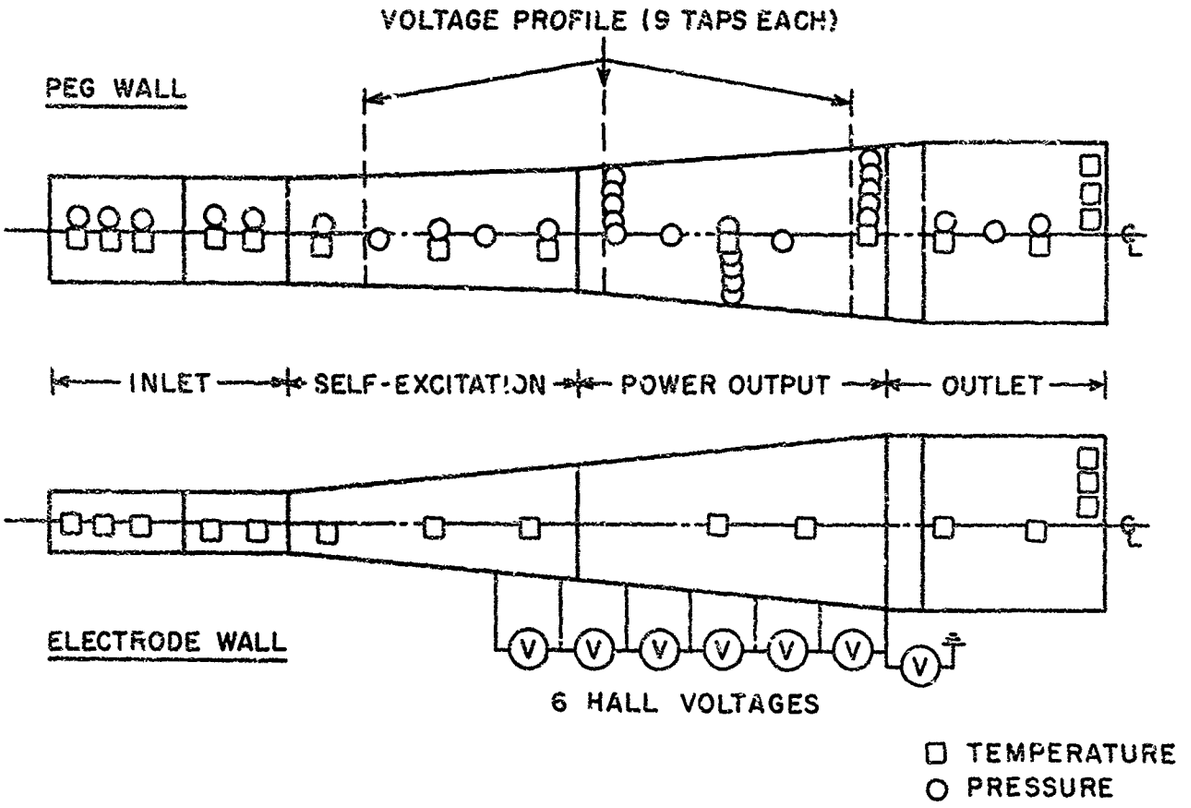

Figure II-F1 Channel Monitoring Instrumentation

A1411

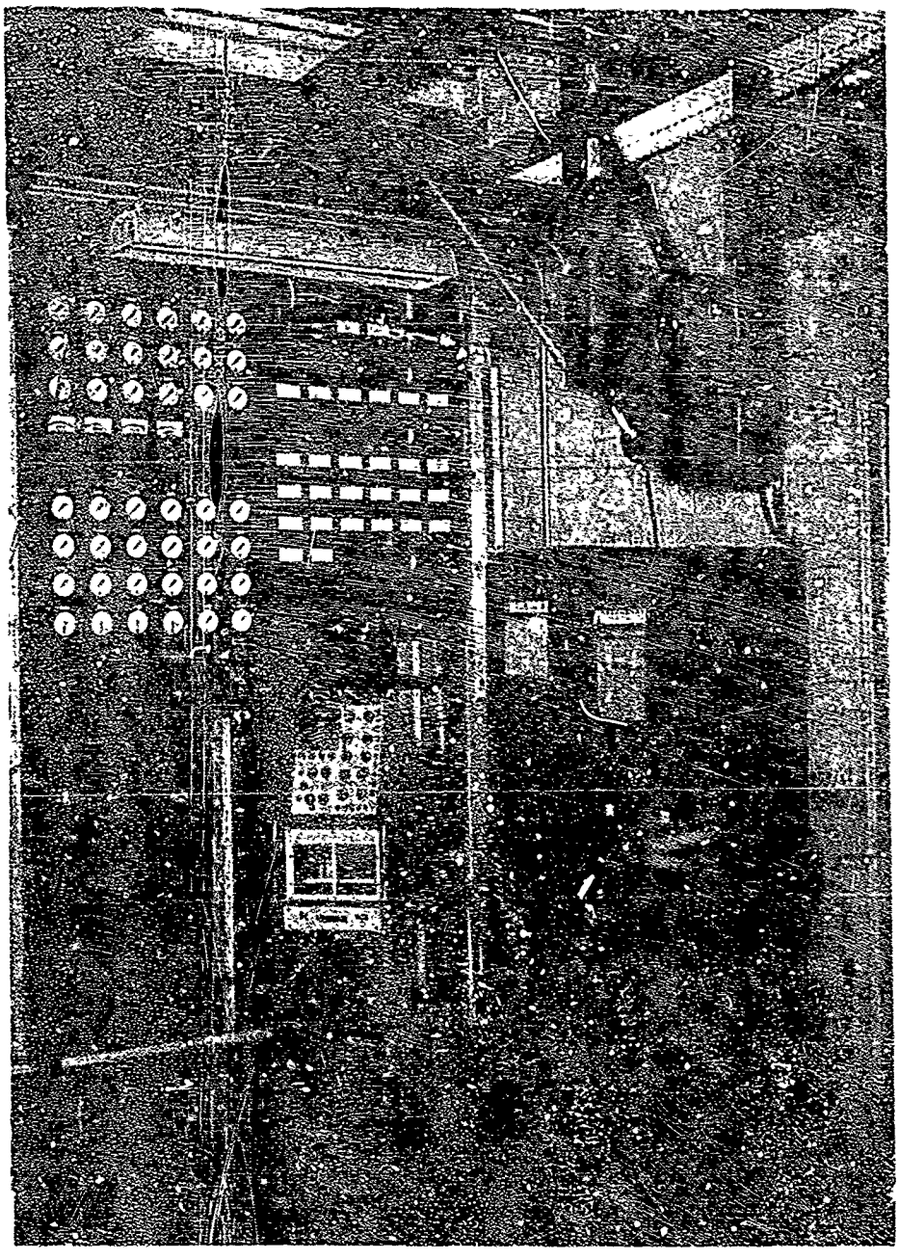

Figure II-F2 Mark V Instrumentation Panel, Recorders and Cameras

A1421

III. COMPONENTS TESTING AND MODIFICATION

In order to check the integrity of the various generator components, and verify design parameters, a testing program was performed. Many important problems were encountered and solved during the program, which necessitated changes to some generator components.

A. BURNER

Initial burner operation was done with a water-cooled dummy channel which permitted normal operation of the burner prior to the delivery of the power generating channel. Burner testing demonstrated that smooth full flow starts and stops could be made and that there were no detectable combustion instabilities.

These tests were conducted at low mass flows in order to check heat transfer rates at low levels. All heat transfer rates appeared to be normal except for the injection section which appeared to be high. At higher mass flows the nozzle and chamber section heat transfer rates were found to be proportional to mass flow indicating that the heat transfer is primarily convective. The rate to the injector plate is not proportional to mass flow indicating that a portion of the heat transfer is radiative. This not unexpected result is fortified by the noticeable increase in heat flux when the fuel is seeded. At 2 mole % seed the radiant heat flux to the injector is about half of the total flux. The measured values of heat flux vs mass flow are shown in Figures III-A1 through III-A4. It can be seen that measured heat fluxes are somewhat lower than design values.

Figure III-A5 shows the main burner chamber pressure as a function of mass flow. As can be seen in the diagram the experimental data for higher mass flows is in agreement with the predicted values, but at lower values the obtained data is lower than the predicted. It is felt that an error existed in the control system, resulting in a nonstoichiometric combustion.

1. Injector Assembly

a. Injector Face Plate

With increased mass flow the Inconel X and stainless steel injector plates both experienced overheating and high thermal stresses at mass flows near 40 Kg/sec, which in some cases meant repair by a welding and a machining cycle. Inspection of the gas surface of the stainless steel

injector plate revealed that overheating and high thermal stresses were prevalent near the outer two rows of oxygen nozzles and that a much better condition existed in the center two rows. It was decided, therefore, to enlarge the oxygen and fuel nozzle orifices in the two innermost rows. The result of this change was to inject a higher percentage of the total mass flow into the center of the combustion chamber so that the outermost two rows of nozzles would be subjected to a lower total heat flux. The data also showed that a sizeable portion of the total heat transfer to the injector plate was due to the radiation component, which could be reduced by electroplating the gas surface of the injector plate with a reflective material. Investigations revealed that a 0.0001 to 0.00015-inch gold plate over a 0.0005-inch of nickel would be optimum for the application since these materials have high operating temperature limits along with oxidation resistance and good ductility. Several tests revealed the modified injector was still subjected to high thermal stresses, and so to be able to realize the full capability of the generator, a design of a new injector plate was started. The prime consideration for this design was the lowering of the combustion side surface temperature, and hence the minimization of thermal stresses. After a thorough materials search, silver bearing copper and everdur were chosen for the new injector plate.

The copper injector assembly is shown on Figure III-A6. The injector assembly is divided by a series of plates or diaphragms to provide passages for cooling water, oxygen and fuel. Starting from the left side of the figure, first is a plate which forms the back wall of the combustion chamber and the oxygen nozzles. The oxygen nozzles have a rounded entrance for a smooth flow and are sized to produce sonic velocity at the throat. Behind this plate is the cooling water passage which is formed by the addition of a support plate. Everdur was chosen as the material for the support plate because of its high strength and its ease in being welded to copper. The third plate closes the oxygen passage and contains the fuel injectors. Since the length of the fuel nozzles was found quite critical, the new nozzles were moved farther into the combustion chamber to minimize the recirculation of hot combustion gases. The last plate closes the fuel plenum and adds to the structural rigidity of the entire assembly. The center of the injector assembly is designed to accept the pilot burner and igniter assembly. The cooling water flow in the new backplate was modified to cool the pilot burner throat. This eliminates a separate cooling water system and also eliminates the welding on the hot gas side of the plate which was required in the stainless steel injector plate. To reduce the radiation component of heat transfer, the hot gas surface of the copper injector plate was gold-plated in a manner similar to the stainless injector.

The new injector plate was installed and a burner testing program was initiated using the dummy channel. The first test of the new backplate was performed at a mass flow of 32 Kg/sec. Analysis of the test data indicated no unforeseen problems, and tests with mass flows of 40 and 46 Kg/sec were performed. The resulting heat flux on the backplate and a comparison with the stainless steel plate is shown on Figure III-A7. The

lower heat flux is attributed to modified cooling water flow, and fuel nozzle placement.

The design of a copper backplate required a thicker section to prevent buckling from water pressures. Due to copper's higher thermal conductivity, the thermal stresses are approximately 1/6 of those realized in the stainless steel backplate. Visual inspection of the backplate after approximately 35 tests revealed no distortion or buckling, proving that the thermal stresses had been the largest contributor to buckling.

b. Fuel Nozzles

A rapid erosion of the fuel nozzles was observed as the mass flow and seed rate were increased. The mechanism for this erosion is believed to be as follows: The high velocity oxygen stream flowing past the fuel injector separates and recirculates at the fuel nozzle tip. The fuel nozzle tip is hot due to radiant heat transfer, and the oxygen reacts with the hot metal to produce accelerated oxidation. It is also possible that there is some combustion occurring in the recirculating flow. In order to find a solution to this problem, a few fuel injectors were made of different materials and with different shapes. By far the most successful was a nickel injector with a shape intended to eliminate or reduce flow separation and recirculation. The fuel injectors were changed over to this design, and no further difficulty occurred.

c. Pilot Burner

The pilot burner liner showed evidence of inadequate cooling after a few runs. This injector was a standard design intended for use with liquid fuels. The change to gaseous fuel eliminated any effective regenerative cooling and overheating resulted. A revised injector was constructed incorporating directed water cooling and a change in material from stainless steel to copper. The new injector has proved to be entirely satisfactory. At the same time a crack appeared in the pilot burner chamber liner. This piece had been spun from tubing and apparently welded tubing had been used. The crack was in the weld. A new liner was made from extruded copper and no further difficulty has been experienced.

2. Main Burner Chamber Liner

Examination of the burner liner after increasing the mass flow revealed a progressive degree of overheating near the injector plate. This overheating of the liner caused failure of an "O" ring after several tests which in turn allowed water to enter the combustion chamber. To remedy

the overheating, N_2 film cooling of the liner was effected. The mass flow of N_2 is approximately 0.5 Kg/sec, and has a sonic throat formed by the burner liner and injector plate. In addition, the spacer ring, which made up the water cooling passage at the end of the liner was modified so as to increase the local water velocity near the "O" ring groove. These changes remedied the problem completely, but it was further helped by the new copper injector plate which was designed to protrude farther into the combustion chamber to eliminate high heat transfer rates near the "O" ring.

3. Nozzle

Since the burner nozzle provides the necessary change in shape and connects the circular combustion chamber to the rectangular channel, this section is very susceptible to thermal distortion due to the great variance of mass in any specific cross section. The nozzle was made in two pieces to facilitate machining, and after repeated thermal cycling distortion of the burner nozzle sections became sufficient to allow water leakage into the combustion chamber. These leaks were located in the junction of the nozzle sections and between the nozzle throat and inlet flange of the channel, and were of such a magnitude as to seriously affect generator performance. The burner nozzle was disassembled, straightened, and the two sections welded together to resist the high thermal stresses and provide a positive water seal between the nozzle sections. In addition, a more positive seal between burner and nozzle was effected by increasing the diameter of the "O" rings in the joint. The welding and modified seals have eliminated the water leaks.

4. Test Results

In conclusion, the Mark V burner has operated throughout the testing program in a very reliable manner and with only a minimum of maintenance. The only precaution other than those normally associated with a rocket motor of this type is the flushing of the fuel nozzle with water after each test, so that evaporating fuel will not leave a seed deposit. On one test in this series a poor excitation was observed, caused by several blocked fuel nozzles, which gave rise to a lean combustion and resulted in a lower than expected stagnation temperature of the working fluid.

The last power tests have been performed at a total mass flow of 52.3 Kg/sec using a 50/50 mixture of ethyl alcohol and methylcyclohexane. The heat release of this fuel mixture is equivalent to that attained with a total mass flow of 60 Kg/sec, using ethyl alcohol and the stoichiometric amount of oxygen. The reasons for using the new fuel mixture are explained in the Testing Program on Page 127.

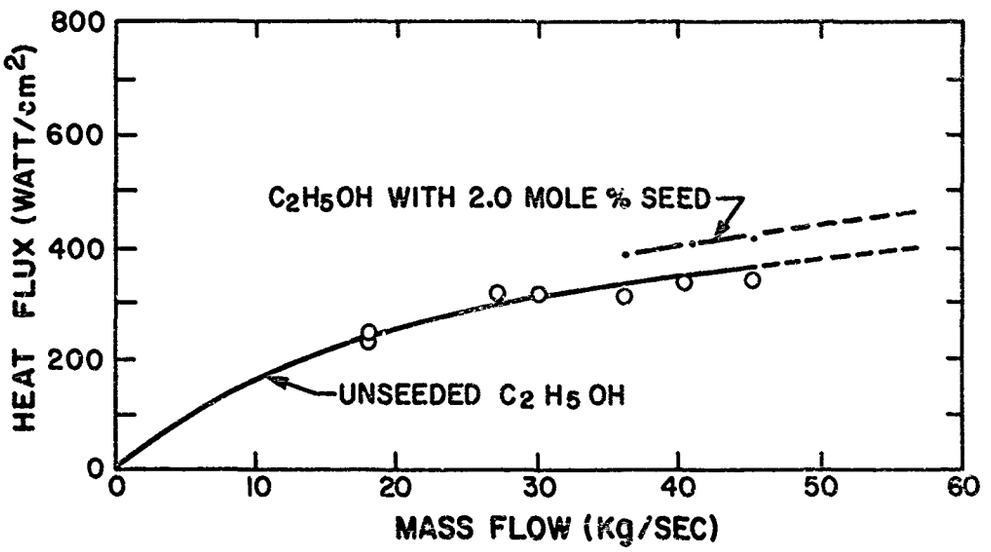

Figure III-A1 Injector Plate Heat Flux Inputs

A22216

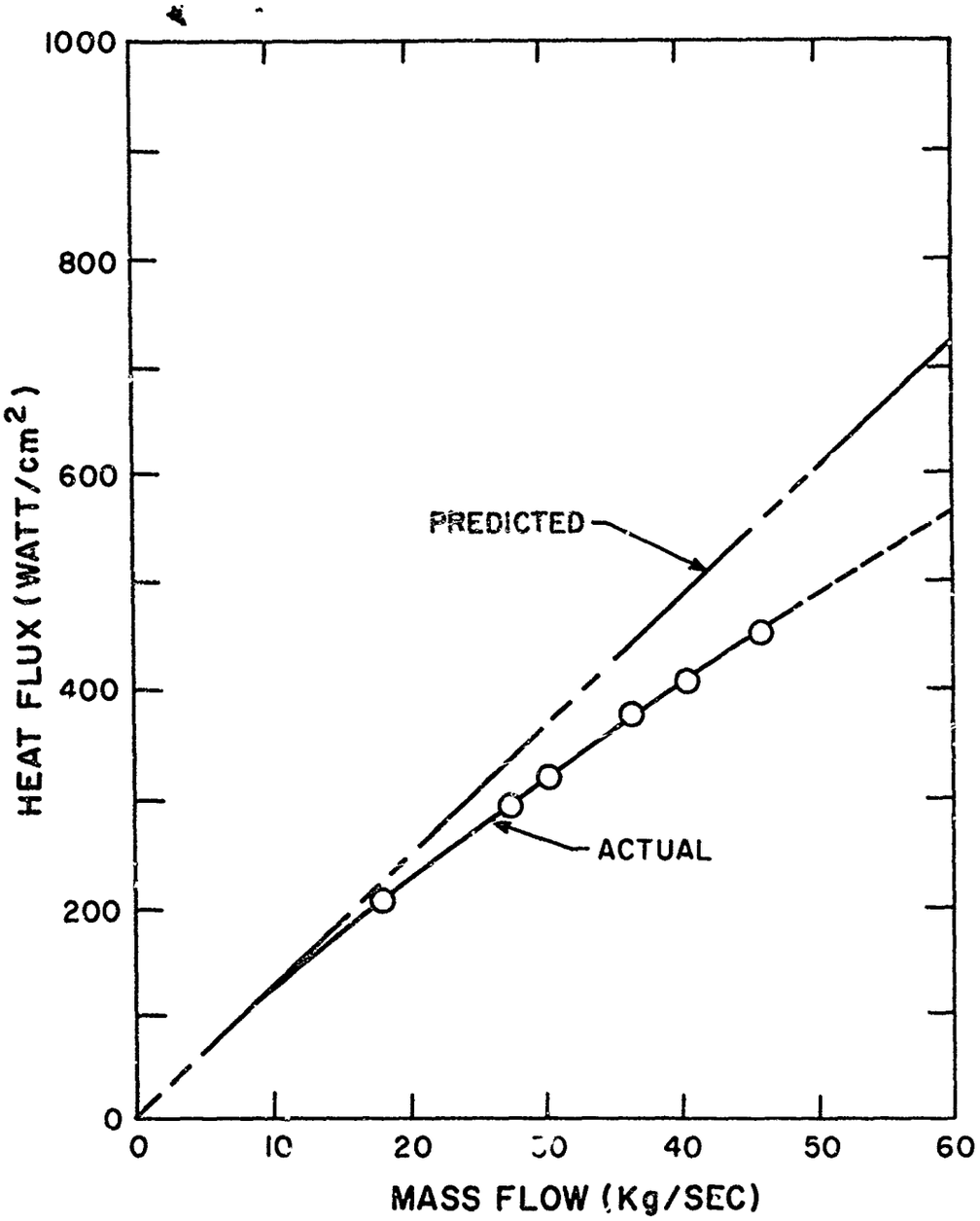

Figure III-A2 Heat Flux for Chamber Liner

A4462

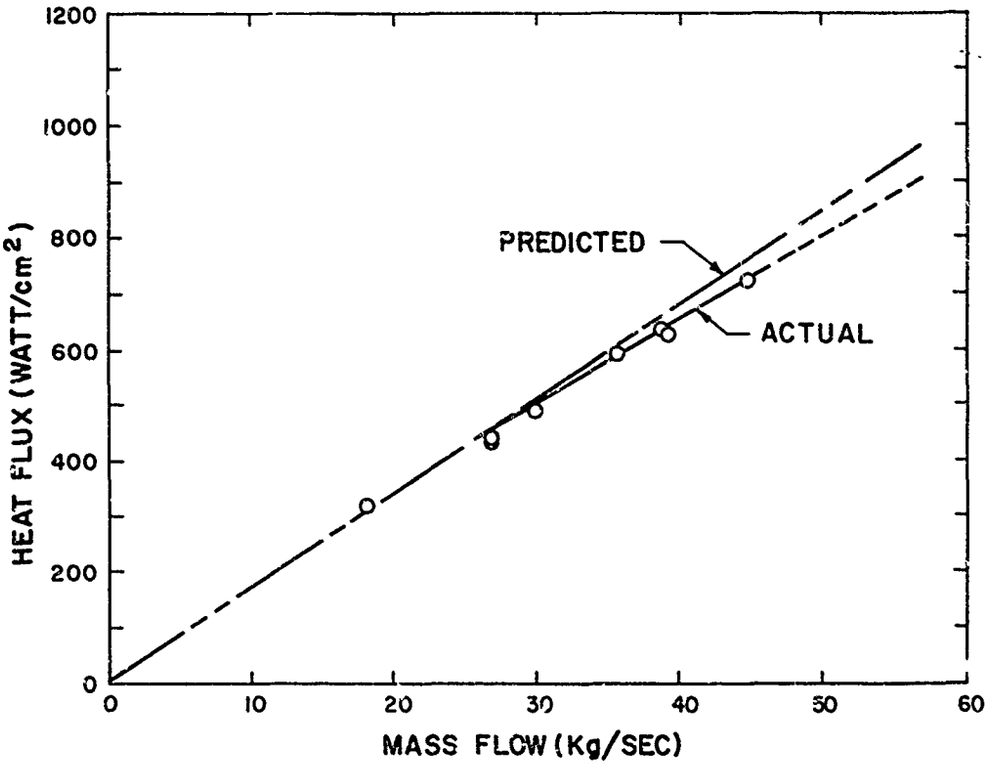

Figure III-A3 Heat Flux Input for Nozzle Throat

A4463

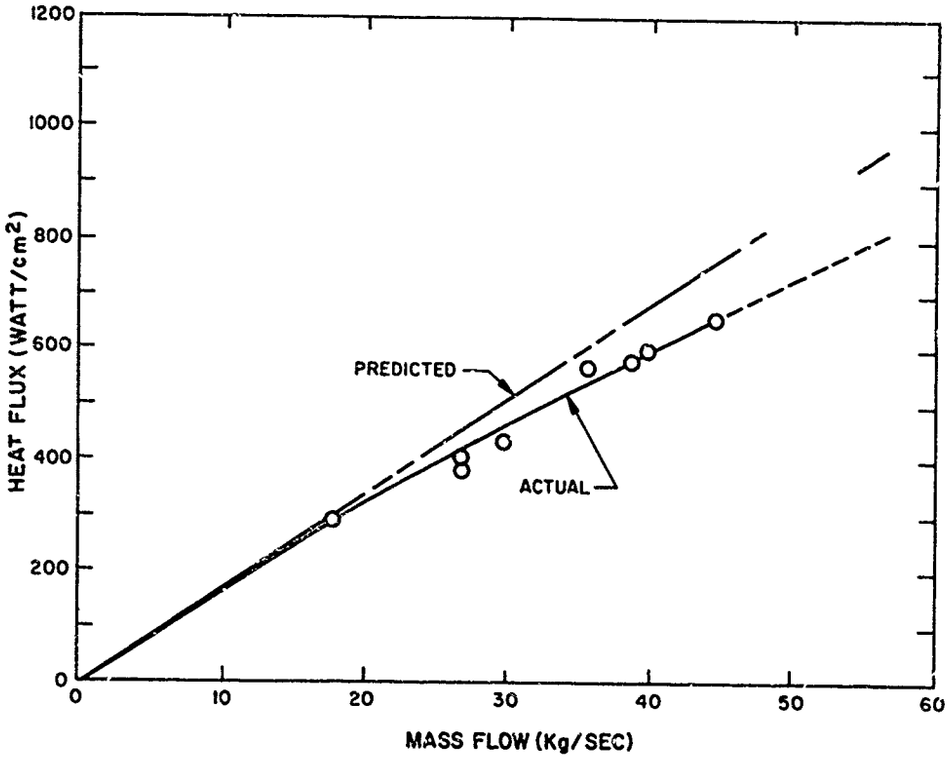

Figure III-A4 Heat Flux Input for Nozzle Transition Section

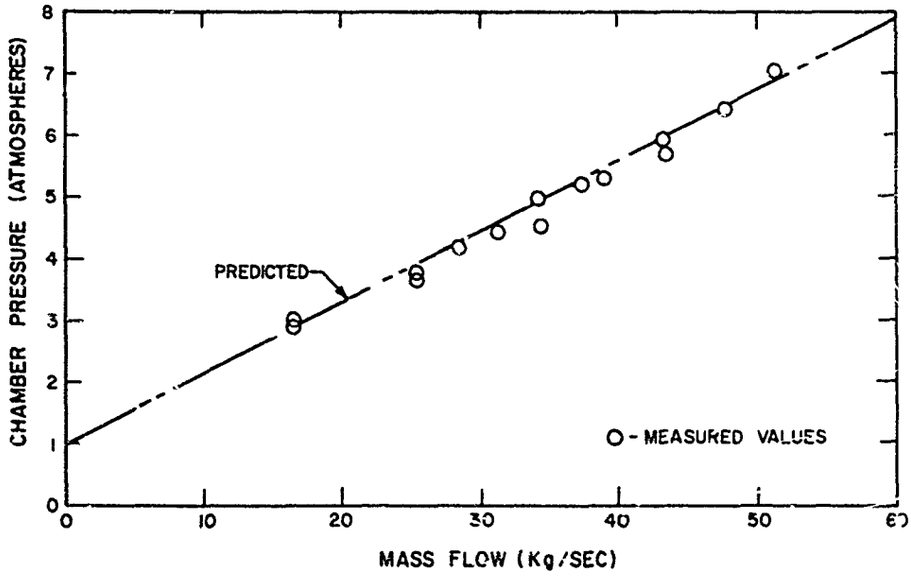

Figure III-A5 Main Burner Chamber Pressure

A4461

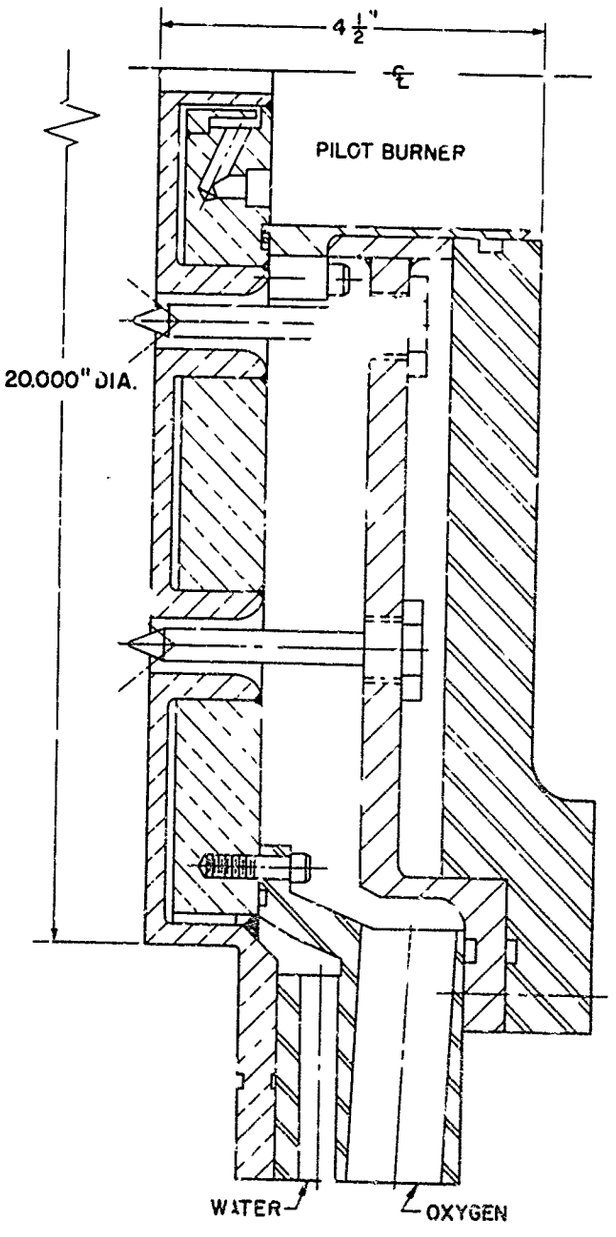

Figure III-A6 Copper Backplate Assembly

A2722

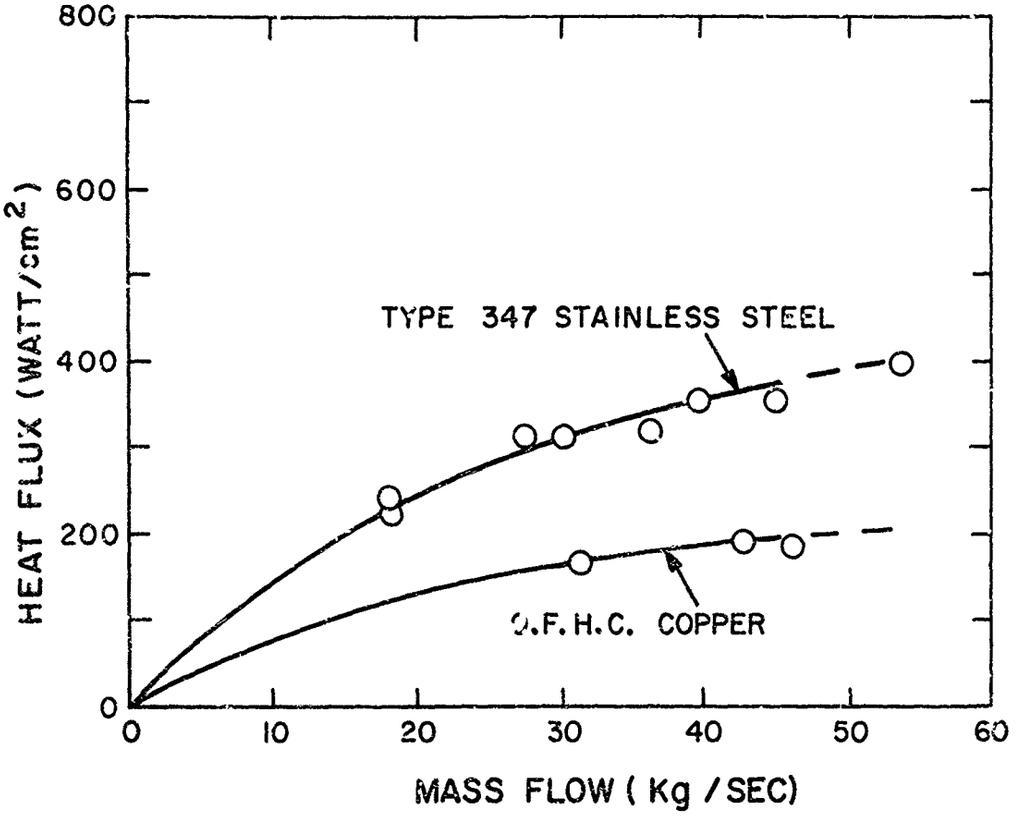

Figure III-A7 Heat Flux Inputs to the Stainless Steel and to Copper Injector Plate

A2723

B. MAGNET

The magnet was brought up to the maximum current and field obtainable with the battery bank, and field measurements were made at several locations along the magnet centerline to verify predicted performance. The field strength was measured by a pickup coil connected to an oscilloscope. The pickup coil produces a voltage which is proportional to dB/dt during magnet buildup. The field strength is determined by integrating the scope trace on the photograph.

During testing the magnet has been brought up to a maximum current of 19,000 amperes or a field strength of 31,700 gauss. Figure III-B1 shows the predicted and the measured field strength along the magnet centerline. The measured field strength is approximately 1500 gauss greater than predicted, due to the low reluctance path provided by the reinforcing steel. This amounts to a field increase of approximately 4%, or a maximum field of 36,500 gauss at design current.

On two occasions during this testing program, minor damage was incurred by the magnet. The first of these was caused by channel gas leaks which burned through the protective epoxy coating of the magnet, the second was a result of external arcing on the channel. These arcs were forced into the copper by the j x B forces, shorting out several turns of the magnet. In both cases, repair was effected by grinding out the damaged section, reinsulating, and covering with a protective epoxy coating. Magnet tests were performed using the battery bank as a check on magnet integrity. The magnet resistance remained at 0.0318 ohms, showing no permanent damage.

Insulation between reinforcing steel and tie rods was improved after external arcs from the magnet tie rods to the reinforcing steel occurred. The original insulation was sufficient for all voltages anticipated during operation of the magnet, but when the channel extension became shorted to the reinforcing steel by a loose water connector, voltages occurred which broke down the insulation between the tie rods and reinforcing steel and ground allowing the Hall current to flow. This severely derated generator performance and so all magnet insulation was checked and improved where possible. The modified insulation stopped external flashovers completely.

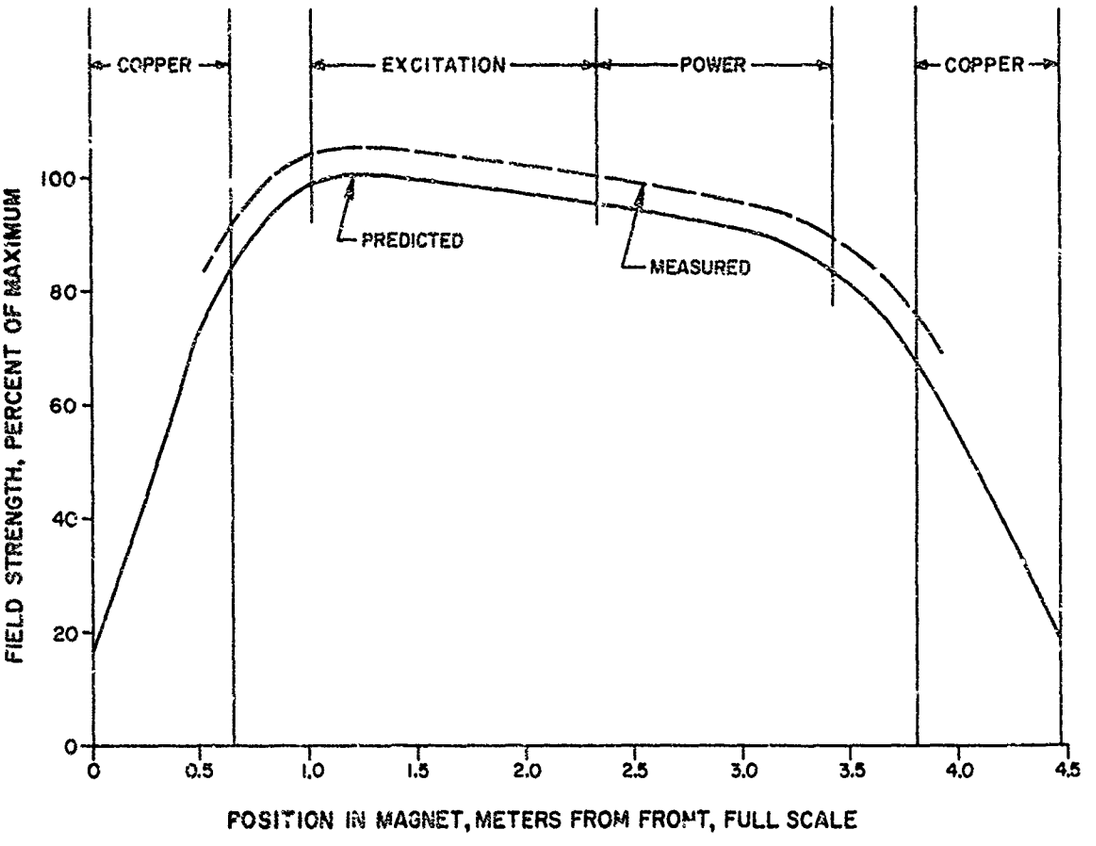

Figure III-B1 Measured and Predicted Longitudinal Centerline Field Strength

A1414

C. CHANNEL AND EXHAUST SYSTEM

1. Mechanical Properties of Channel Walls

a. Heat Transfer

The cooling of the channel has been sufficient under all operating conditions encountered. At no time has a component burned out due to excessive local heat transfer alone. In various instances local pieces of refractory material have been lost, thus exposing water cooling connectors to the high temperature gas.

b. Thermal Stresses

The overall channel design is extremely rigid, and stresses resulting from hydraulic pressure are at a minimum. Thermal stresses, however, have caused some problems on surfaces which are exposed to the gas. These problems have been encountered in the slabs of the inlet and exit sections where the yield point of the copper has been exceeded. The slabs of the inlet section which are parallel to the axis of the channel are subjected to a nonuniform change in temperature. The forces on the restraining screws are such that the threads in the copper bars yield and allow the bars to distort. The distortion disrupts the cooling water seals and leaks are developed. To relieve the stresses on the slabs, a series of grooves were cut in the critical areas. To provide additional clamping forces, steel inserts were placed in the tapped screw holes and additional screws were added where necessary.

The electrode slabs used in the exit section are mounted normal to the channel axis, and have been subjected to a temperature gradient sufficient to cause distortion. The forces involved resulted in a permanent deflection of both exit section electrode walls, but were of such a magnitude that no cooling water seals were disturbed.

c. Refractory

The refractory materials used to provide electrical insulation between metallic segments of the channel walls must meet severe criteria.

The refractory must be:

1) a finely ground preparation which is plastic and trowelable when tempered with water

2) non-slagging in that no destructive chemical reaction can exist between the refractory and external agencies at high temperatures resulting in the formation of a liquid

3) of high strength to avoid spalling from the mechanical, thermal and structural forces which cause cracking and rupturing of the refractory and eventual detachment of segments

4) capable of withstanding a sufficient surface temperature for exposure to generator gases without ablating

5) sufficiently strong to resist erosion of the turbulent, high velocity working fluid

6) an electrical insulator at high temperatures

7) sufficiently dense so that the porosity will not allow the refractory to become saturated with generator seed materials.

These considerations led to the choice of refractories composed principally of alumina. The materials used are furnished in a dry form and are mixed with water at the time of application. The material used for the greater portion of the test program was fairly satisfactory. However, some erosion of the material was experienced throughout the program. Most seriously affected were grooves aligned parallel to the gas flow. After each test it was necessary to add material to some of these sections. The refractory material created some problems in that the seed material would diffuse into its surfaces and drastically reduce the insulating capability. In some cases it became necessary to mechanically remove old mortar and replace it.

Spalling of the refractory has occurred although it is difficult to determine the exact nature of the spalling. The refractory in the entire channel is exposed to a thermal shock upon burner startup with the refractory of the inlet exposed to additional mechanical and structural shock due to internal gas pressure and the distortion of components due to thermal stresses. This latter problem was extremely troublesome in that the cooling water connectors are near the hot gas surface and the loss of refractory directly exposes the cooling water connectors to the gas. The net results are burned seals and connectors which caused water leaks.

The fact that all rocket type gas generators vibrate adds additional stresses to refractories and increases the possibility of losing refractory which was not properly bonded to the metal surfaces.

New refractory materials have been incorporated during the program as they were found more satisfactory through tests conducted in smaller MHD experiments. The newest refractory used was 99% pure aluminum oxide with an extremely low concentration of calcium oxide (0.1%). When this refractory is tempered using a sodium silicate solution, the re-

sult is an extremely dense and strong material with excellent high temperature electrical properties. Experiments performed using this refractory in various sections of the channel indicated that seed diffusion was down, erosion was less, and the electrical quality of the wall superior to other sections of the channel in which the older type refractory was used.

2. Electrical Properties of the Channel Walls

Arcing has occurred in every section and considerable effort was placed on repair and revisions to the generator channel.

In the early phase of the program a method of removing and replacing damaged electrodes or pegs within the channel, without removing entire sections, was developed. In conjunction with the first arcing experienced, a repair cycle was initiated to repair components damaged by the arcs. This repair was important since not only was complete replacement of the parts expensive, but it would be most of all time-consuming.

The repair cycle was basically to clean the damaged area and redeposit the base material through a heliarc welding process. The puddle welded material was then removed to return the component to the original dimensions. In this manner localized damage could be repaired with the minimum of inconvenience to the testing program.

a. Changes Made to Channel Electrode Walls

1) Inlet Section: One major modification was performed to the channel inlet section electrode wall to blend the open circuit voltage of the inlet section with the output voltage of the self-excitation section and prevent arcing. Nine slabs which were adjacent to the self-excitation section on the electrode wall were converted to working electrodes. This modification involved the removal of the slabs and machining of grooves on the gas surface. The grooves were then filled with zirconium oxide refractory material used in all working electrodes. Electrical power taps and bus bars were designed and manufactured, together with electrical cables to connect the electrodes to the load leads.

2) Self-Excitation Section: The self-excitation section has performed as expected, electrically. No modifications or repairs have been performed on the electrode walls in this section.

When it became necessary to remove the channel after almost every test, the manner of connecting the self-excitation section to the magnet was improved. The original hookup consisted of a series of 26 leads from each side of the channel to the magnet. These were replaced by bus

bars and this improvement has saved many hours of hookup time throughout the program.

3) Net Power Section: This section has required attention throughout the program. The major portion of the channel repairs and modifications have been made in this section.

Many electrodes were repaired using the welding cycle previously described.

Edge pegs which line the top and bottom of both electrode walls were found to break down to the reinforcement steel of the adjacent electrodes. To remedy this situation without a large machining operation, the edge pegs were completely insulated from the reinforcing steel. The pegs were mounted on a thin strip of mylar insulating material and the material of the bolts which clamp the pegs to the reinforcing steel wall were changed from stainless steel to nylon.

One major change was made to the anode electrode wall when all 50 electrodes were modified to a new electrode design which incorporated the latest electrode technology. This change is more thoroughly described in the electrode section of this report.

The joint electrodes between the self-excitation and net power sections were modified to increase the electrode drop in the beginning of the net power section (see Power Testing). The electrodes were cleaned of all refractory material and the grooves were filled with the base metal using the welding repair cycle.

4) Exit Section: The performance of this section was as expected until the latter portion of the test program. At this time severe arcing damaged both electrode walls such that it was necessary to remove and repair all electrodes and the stainless steel support bars. Approximately 50% of the edge pegs in this section were so heavily damaged it was found to be more expeditious to completely replace the pegs. The last three electrode slabs on each wall were split down the middle to provide more insulation.

c. Changes Made in Insulating Walls

1) Inlet Section and Self-Excitation: The joint formed in the insulating wall between the inlet and self-excitation was found to be improperly insulated. The problem involved the proximity of peg retaining screws to external joint support bars. Insulation was added between these components with satisfactory results. The remainder of the insulating wall presented no electrical problems during the testing program.

2) Net Power and Exit Sections: Twice in the program it was necessary to increase the insulating capability of the top and bottom peg

walls of the net power and exit sections. The trouble area included the last 40% of the net power section and the first 10% of the exit section. In the instance of the first repair, approximately 200 pegs were modified by having 0.76 mm removed from one side and later approximately 800 pegs, including some of the first modified, had 1.0 mm removed from one side. When damage did occur on the insulating walls, considerable work was involved. The major portion of the damage was to the plastic wall on which the pegs are mounted. Some arcing occurred between pegs on the plastic surface and caused the plastic to char, forming permanent short circuits between pegs. It was necessary to grind out the charred areas and replace the removed plastic with glass-filled epoxy.

A problem was also encountered with external arcing on the stainless steel reinforcing bars in the exit section. To prevent a recurrence of this problem, the metal sealing bars in the channel joints were replaced with plastic bars, while the external support bars for the top and bottom walls of the exit section were also replaced by plastic bars.

3. Electrodes

During the testing program arcing was experienced between electrodes in the power section with voltage gradients far below design values. It was believed that the zircoa was operating at a sufficiently high temperature to melt and flow across adjacent electrodes and thereby trigger arcing at low voltage gradients. For this reason the zircoa was removed from the downstream groove and replaced with alumina. Results of this test showed that arcing occurred when the voltage differential on the anode wall exceeded a value of 25 volts between electrodes which indicated a more extensive design change was necessary. Damage was more severe on the anode wall since the j x B forces drive the arc current into the wall while arcs on the cathode wall are forced into the gas stream. Arcs on the anode wall resulted in damaged water seals causing leaks. It was therefore decided to remove and modify the electrodes on the anode wall of the net power section. The downstream half of each electrode became a copper slab while the upstream half was solid zircoa. This type of electrode had been found to give excellent performance in tests conducted at the Avco-Everett Research Laboratory Long Duration Test Facility under our commercial MHD development program. The zircoa used in this modification has improved electrical characteristics due to an increase in the amount of calcium oxide. In addition, the sharp edges of the electrodes were radiused to prevent electric field concentration.

Due to the current concentrations that exist in the downstream end of the self-excitation section cathode wall, several electrodes in this location were also modified to the high performance design.

Another important change in the electrode walls was that the electrode slabs in the critical junction between the self-excitation and power

sections were modified. Due to L di/dt, high ΔV's are experienced in this critical junction during excitation and in order to increase the breakdown voltage in this junction, a cold boundary layer was created by converting a copper-zirconia electrode to a copper slab.

After approximately thirty power tests, few problems have been encountered with the design. In conjunction with these modifications, important changes were made in the exhaust system which partly contributed to the success of the new electrodes.

4. Exhaust System

The major change to the exhaust system was the addition of a new transition. The new design was made to alleviate the problem of flow separation in the channel, as fully discussed in Section II. The new transition section is rectangular in cross section, 3.67 meters long, and fabricated of mild steel plate. It is designed to withstand a heat flux equal to that of the channel exit section (190 watts/cm^2) for its entire length. Total cooling water flow is 2000 gpm or 500 gallons per wall. This quantity of water is needed as the water supply is previously used to cool the loads and so it may enter the transition section at temperatures up to 60°C, depending on the power dissipated in the loads. Mechanically, the transition section is constructed as a double box with spacers to maintain the cooling water passages. Both boxes are plug welded together in a manner to provide the necessary strength to resist thermal and mechanical stresses. After several tests it was necessary to repair some defective plug welds. Since their repair, it has been repeatedly operated without incident.

As the power levels have increased, the Hall voltage in the channel has increased and on several occasions arcs have been experienced between the channel and channel extension, then channel extension to exhaust duct and exhaust duct to ground. In an effort to eliminate any external arcing, the channel extension was insulated from the channel, and the insulation between the exhaust duct and transition and exhaust duct and ground was improved. Results of these changes have eliminated arcing in the exhaust system, and no insulation problems have been observed while running under more severe conditions.

D. GENERATOR CONTROL AND INSTRUMENTATION

1. Control System

The burner and magnet control systems have operated in a trouble-free and reliable manner throughout the testing program, except for a few problems with the ignition coil used to fire the igniter burner, and some pressure switches going out of calibration. These problems were corrected by an improved maintenance program.

The resistor bank has been utilized to its full capability with a large number of load resistor variations being obtained. Overall, the load resistor bank has performed as expected, and gave the desired degree of flexibility.

2. Instrumentation

The original instrumentation system used to record and monitor the test performance of the Mark V generator has been supplemented throughout the program.

The changes and additions which have been made were done so as to more fully evaluate and understand the phenomena which were occurring within the generator and to more intelligently control the operation of the generator.

During each run, measurements of mass flow, plenum pressure, static channel pressures, magnet voltage and current, external voltage along both walls and the centerline of the channel, and voltage distribution across the channel are obtained. These measurements are obtained from multi-channel recorders and photographs of the instrumentation panel. The measurements have been proven to have sufficient accuracy to analyze the generator performance.

Meters used to measure current in the load resistors were converted to voltmeters to improve the flexibility of the system. These meters could then be used to measure any voltage on the channel without the limitation of shunts. In all, the voltage instrumentation has been expanded to 92 meters or an increase of 54 meters over the original installation.

To obtain a picture of the equipotential lines which exist within the channel, the instrumentation system was expanded, utilizing the copper pegs of the insulating walls as Langmuir probes, to measure the transverse voltage distribution at five separate locations along the net power section of

the channel. Five complete sets of 20 leads were installed from the channel to the instrumentation panel. The panel is wired to a stepping switch, and then to one set of volt meters. As the test progresses, the switch may be used to read out the voltages at any one of the five desired locations.

In the original design no provisions had been made to measure the open circuit or Hall voltages after electrode #50. To do this, the channel was equipped with high voltage instrumentation leads on each copper slab of the electrode wall from electrode #50 to the exit. In addition, leads were added to the channel at various locations along the centerline. Twenty sets of leads were then drawn from the channel exit to the instrumentation panel.

To minimize damage from arcing inside the channel, a voltage monitoring system was installed. This system gives the monitor a complete picture of the voltage distribution which exists on the entire length of the net power section, as well as any abrupt change in voltage gradients. These abrupt changes were always associated with arcing, so by terminating the test on the first indication of adverse gradients, damage from arcing and in turn the repair work was minimized. When the problem of external arcs arose, the voltage monitoring system was expanded to measure the open circuit voltage in the exit section as well as the Hall voltage of the channel extension and exhaust duct.

To record the ΔV between electrodes along an entire electrode wall, a 52-channel oscillograph recorder was obtained and installed in the instrumentation system. Voltage dividers were designed and assembled to protect the recorder from high voltages, and allow changes in calibration and dampening of galvanometers.

The channel is equipped with pressure taps to measure both the axial and transverse static pressure distribution. With the original pressure tap spacing along the channel, it was difficult to distinguish between a continuous pressure increase due to a large eddy current, or a step increase due to a shock or a superposition of both effects. For this reason additional pressure taps were installed on the channel centerline in the region of electrodes 30 through 50.

The channel extension section added during this testing program included provisions for measuring the static pressure at five locations along its length. The addition of this section required no further revisions in the data-taking system.

IV. TESTING PROGRAM

A. INTRODUCTION

Originally, it was intended to study the performance of the Mark V generator over a wide range of seeding, mass flow, and loading configurations. However, as the testing program progressed, the main problem was to find an operating configuration which would lead to the production of a net power output of 20,000 kilowatts. Since the Mark V generator was to be self-excited, one section of the generator channel is used to provide the necessary power for the generator field coil, and since self-excitation had never been demonstrated, or for that matter attempted, it was natural that the first objective of the program should be to achieve self-excitation of the generator. It was further known that the exact self-excitation conditions which would be required to bring the generator to rated output would have to be studied and that several tests were needed to gain sufficient knowledge of the self-excitation mechanism. For this purpose the testing program was divided in two sections: first a study of generator self-excitation followed by a concentrated program of net power generation tests.

The main objectives sought in the self-excitation phase of the testing program were a knowledge of the relationships between battery voltage, magnet current, and L di/dt, which must exist before and after the main combustion chamber is fired. Further, the rate of self-excitation must be well known in order to properly load the generator and prevent unfavorable voltage distributions in the region between the self-excitation section and the net power section. Once these objectives have been attained, it was possible to determine the burner firing point for any specific battery voltage and length of self-excitation section.

The power generation phase of the program was initially believed to be readily accomplished once the self-excitation mechanism was understood, since during self-excitation tests some experience of loading the net power section would be gained, as well as a good knowledge of actual gas conditions.

The major problem encountered during the testing program was arcing. From the discussion of the testing program, it will be seen that during some experiments the arcing was triggered by water leaks, while at other times the water leaks were the direct result of arcing. Poor performance was experienced in some tests, caused by the introduction of water into the working fluid, which required the repetition of the test to obtain the desired data.

Fifty-six power generation runs were conducted with the Mark V generator during the testing program and self-excitation was easily and reliably achieved. A maximum net power output of 23,600 kilowatts was

produced, exceeding the design value of 20,000 kilowatts. The maximum gross power output was 32,000 kilowatts. These performances were achieved using a mixture of ethyl alcohol and methylcyclohexane combusted with the stoichiometric amount of oxygen. In order not to exceed the design heat release value, the above mentioned power outputs were obtained using 87% of the design mass flow.

B. GENERATOR SELF-EXCITATION

In order to best show the progress made in self-excitation of the generator, curves from the most interesting tests are presented and described, and, where applicable, compared. It should be noted that the cathode electrode and anode electrode are defined as the positive and negative electrodes of the generator, respectively.

After the first series of generator tests, the problems which were to be experienced with the self-excitation of the generator were evident. These included determining the initial value of battery voltage, the magnet current at which the burner was to be started for a specific battery voltage, the value of L di/dt at the time of burner start, the problem of avoiding arcing to electrodes adjacent to the self-excitation section, and a method of controlling L di/dt when the generator was operating in a burner only configuration.

Testing started with a mass flow of 33.2 Kg/sec and a seed concentration of 2.0 mole % of K in the combustion gases, at a temperature of 3000°K, and at a static pressure of 1 atmosphere. After a few operational tests, the mass flow was increased to 36.4 Kg/sec, and, in Test #3, the first successful self-excitation of an MHD generator was achieved.

As can be seen from Figure IV-1, the current delivered to the magnet by the batteries was 4500 amperes, when the main burner was started. The battery bank and the generator ran in parallel for approximately three seconds, the time it took the battery circuit to decrease to 1000 amperes and automatically cut out. Before this happened, the generator current was 4600 amperes, and as soon as the switch in the battery circuit was opened, the generator ran self-excited for a period of twenty seconds. This corresponded to 2100 kilowatts delivered to the magnet and 400 kilowatts net output to the loads, for a total gross output of 2500 kilowatts. Magnet voltages appear on Figure IV-2. The upper curve is the magnet voltage and the lower curve is the voltage drop due to the internal impedance of the magnet, the difference between the two curves being L di/dt. As can be seen in the diagram, the magnet voltage increased rapidly during the time the battery bank and generator were working in parallel. When the battery circuit was opened, the generator had to deliver instantaneously 1000 amperes, which caused the sharp change in magnet voltage and L di/dt. Due to the low value

of L di/dt, excitation was slow, but self-excitation was clearly demonstrated with the magnet current reaching a value of 8000 amperes. The test utilized the design length of the self-excitation section.

The first major arcing was experienced during this run and occurred on the anode wall of the net power section. The arcing was the result of an excessive potential difference between adjacent electrodes with the resultant arcs developed forced into the electrode wall by the j x B forces. The arcs attacked the water seals between adjacent electrodes and water leaked into the channel shielding the electrodes.

To develop the technique of proper generator startup and control of self-excitation through the transient condition, the electrodes in the net power section were initially paralleled with those of the self-excitation section. This generator configuration would then produce a constant voltage through the loaded section and hence a zero voltage gradient between the loaded electrodes. Both ends of this loaded section then became the only area for possible arcing, due to the steep voltage gradient at these locations caused by the difference between the output voltage in the loaded section and the open circuit voltage before and after the loaded section. The ΔV's in these regions could, however, be monitored and the tests discontinued if the ΔV's exceeded the prescribed voltage. The next series of tests was then conducted using various resistors in parallel with the generator magnet as well as various battery voltage startup conditions.

The voltage monitoring system described in Section II was installed and proved effective, enabling the generator to be shut down before any severe arcing could be established.

Figure IV-3 shows the excitation characteristics for Test #6. The mass flow for this test was 39.1 Kg/sec with 2 mole % seed. This test utilized the design length of self-excitation section plus electrodes 1-16 of the net power section operating in parallel. To control the value of L di/dt at burner startup, a fixed shunting resistor of 0.118 ohms was placed in parallel with the magnet and self-excitation sections. As can be seen in the figure, at 5.8 seconds the burner was fired and the generator started to overtake the battery bank. At 20 seconds, the battery current has gone down to zero, and the generator becomes self-excited. By having the battery circuit open at zero current value, a smooth transition to generator only operation was achieved instead of the sudden output voltage drop shown in Figure IV-2. This test clearly demonstrates that if the generator is to be self-excited to design condition using external shunt resistors without exceeding predetermined values of L di/dt, it cannot be done using fixed resistors, since magnet current will level off at a value lower than the design value; therefore, the shunt resistance must be variable. Figure IV-3 shows, once the generator was started, the value of L di/dt was continually decreasing although the rate of decrease was slow and the generator was still self-exciting. Therefore, it would have taken the generator a relatively long time to reach

the steady state point. Based on the results of this test, it was decided to install a switchgear which could be used to take loads in and out of parallel with the magnet and hence have more control over the rate of self-excitation.

To more effectively control the voltage potential between loaded and unloaded electrodes, a system of bleed resistors was installed. This system of bleed resistors was such that the potential developed between electrodes could be controlled and kept within tolerable values.

Figure IV-4 shows the excitation characteristics for Test #10. The tests conducted prior to #10 were made using higher values of battery voltage and different values of loading in parallel with the self-excitation section. The tests indicated that the arcing problem would be more severe at higher voltages in the burner start point; therefore, Test #10 was conducted using a mass flow of 39.1 Kg/sec, 2 mole % seed, and a battery voltage of 204 volts, with electrodes 1-17 in the net power section connected to the self-excitation section and a load resistor of 0.110 ohms in parallel with the magnet. The burner start point is exactly the same as that shown in Figure IV-4, with the exception of battery current, which is slightly higher due to the change in loading caused by the bleed resistors. As can be seen, a relatively smooth transition from generator and battery operation to generator only operation was achieved. Generator self-excitation is improved and the decrease in L di/dt is less than that exhibited in Figure IV-4. When the magnet current attained a value of 10,000 amperes, which is approximately 50% of the magnet design field strength, there was a gross power output of 4900 kilowatts (1400 kilowatts net), as well as 40 volts positive L di/dt. At this point there occurred a sudden decrease in generator output current to the load shunting the magnet. The sudden decrease in the current value was due to an arc which had developed in the inlet section of the channel between the burner and self-excitation section. The occurrence was detected on test monitoring instrumentation and the generator was immediately stopped.

The inlet section had been operating open circuited and the arcing which occurred made it necessary to control the voltage distribution in this section. A modification was then made to convert nine inlet slabs into working electrodes and thus provide the possibility to load 30% of the downstream end of the inlet section. These nine new electrodes were then loaded in such a manner as to produce a favorable voltage distribution and an acceptable value of ΔV between electrodes.

For Tests #11 and #12 the mass flow and load in parallel with the magnet were varied from 41.8 Kg/sec and 0.104 ohms to 45.0 Kg/sec and 0.156 ohms. In addition, the inlet section electrodes were now individually loaded and electrodes 18-23 in the net power section were separately loaded. The loading at each end of the self-excitation section was such that the load voltage would blend with the open circuit voltage of the unloaded section of the channel. The generator failed to self-excite in Test #11 as too much power was dissipated in the parallel load, while in Test #12 the gen-

erator self-excited, but did not attain the anticipated magnet current. It was then discovered that the burner injector plate was damaged, admitting water to the combustion chamber, and hence the results were lower gas conductivity and a correspondingly derated generator performance; in addition, the lower gas conductivity also caused an unfavorable voltage gradient which resulted in electrical breakdown at both ends of the self-excitation section.

This occurrence clearly demonstrates that, if the generator loading is set up for specific gas conditions, and if these conditions are not met within reason, unfavorable voltage gradients will exist over which there is no control once the test has been started. Knowing that the problem of poor gas conductivity was solved by the elimination of the water leaks, and since it was necessary to check out the repaired burner, the next test (Test #13) was made at a reduced mass flow of 39.1 Kg/sec. The length of the self-excitation section was reduced to include only up to #1 electrode in the net power section, while electrodes 6-17 were loaded so as to blend the voltage gradient of the last loaded electrode with the open circuit voltage of the first unloaded electrode and thus prevent the occurrence of too high a ΔV. Figure IV-5 shows the excitation characteristics for Power Test #13. The result of this test was a smooth performance which attained 7800 amperes magnet current or nearly what was achieved in Power Test #12. However, this test was conducted using a shorter length of self-excitation section and a mass flow which was 10% less than that used in Test #12. The test was stopped when it became apparent that the rate of excitation was slow. Since generator performance again indicated the presence of water in the working fluid, an investigation was made and it was discovered that the water had been introduced into the storage tank of the fuel system. The ΔV in the junction of the inlet and self-excitation sections was found to be tolerable, but arcing occurred at the junction of the self-excitation and net power sections.

The arcing which occurred demonstrated that a good knowledge of the electrode output voltage along the channel length was required to operate the generator in a segmented configuration. Since the ΔV at the junction of inlet and self-excitation was found to be tolerable in the preceding test, it was decided to concentrate efforts to obtain a satisfactory ΔV at the junction of the self-excitation and the first loaded electrode in the net power output section.

Figure IV-6 shows the excitation characteristics for Test #14. This test was made using a mass flow of 39.1 Kg/sec, 2 mole % seed, and a battery voltage of 204 volts. The net power section was operated open circuit to obtain a better understanding of the existing voltages, while the inlet section, which was working properly, was loaded as in the preceding test. To verify the gas conductivity, electrode #2 of the net power section was set up so that loads could be switched in a few seconds after burner start. It was further planned to stop the test at approximately 6000 amperes magnet current, but the rate of self-excitation was such that the magnet

current reached a value of 11,000 amperes before the test plan was completed. Comparing Test #13, Figure IV-5, with Test #14, the effect which a relatively small percentage of water in the fuel has on the gas conductivity is clearly evident. The rate of magnet excitation in Test #14 was the highest of any test which had yet been experienced, with a maximum value of L di/dt of 130 volts. Close examination of Figure III-6 shows that within the first second after burner startup, arcing occurred as is indicated by the inflection in the curves. This means that there was arcing inside the channel from time 15 seconds to burner shutoff.

Figure IV-7 is a plot of the total ΔV between electrode #1 which was attached to the self-excitation section and electrode #3, which at burner startup was operating open circuit. The figure shows an instantaneous total ΔV of approximately 270 volts within one second after burner startup. Arcing then caused the decrease of this voltage and the steps in this curve resulted from the switching in of the two loads, one at 5600 amperes and the other at 7700 amperes. It is therefore evident that arcing was established by this voltage peak. The results of electrical gas conductivity measurements showed a value within 10% of the theoretical value. The test also demonstrated that a lower initial value of battery voltage would facilitate a smoother transition between battery only and generator only operation, and that the ΔV can be reduced by proper loading as indicated in the steps of Figure IV-7.

Severe arcing occurred on both electrode walls. The arcing began at electrode #2 and was then spread to other electrodes as cooling water connectors were damaged and allowed water to enter the channel. The gas conductivity and excitation rate were as expected, so it was decided to individually load the first thirty electrodes in the net power section based on the data obtained from Test #14, while keeping the loading in the inlet section the same as for the previous tests. Bleed resistors were used from electrode #1 to electrode #5 and the battery voltage was reduced from 204 volts to 120 volts. Test policy was to bring the generator to as high a magnet current as that attained in Test #14 and to also find the value of ΔV without having arcs from burner start.

Figure IV-8 shows excitation characteristics for Test #15. The test was made using a mass flow of 39.1 Kg/sec and 2 mole % seed. The figure shows a smooth transition from battery only to generator only operation. The rate of self-excitation was continuously increasing to approximately 17 seconds after burner startup. At this time the maximum value of L di/dt of approximately 110 volts was obtained. From this point on arcing was occurring in the channel, causing a large dip in magnet voltage as can be seen at 26 seconds after burner startup. The net results of the test were a smooth transition from battery to generator, and further proof that it was necessary to have better control over the rate of magnet self-excitation and hence be better able to control the value of L di/dt.

Extreme arcing occurred on the anode wall. The worst damage was on the top and bottom of the electrodes where special edge pegs

were severely damaged as arcs had been driven deep into the wall so as to damage the stainless steel electrode support bars. It was determined that the arcs were initiated on the edge pegs, caused water leaks, and led to the breakdown. Since the electrical insulation of the edge pegs was not sufficient to meet the ΔV's which were occurring in the generator as the magnetic field strength was being increased, a program was set upon to completely insulate the edge pegs from the electrodes.

Analysis of the data showed that the test had been the best to date regarding total power output. A total power of 7400 kilowatts wa achieved, with 3850 kilowatts being in the magnet and 3550 kilowatts net power. This test indicated that it was necessary to have better control of the value of L di/dt, which could be done by several methods, such as controlling the length of the self-excitation or better still by switching loads in and out of parallel with the magnet. It was decided that a series of tests should be made in which the effects of magnet shunting could be found, using the previously installed switchgear. Since parallel operation of the electrodes in the net power section with the self-excitation section greatly reduces the danger of any arcing, it was decided to parallel the first 30 electrodes in the net power section.

Ten load resistors were each set at 0.305 ohms and set up such that five fixed loads could be connected in parallel with the magnet while the remaining five loads were installed such that they could be switched in and out of parallel with the magnet. The policy for this series of tests was to obtain a smooth transition in the magnet voltage between battery only and generator operation, and to stop the generator at 15,000 amperes magnet current.

Tests 16-20 were therefore conducted with a parallel loading configuration. Various lengths of self-excitation section and loading were utilized while the loading could be varied during the test by switching loads in and out of parallel with the magnet. For these tests the burner operating conditions were kept at a mass flow of 39.1 Kg/sec, a seed rate of 2 mole %, and an initial battery voltage of 156 volts, with the burner being fired when the magnet current reached a value of 2500 amperes. The most significant of these tests are Tests #18 and #20. The excitation characteristics for Test #18 are shown in Figure IV-9. The test was started with five switchable loads in parallel with the magnet. After a 10-second pre-excitation by the battery bank, the burner was ignited. The presence of this impedance was reflected in the low value of L di/dt immediately following burner ignition. Some of the shunt resistance was then switched out and the generator began to excite at a rapidly increasing rate. One shunt resistor was kept in until approximately 33 seconds when additional shunt resistors were again added to the extent that a negative L di/dt resulted as is shown in the figure when the magnet voltage curve drops below the IR curve. At this time some of the shunt circuits were opened and the generator showed a rapid excitation rate. When the magnet current obtained a value of 15,200 amperes (70% of the design maximum current), the burner was extinguished as had been programmed. The reason 15,200 amperes had been set as a maximum

for this test was that the magnet current and stresses exceeded those of any previous run, and it is not desirable to go too far with the excitation at a single step. Besides having attained a power output of 31,200 kilowatts with the test, the fact that L di/dt could be easily regulated using the proper shunt resistors was proven.

Figure IV-10 is a plot of the axial voltage distribution for the indicated electrode pairs measured during Test #19 and is plotted for three times during the test. From these curves it can be seen that the loading in the inlet section produces voltages which blend smoothly with the magnet voltage. The voltage on inlet electrode 1I to 6I varies directly as the magnetic field strength, but the voltage on electrodes 7I through 9I is influenced by a combination of magnetic field strength and L di/dt through a network of bleeder resistors interconnecting these electrodes. The voltage variation in electrodes 7I through 9I is therefore greatly affected by the value of L di/dt. This influence is most pronounced in the curve for 17 seconds where the L di/dt is a large percentage of the magnet voltage. Electrodes #1-30 are operated at the same voltage as the magnet since they are shorted to the self-excitation section. Electrodes #31-50 are operated open circuited. Since there exists a fringing effect of the current flow through the gas, the excess voltage which would be expected to exist on electrode #31 is spread out to the neighboring electrodes and hence a blending of voltage between #30 and #31 is obtained.

The excitation characteristics for Test #20 are shown in Figure IV-11. The generator operating conditions and start point are exactly the same as those used in Test #18, except that the number of shunt resistors connected at burner start are reduced and the loading configuration includes electrodes #1-50 in parallel with the magnet, while Test #18 used only electrodes #1-30 in parallel with the magnet. The figure shows smooth transition from battery to generator only operation. The curve of the magnet voltage demonstrates that the use of switchgear to shunt the magnet causes large changes in the magnet voltage. From the curve it can be seen that at 18 and again at 20 seconds loads were removed from the circuit in parallel with the magnet. This is indicated by the instantaneous rise in magnet voltage. Upon removal of these loads the rate of generator self-excitation increases rapidly. The smooth excitation continues to approximately 30 seconds, at which time an electrical breakdown caused a sudden drop in the magnet voltage. The power dissipated elsewhere in the channel as the result of the electrical breakdown promotes a decrease in L di/dt and hence degrades the entire generator performance.

At this point in the program the most serious problem was the high voltage gradient between the last working electrode in the self-excitation section and the first electrodes in the net power section. Several methods besides loading were investigated to minimize this problem, but the best was to cool the gas boundary layer in this critical junction and thus present a high electrode drop which must be overcome before arcing can occur. This method removed the refractory materials which filled the grooves of electrode pairs 9sx and #1 (see Figure II-D1), and then the

grooves were filled with solid metal and hence became flat copper electrodes. The net result of this change was an increase in heat transfer by virtue of the increased heat conducting surface exposed to the working fluid, which resulted in a lower boundary layer temperature and a correspondingly higher breakdown voltage between electrodes.

The following tests were devoted to obtaining an ever smoother generator startup and eliminating the arcing problem between the self-excitation section and the net power section, while operating the net power section in a segmented configuration.

Power Test #21 was run at a mass flow of 38.7 Kg/sec, with the battery voltage reduced from 156 to 120 volts, and the main burner being started when the magnet current attained a value of 2000 amps. A bleeder network was installed between the self-excitation electrodes and the first six working electrodes in the net power section. Resistors used to shunt the magnet for the control of L di/dt were removed from the test hookup, since the generator would start at lower field strength and the value of L di/dt would be low. A smooth transition was achieved, and L di/dt was approximately 100 volts when the test was stopped at 5500 amperes. Figure IV-12 shows the transverse voltage distribution as a function of channel length. As can be seen, there is a sharp decrease in output voltage occurring in the middle of the net power section. This sharp voltage drop and hence poor performance may be attributed to the introduction of water into the gas stream. The result of this voltage distribution and hence large voltage gradients along the electrode walls is arcing.

The results of several tests indicated that a lower battery voltage would insure a smoother transition from battery only to generator only operation; a bleeder network installed at the critical junctions of each end of the self-excitation section would eliminate arcing, and that the channel must be perfectly watertight to obtain reliable generator performance.

This series of tests was plagued by minor difficulties, such as individual water leaks in the channel, plugged fuel nozzles, and the presence of eddy currents in the downstream end of the net power section. However, the critical junctions of the generator at both ends of the self-excitation section operated satisfactorily.

The most significant of these tests was Test #28, in which the switching was again used to shunt the magnet and control the excitation rate. The excitation characteristics for Power Test #28 are shown in Figure IV-13. This figure shows that two shunts were added to the magnet circuit at 14 and 18 seconds and were removed at 43 and 47 seconds. The magnet current reached a maximum of 7700 amperes and L di/dt was 60 volts when the collapse occurred initiating shutdown. The net power output for this test was approximately 5000 kilowatts and no arcing was experienced in the junction between self-excitation and net power section.

The program had now reached the level of progress where it was felt that a sufficient knowledge of the generator startup had been attained, and that self-excitation of the generator could easily be attained without the occurrence of arcing in the critical junctions of the self-excitation sections. Sufficient experience in magnet shunting to control L di/dt was obtained, and during the process a good knowledge of proper loading techniques for the net power section had been obtained. The goals of the program were now within reach, so the remainder of the program may be considered as power testing to achieve rated generator performance.

C. POWER GENERATION

In conducting the net power tests the generator starting conditions were fixed to be an initial battery voltage of 120 volts, burner firing point of 2000 amperes, and every electrode in the net power section individually loaded. In addition, the mass flow was kept constant at 46.4 Kg/sec, with a seed rate of 2 mole % Potassium. These conditions were not changed until the latter part of the testing program where new conditions are then noted.

The first test in the new series presented the most critical problem encountered in the program. Special voltage monitoring systems showed that during the test there occurred a voltage collapse and severe arcing in the region of electrodes 20 through 40. It was felt that the loading pattern had not been properly selected and that arcing had been initiated causing water leaks and hence the collapse.

The loading for the next test was adjusted and again the voltage collapse, accompanied by arcing, was experienced. The potential difference at which the collapse occurred was identified to be in the region of 25 to 30 volts per electrode spacer. Figure IV-14 shows the transverse voltage distribution for two different magnet currents, one just prior to, the other just after the collapse. During this test the generator excitation rate was less than expected, and a thorough investigation and checkout of all generator components and control systems revealed water leaks in the joint between the channel inlet flange and burner nozzle. This explained poor generator performance and since the leaks were on the anode side, another test was necessary in which no water leaks occurred to identify the arcing problem. The test was made duplicating previous conditions only with no water leaks in the channel. Again the voltage collapse occurred at exactly the same voltage gradient.

Since the electrodes could not withstand a ΔV of more than 25 volts, it was decided to improve the electrical characteristics of the anode wall by modifying the electrodes. The modification made was as described in Section II of this report.

Water leaks in the channel inlet section plagued the next series of tests. These water leaks were of sufficient magnitude so as to shield the downstream end of the net power section such that no voltage output could be developed. Some slight arcing was now experienced on the cathode wall, but the modified electrodes on the anode did not arc and appeared to be in excellent condition.

Upon repair of the inlet section another test was made and once again the voltage collapse occurred. However, no damage was experienced in the channel, no water leaks could be found and the excitation rate was good with a value of L di/dt of 100 volts remaining when the test was stopped.

With the conclusion of this test all factors indicated that the voltage collapse experienced was the result of recirculation of cooling water used to quench the exhaust gas. The theory of such an occurrence is well known; however, prior to this test the other problems had not been eliminated and the problem could not be placed on recirculation.

From the pressure distribution it was evident that fluid in the channel was being expanded to a pressure less than that of the exhaust system, and due to this overexpansion of the flow, a shock induced boundary layer separation occurred. Since pressure taps are located in one insulating wall, the location of the separation point on the electrode walls can be better found using electrical test data. From published aerodynamic data it was found that separation of the jet from the wall would occur whenever the channel (nozzle) pressure is approximately 0.38 to 0.40 of the exhaust pressure.*

The flow separation is the result of the shock and boundary layer interaction, which creates a region of oblique shocks with regular or Mach type reflections proceeding downstream while the flow remains supersonic. The fact that the flow remains supersonic and therefore that only oblique shocks exist has been verified by the channel voltage distributions, as can be seen in Figure IV-14. The pressure gradient from the shock location to the exhaust duct allowed water vapor to mix with the separated flow, which recirculated creating a layer of relatively cold non-conducting gas which effectively shielded the electrodes. Presumably, as the output power increases, the flow Mach number decreases, causing a pressure rise which would relieve the separation. However, before sufficient power could be developed to raise the static pressure, water has recirculated, derating the operation. In an effort to move the separation point from the power section to the exit section, mass flow was increased from 39.1 Kg/sec to 47.8 Kg/sec, resulting in moving the separation point from electrode #18 to electrode #25 (see Figure IV-15). After changing the mass flow, arcing, which was usually concentrated near electrode #18, began at electrode #25. To move the separation point out of the power section by increasing mass flow

*M. Arens and E. Spiegler, AIAA Journal, Vol. 1, No. 3, March 1963.

required mass flows in excess of the original design conditions, and so other means of moving the separation point and eliminating water were investigated.

It appeared the simplest solution was to eliminate the water by modifying the transition section and channel cooling water discharge system. While design of such an apparatus was underway, testing was continued by temporarily modifying the channel cooling water discharge and by adding a simple spray cooled extension to the existing cylindrical transition section. Results of this test were encouraging as no voltage collapse or arcing was experienced. Tests using the modified transition section were terminated due to overheating of the spray cooled transition section.

A new transition section was made to prevent cooling water from entering the channel and act as a diffuser for the supersonic flow, allowing for a controlled pressure recovery between the channel and exhaust duct. The transition section matches the shape of the channel exit, is water-jacketed, and approximately four channel diameters long. For the supersonic flow a constant cross section rather than a converging diffuser was made. The reasons for this were ease of constructing a rectangular duct, and most important, the possibility of inducing a normal shock in the diffuser was practically eliminated so that a really good diffuser was not required. In order to design a converging diffuser for a separated supersonic flow, many tests would have been required to compile significant design data; this in itself being time-consuming and costly. For the small decrease in efficiency, a constant cross section diffuser was deemed the best for the purpose. A comparison of the pressure distributions before and after installation of the diffuser is shown on Figure IV-16. It is seen that the addition of the diffuser shifts the point of separation well downstream of the net power section, eliminating recirculation of cooling water on the electrodes.

Upon installing the diffuser, the separation problem became unimportant to the generator performance and no further difficulties in this vein were experienced for the remainder of the testing program.

Power Test #40 was the first test performed with the water-jacketed channel extension duct. The test was conducted under identical conditions to those which existed in previous tests. The data revealed that the separation point was moved further downstream, the excitation was good, and the output voltage and the open circuit voltage came up as expected in the exit section.

The test was stopped due to arcing between external steel support bars on the exit section of the channel to the magnet. The maximum magnet current was 7500 amperes, and the L di/dt at the end of the test was 110 volts.

The damage to the generator was minor; however, the material for the support bars on the exit section of the channel was changed and the damage to the magnet was repaired.

For the next series of tests the mass flow was increased to 47.8 Kg/sec to insure that the separation point was located outside of the net power section as the load was increased. The test configuration was the same as in Test #40, with the exception that the last three inlet electrodes were connected to the self-excitation section to increase the rate of excitation. The test was stopped at a magnet current of 8700 amperes due to the failure of a cooling water fitting on the channel extension duct. The rate of excitation was markedly improved despite the existence of slight water leaks in the top wall of the inlet section.

The next tests were conducted using identical testing conditions. The tests were each stopped when external arcing occurred in the exhaust system. The overall performance of the tests was derated by these external arcs, and the electrical insulation in the exhaust system was further improved for each test. During Test #45 arcing was experienced between copper slabs in the electrode walls of the exit section. To improve the insulation in this region the width of the refractory grooves was increased.

For these tests the loading was adjusted slightly to optimize net power output. The maximum magnet currents attained were between 9200 and 10,000 amperes. Figure IV-17 shows the best excitation rate achieved, with 120 volts L di/dt remaining when the test was discontinued.

A maximum magnet current of 12,200 amperes was achieved in the next test which was stopped at this point due to a decrease in the excitation rate. Severe damage from arcing was experienced on both "electrode-type walls" (see Figure II-2) in the exit section as well as between electrodes on the negative wall of the power section. The breakdown in the end of the exit section occurred at a voltage gradient along the electrode wall of 1600 volts per meter, or approximately 80 volts per insulator. The results of this test showed that the widening of the refractory grooves was not sufficient to prevent arcing and to bring the generator to rated performance, so to further improve the insulating capabilities of the wall, a finer segmentation of the "electrode" wall in the exit was made by splitting the copper slabs in the end of the exit section where the voltage gradient was the highest. At the same time the channel extension duct was insulated from the channel to remove the dead short across the insulating walls.

Test #47 reached a magnet current of 11,800 amperes where the test was stopped due to slow excitation. The slow excitation was caused by water leaks in the inlet section; however, no arcing was experienced in the entire generator. This was the highest magnet current attained without experiencing arcing in the channel.

To further increase the power output and lower the Hall voltage, Tests #48 through #50 were performed with an increased seed rate of 2.38 mole %, while keeping mass flow and loading the same as in previous tests. Test #49 was stopped at a magnet current of 10,800 amperes at which time instabilities in voltage output occurred. No arcing occurred on electrode walls, but there were indications of minor arcs on the insulating walls. After cleaning the channel and repairing refractory, Test #50 was performed which achieved a magnet current of 12,800 amperes, as can be seen in Figure IV-18. The test was stopped when a decrease in the rate of excitation was observed, caused by water leaks developing in the channel at a magnet current of approximately 9000 amperes.

Inspection of the channel after the test revealed no damage to the electrode walls, but arcing had occurred in the insulating walls. The arced region was from the end of the self-excitation section anode wall to the end of the net power section cathode wall. Figure IV-19 is a diagram showing the voltage distribution in the power and exit sections. The voltage across the arced region is 2900 volts and is equivalent to 88 volts per insulation in the insulating wall, a value exceeding the design conditions because of a high value of $\omega\tau$ caused by the overexpanded flow.

Figure IV-20 is a diagram showing power vs magnet current for Test #50. The power level in the end of the test was 14,000 kilowatts net and 19,200 kilowatts gross, which was the highest power level achieved at that time. Predicted power is also shown in Figure IV-19, the difference between expected and actual power being caused by the water leaks and arcing.

The capability of the insulating walls to withstand higher voltages was improved by increasing the distance between pegs as described in Section II.

In order to reduce the voltage gradients in the channel and to increase the excitation rate, a fuel mixture of 50% ethyl alcohol and 50% methylcyclohexane was used for further testing. The properties of methylcyclohexane compare closely to JP-4 with the exception that methylcyclohexane will mix with seeded alcohol while JP-4 will not. For a corresponding mass flow, this new fuel mixture has a 20% higher heat release and a higher stagnation temperature and in turn higher conductivity. For this reason, the internal resistance of the channel is lowered, so the external loads must be reduced to maintain matched loading. The external loads for the same power level draw a higher current which causes a lower transverse voltage but a higher Hall voltage. The net effect is a decrease in the channel voltage gradients since the increase in Hall voltage is less than the decrease in transverse voltage.

The test was conducted using a mass flow of 47.8 Kg/sec of fuel oxidizer mixture, 1.3 mole % seed, 120 volts on the battery bank, and a burner start at 1700 amperes magnet current. Starting at a lower magnet

current was done to eliminate voltage peaks in the startup due to the expected increase in excitation rate. Figures IV-21 and IV-22 show the excitation characteristics and power vs magnet current for Power Test #51. The test was highly successful in that the excitation rate was as expected and a net power output of 19,100 kilowatts was achieved at a magnet current of 12,800 amperes. The gross power output was 24,300 kilowatts. The improvement in the electrical properties of the gas is evident in that a magnet current of 12,800 amperes was achieved at time 28 seconds, while in Test #50, 12,800 amperes was not achieved until approximately time 52 seconds. The rate of self-excitation experienced in this test produced L di/dt's as high as 240 volts and there still remained 193 volts L di/dt when the test was stopped. The test was stopped at 12,800 amperes due to an external flash in the exhaust system. Water leaks had developed in the channel inlet section and every indication was that the performance was being derated by these leaks. No arcs were experienced in any section of the channel.

Tests 52-55 were conducted under conditions similar to those of Test #51. However, due to water leaks and other minor problems, the net power achieved in Test #51 was not equalled, although the magnet was excited to higher field strengths.

Test #56 was performed with a mass flow of 52.3 Kg/sec, 1.5 mole % seed, and a loading pattern and battery voltage identical to those of Test #51. The maximum net power for this test was 23,600 kilowatts with a maximum gross power of 32,000 kilowatts.

Figure IV-23 shows power as a function of time for the entire test. At the time 6.1 seconds the main burner was ignited. At 8.1 seconds the generator overtook the battery bank and from there on the generator was self-excited. The gross power output increased rapidly until the maximum was attained. Since the magnet is of heat sink design, the coil temperature increases with time resulting in a higher magnet impedance. This higher magnet impedance causes a lower magnet current, therefore a lower magnetic field, and in turn, less gross power output.

Figure IV-24 shows the excitation characteristics which reveal this test to have the most rapid excitation of any test in the entire program. The maximum value of L di/dt was controlled by shunting the magnet so as not to exceed a value of 250 volts. As can be seen in Figure IV-24, the magnet voltage reaches a maximum 15 seconds after burner start and L di/dt goes to zero at the time 30 seconds after burner start. At this time the maximum magnet current of 19,000 amperes was obtained corresponding to field strengths of 31,500 gauss. After having reached this value a slight dropoff in magnet current can be seen. This is also due to the previously described ohmic heating.

Figures IV-25 and IV-26 show current and power densities respectively, for various magnet currents. The change in slope of the power and current density plots with increasing magnetic field is due to

changes in the local gas velocity. As the magnet current increases more power is generated and the resulting drag reduces the gas velocity; however, internal joule dissipation and increased pressure result in increased conductivities so that the change in slope of the power and current density curves is slow until the MHD body forces become dominant over the other variables. The rise in the curves from electrode #45 on is due to the loading pattern required to blend the voltage of the last loaded electrode with the open circuit voltage of the exit section.

Figure IV-27 is a typical pressure distribution taken at 16,000 amperes magnet current. The minimum pressure at the time shown is 0.51 atm and this point is located outside of the working section of the channel. It can also be seen that there is sufficient pressure drop available to obtain higher current densities.

The transverse voltage distribution for electrode #21 at a magnet current of 16,500 amperes is shown in Figure IV-28. The shape of this diagram is typical of the voltage distribution throughout the generator. The output voltage for this magnet current is 870 volts. The figure shows that if losses associated with electrodes could be eliminated or reduced a substantial increase in voltage (hence, net power output) would be attained. The losses in this case are approximately 150 volts with 130 volts being on the anode with 20 volts on the cathode side. These "electrode drop" losses are higher than what would be normally expected, but water leaks, upstream on the anode wall, produce the large difference experienced from anode to cathode. The linear portion of the diagram, which traverses the major portion of the channel width, is a direct reflection of the internal impedance and hence the electrical conductivity of the gas.

Figure IV-29 depicts a typical voltage distribution throughout the net power and exit section. The voltage for the anode, cathode and channel centerline is shown, together with the output voltage at a magnet current of 19,000 amperes.

The voltages are measured with respect to ground (in this case, the burner) while the output voltage is measured across the electrode pairs. Hence, the voltage between the anode and cathode lines is the output voltage. After electrode pair #50, the voltage is shown open circuit voltage which accounts for the sharp change in slope of the curves at this point. The maximum voltage gradient is 1650 volts/meter on the cathode wall while the maximum voltage to be withstood is between electrode #2 on the anode to electrode #50 on the cathode which for this case is 2600 volts.

Figures IV-25 and IV-26 illustrate the impulse mode of operation for the Mark V, which was found to perform beyond the design reaction configuration during the test program. The new mode of performance is particularly evident in the power density distribution shown in Figure IV-26. It will be noted in Figure IV-23 that the net power output rises to a maximum at a time of 21 seconds at which time the magnet current is about

15,600 amps, which is substantially less than the design value of 22,000 amperes and corresponds to a magnet power dissipation of about one-half the design value. It is noted from Figure IV-23 that the net power output actually decreases when the magnet current goes above 15,600 amps, and that the best operation would be achieved at the lower magnet current.

The power density of an MHD generator is proportional to the product of the gas density and the square of the gas velocity. Where the combustion gases are used in the Mark V generator, the peak value of the power density occurs at a Mach number slightly below 2. The Mark V generator was designed for maximum flow number of Mach 1.2 at the design condition. The net output of the power section was calculated using gas inlet conditions at the power section corresponding to those which were obtained with the design current of 22,000 amps in the magnet. No calculations of the power section were made for magnet currents below the design value.

With a magnet current lower than the design value the MHD drag on the gas in the excitation section is much less than that predicted. Thus, instead of entering the power section at a Mach number of about 1.1, as was the case with the original design, the flow enters the power section at a Mach number close to 1.7 or 1.8, with a greatly increased power density for a given magnetic field as compared with the design condition. The flow is then decelerated in the power section, the power output being extracted mainly from the kinetic energy of the flow. Figure IV-16 illustrates this very well. At the most efficient magnet current of 15,600 amps, the power density is very high at the generator inlet, and drops through the power section due to the decreasing velocity. At lower magnetic field strengths the power density is relatively flat, due to the fact that the velocity increases while the conductivity drops in the power section. Had the generator been operated in the design mode of operation, that is to say roughly constant velocity, the power density throughout the power section would have approximated that at the exit of the power section in the actual impulse mode of operation, which is only about 60% of the peak power density that was actually attained.

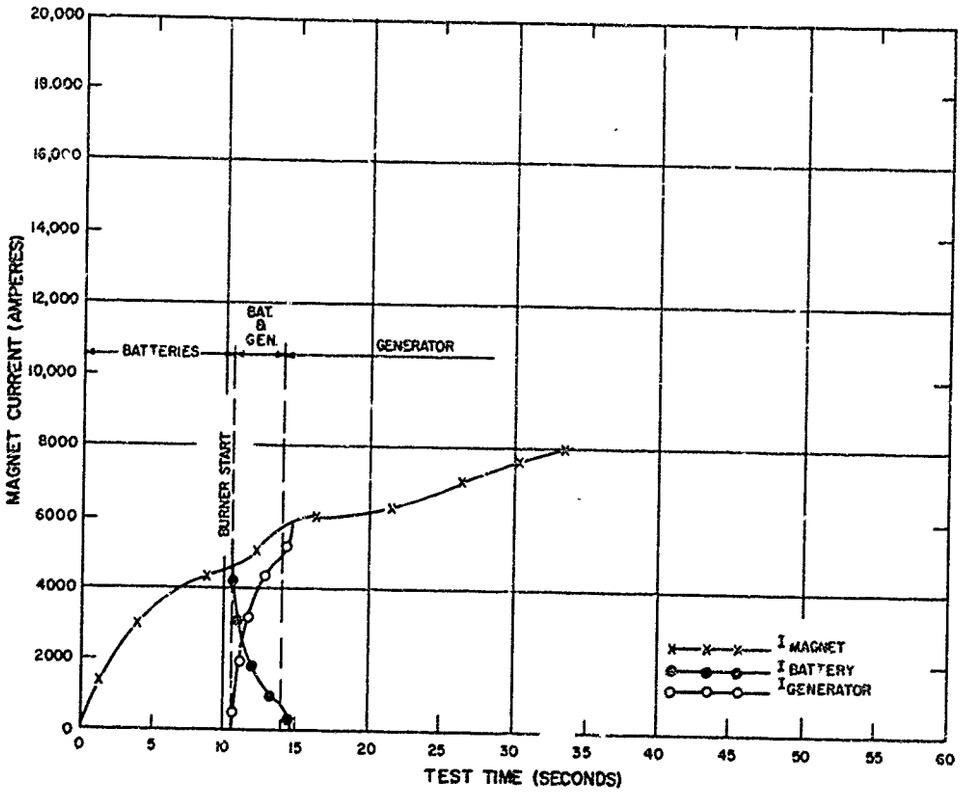

Figure IV-1 Magnet Current vs Time for Power Test #3

A4478

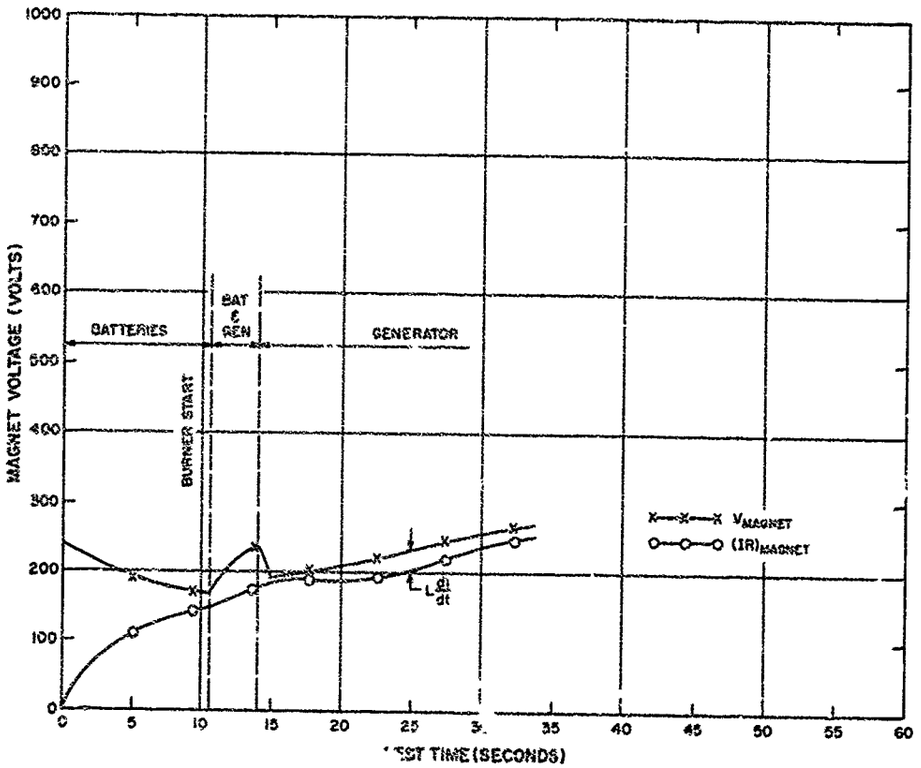

Figure IV-2 Magnet Voltage vs Time for Power Test #3

A4572

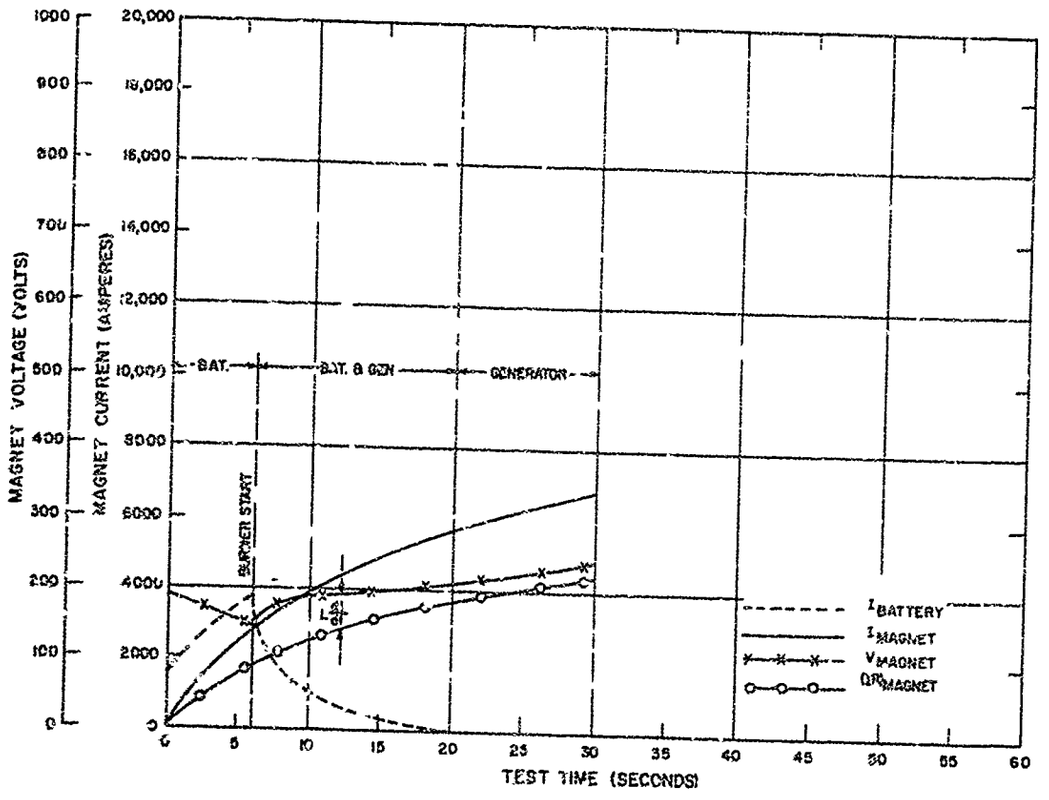

Figure IV-3 Excitation Characteristics for Power Test #6

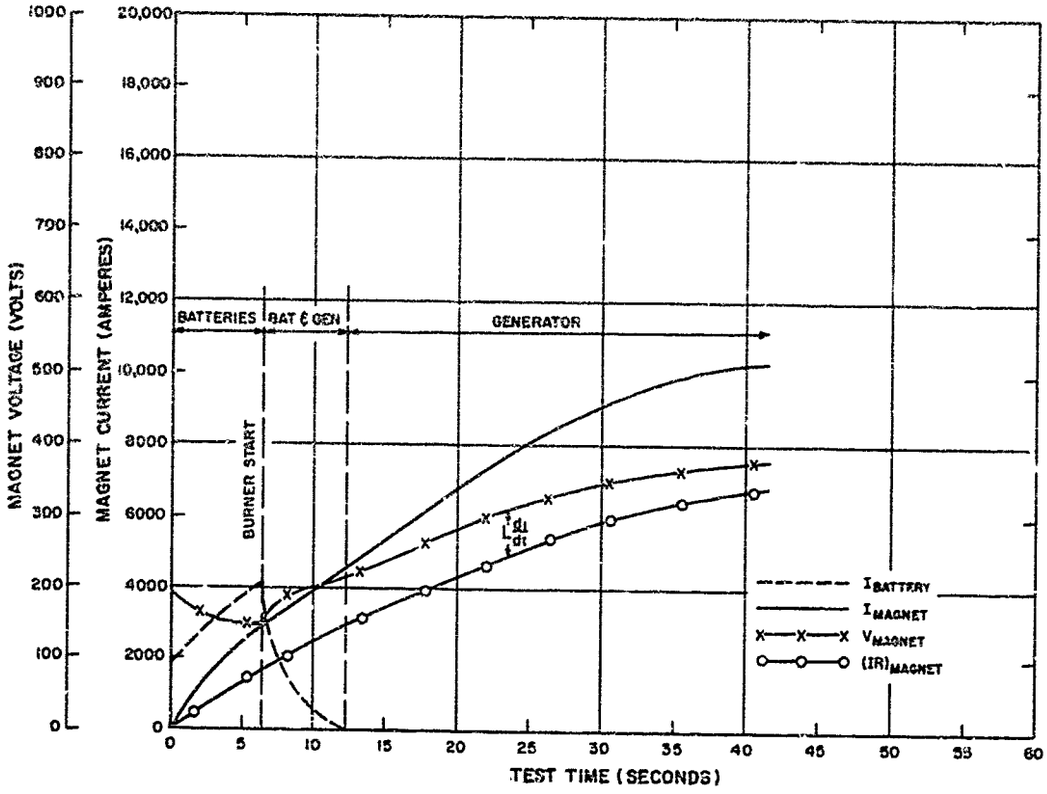

Figure IV-4 Excitation Characteristics for Power Test #10

A4478

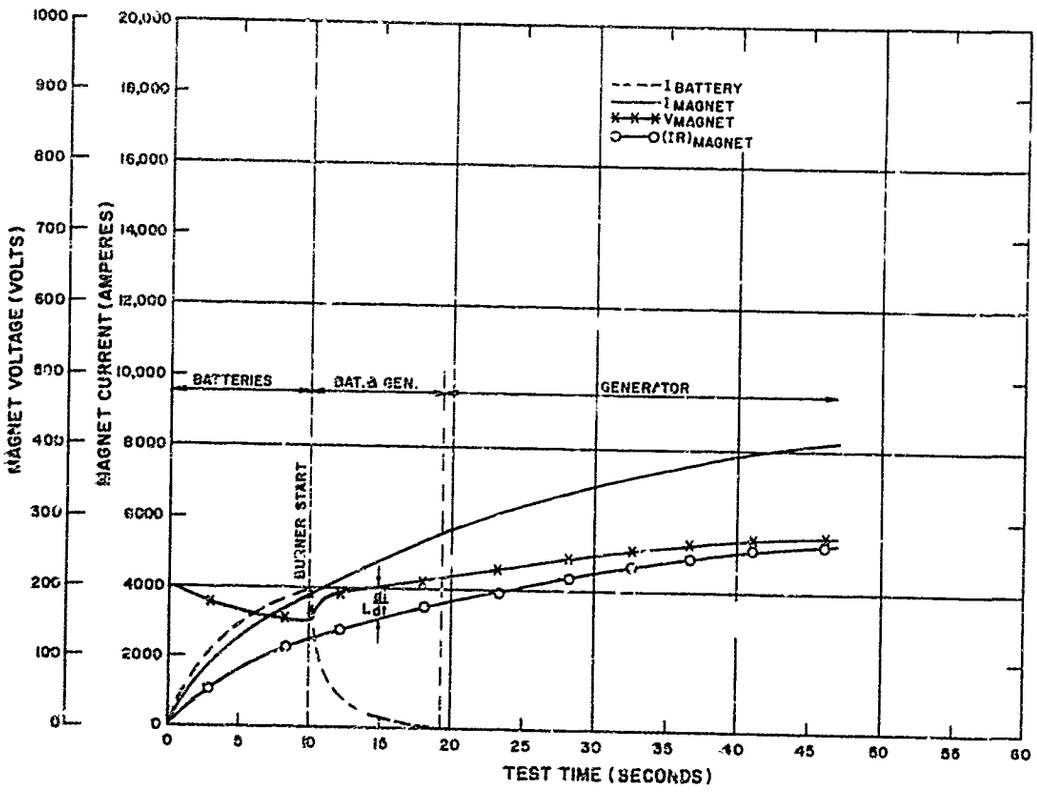

Figure IV-5 Excitation Characteristics for Power Test #13

A4470

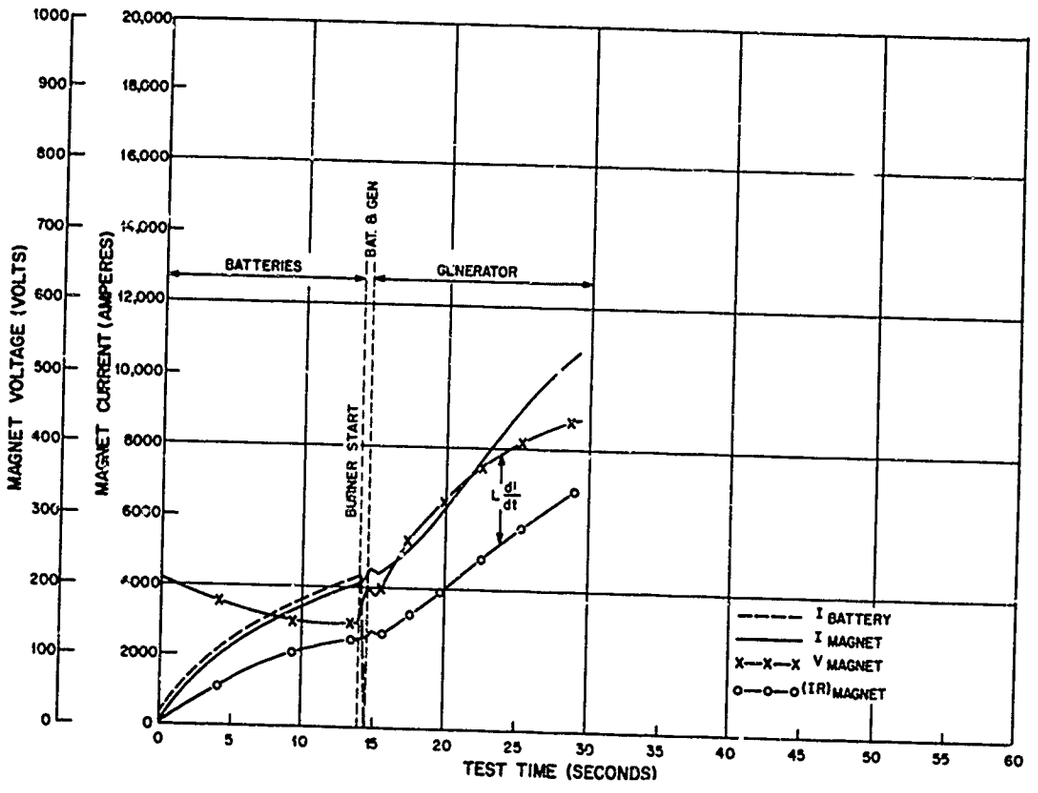

Figure IV-6 Excitation Characteristics for Power Test #14

A4469

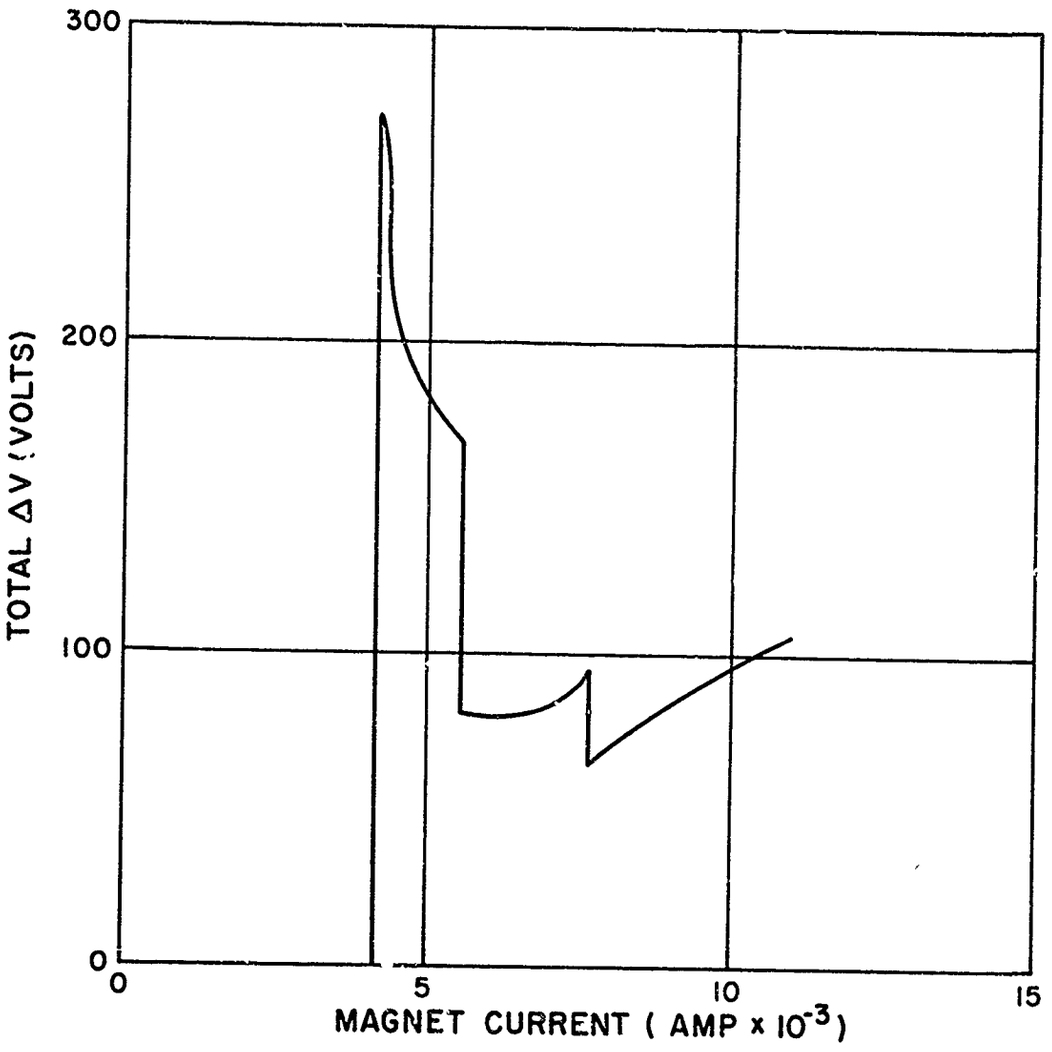

Figure IV-7 ΔV Between Self-Excitation and Electrode #2 for Power Test #14

A2664

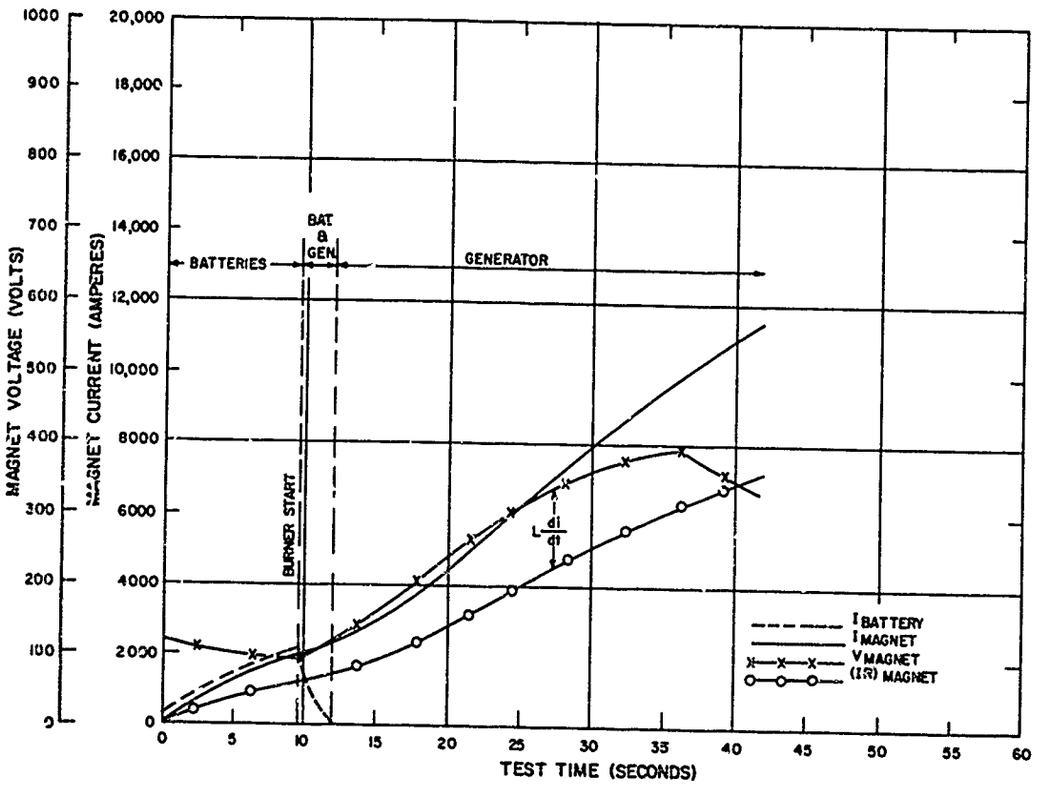

Figure IV-8 Excitation Characteristics for Power Test #15

A4466

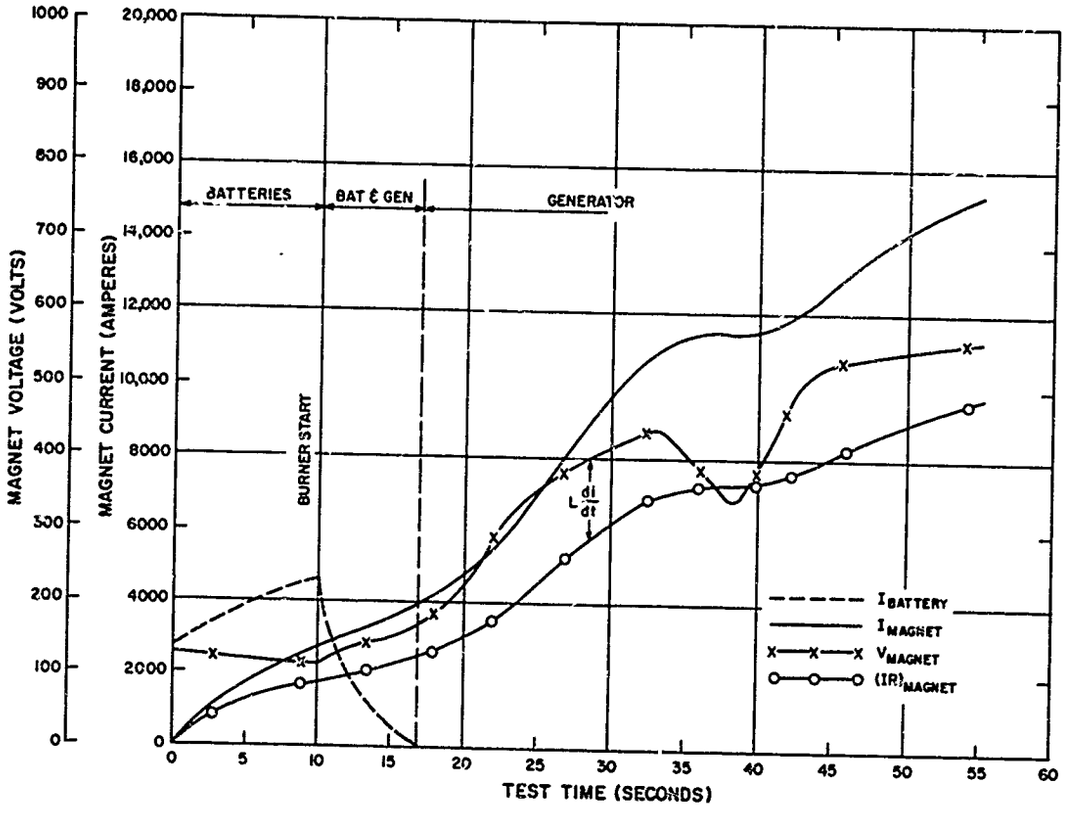

Figure IV-9 Excitation Characteristics for Power Test #18

A4438

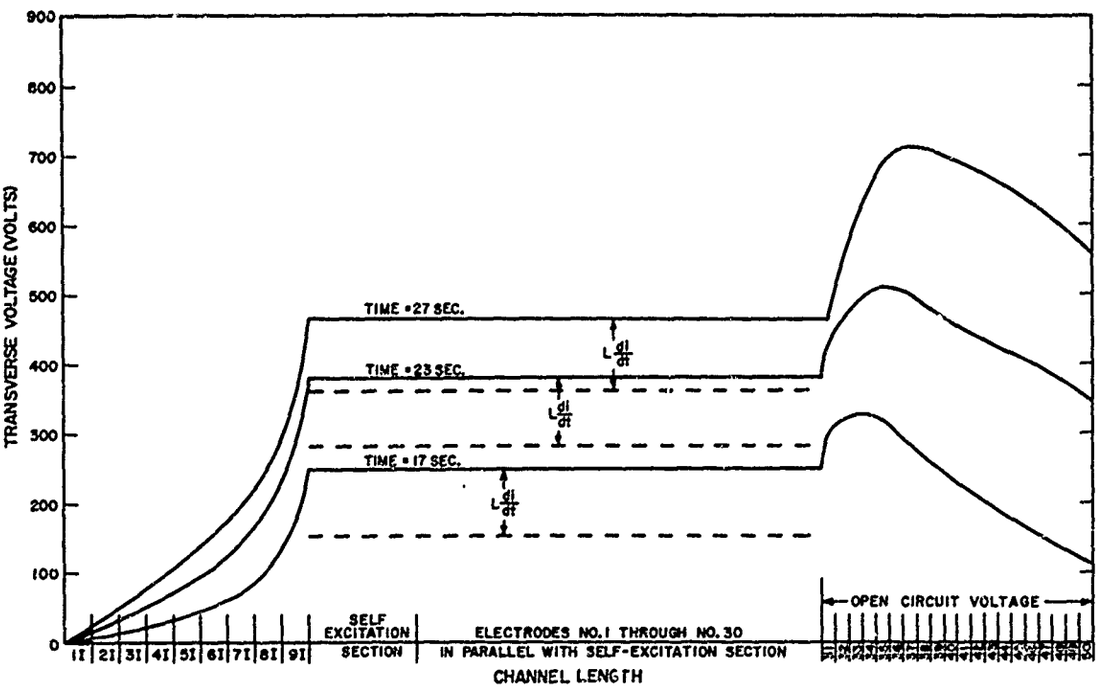

Figure IV-10 Transverse Voltage Distribution for Three Different Times During Power Test #19

A2654

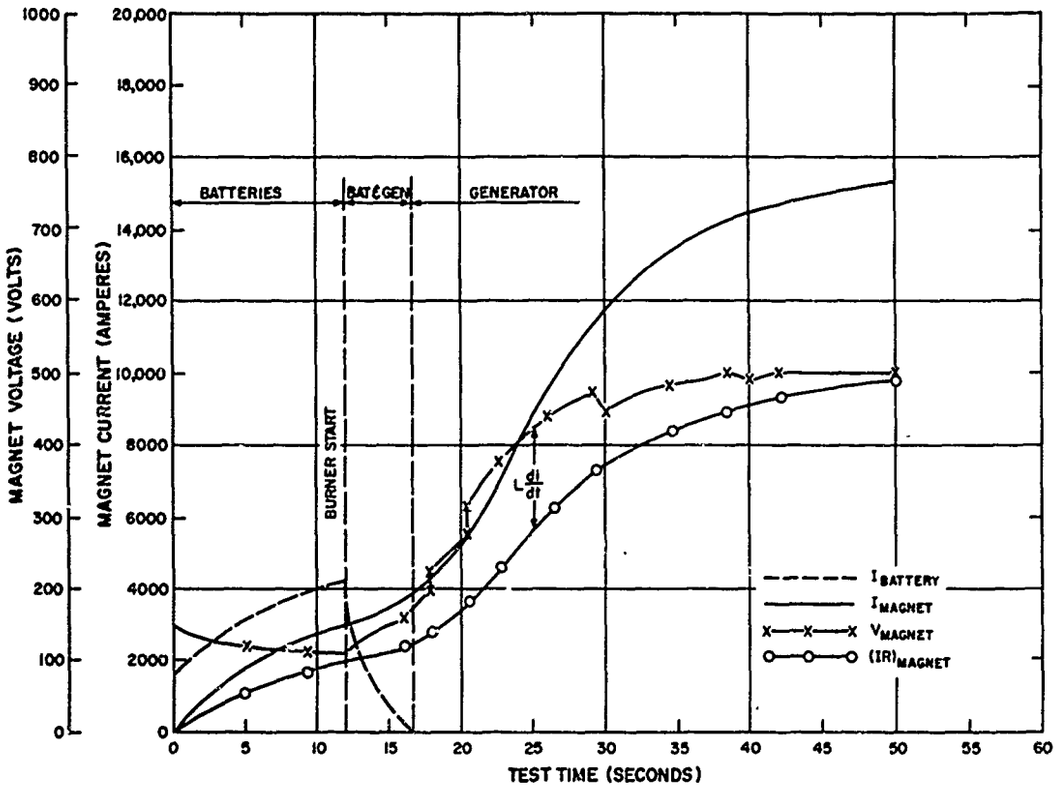

Figure IV-11 Excitation Characteristics for Power Test #20

A4471

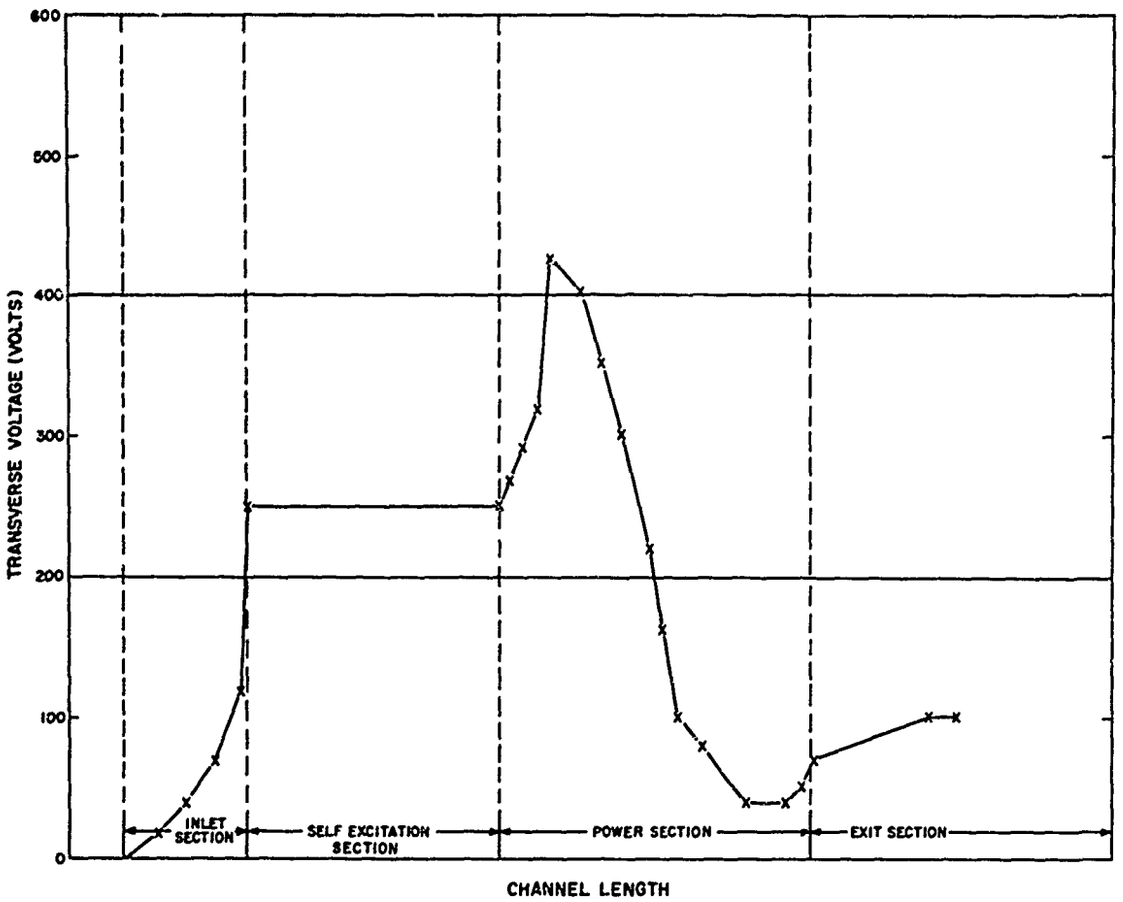

Figure IV-12 Transverse Voltage Distribution as a Function of Channel Length in Power Test #21

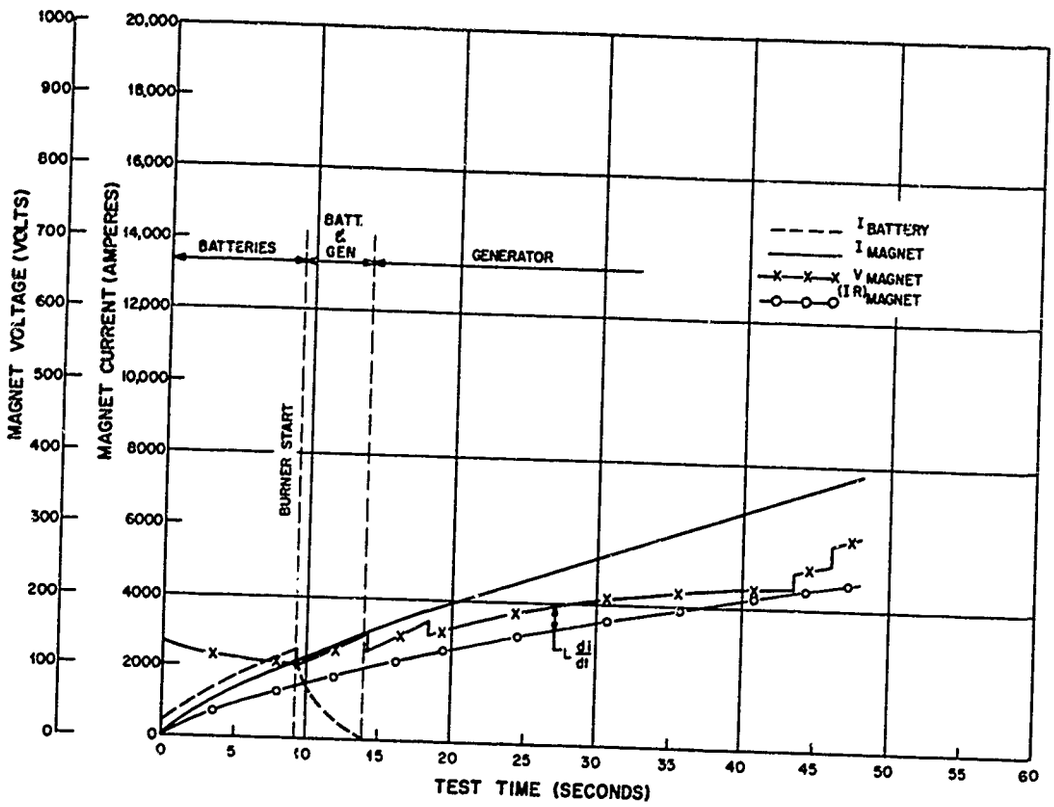

Figure IV-13 Excitation Characteristics for Power Test #28

A4475

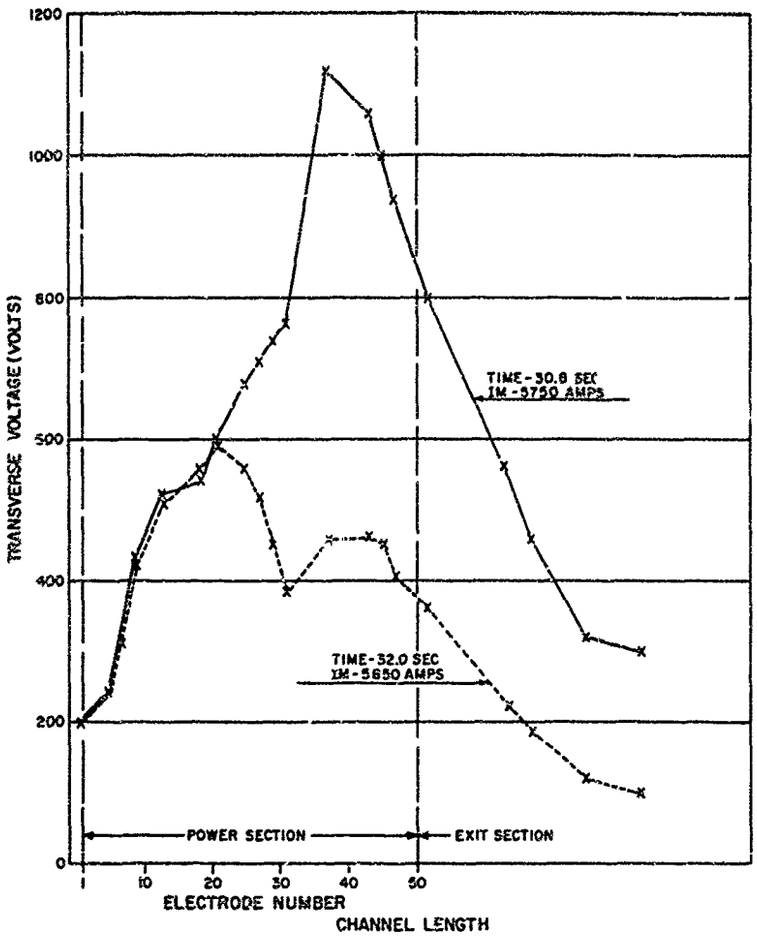

Figure IV-14 Transverse Voltage for Two Different Magnet Currents (Before and After Collapse)

A2814

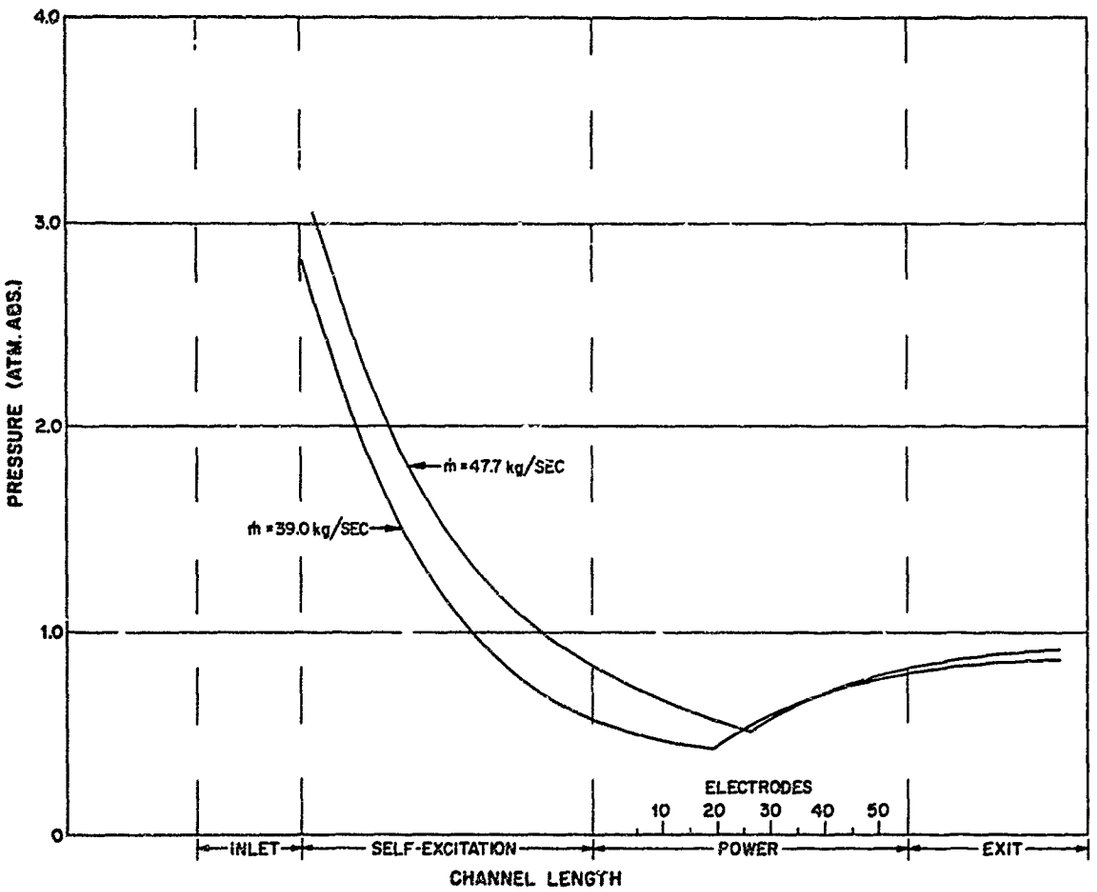

Figure IV-15 Static Pressure vs Channel Length Showing the Moving of the Separation Point by Changing Mass Flow

A3677

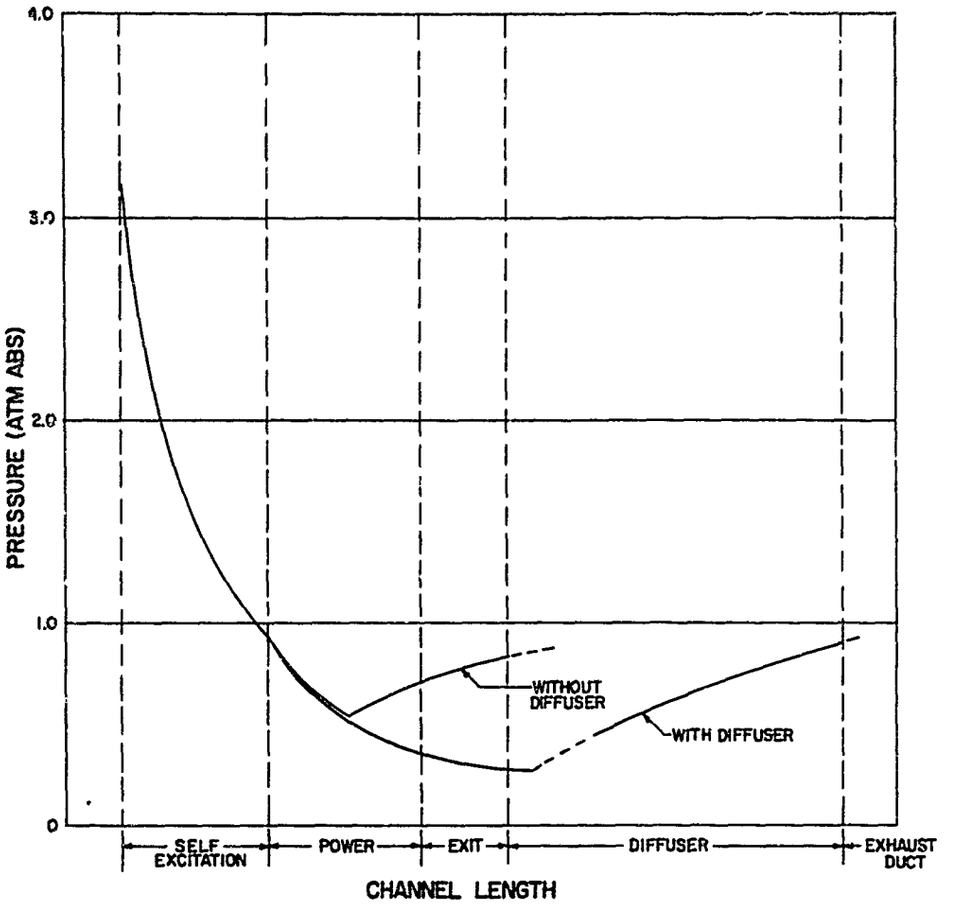

Figure IV-16 Static Pressure vs Channel Length Showing the Location of the Separation Point Before and After Installation of Diffuser

A4454

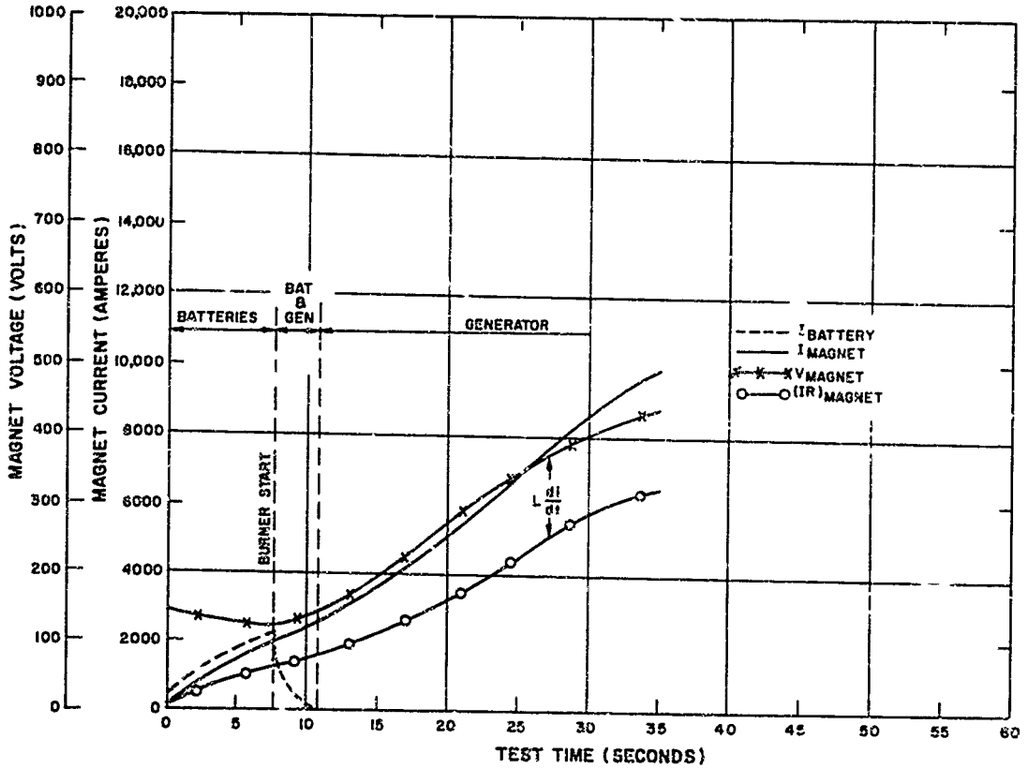

Figure IV-17 Excitation Characteristics for Power Test #45

A4474

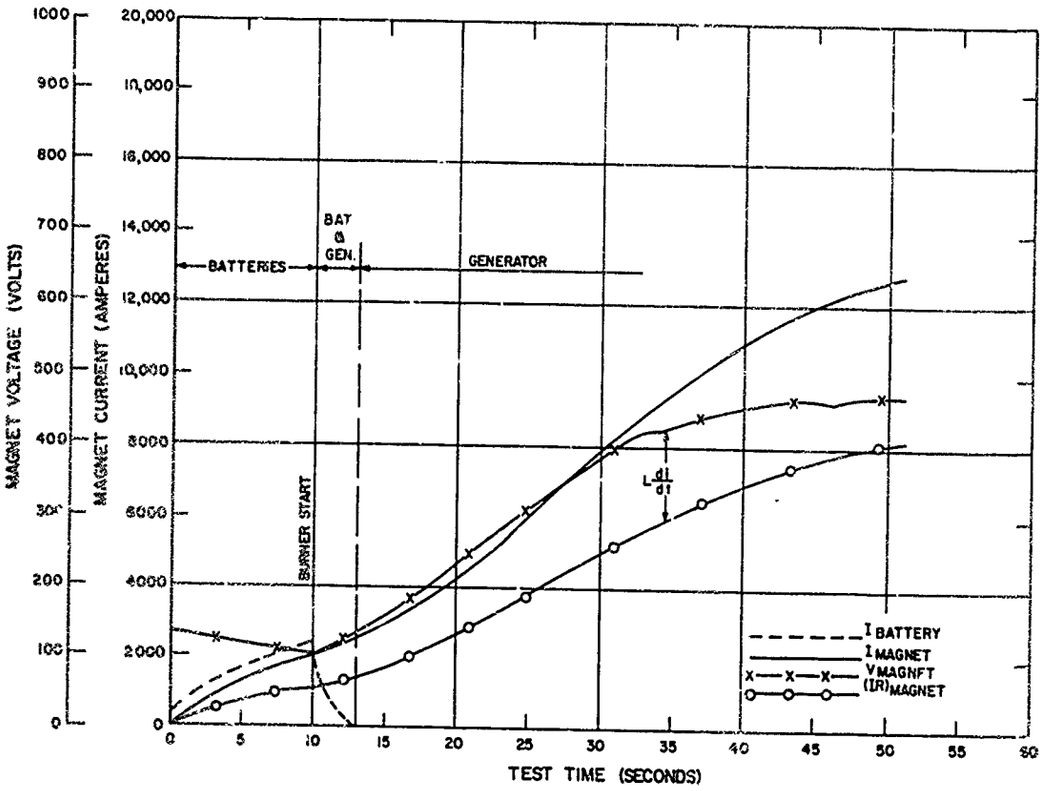

Figure IV-18 Excitation Characteristics for Power Test #50

A6484

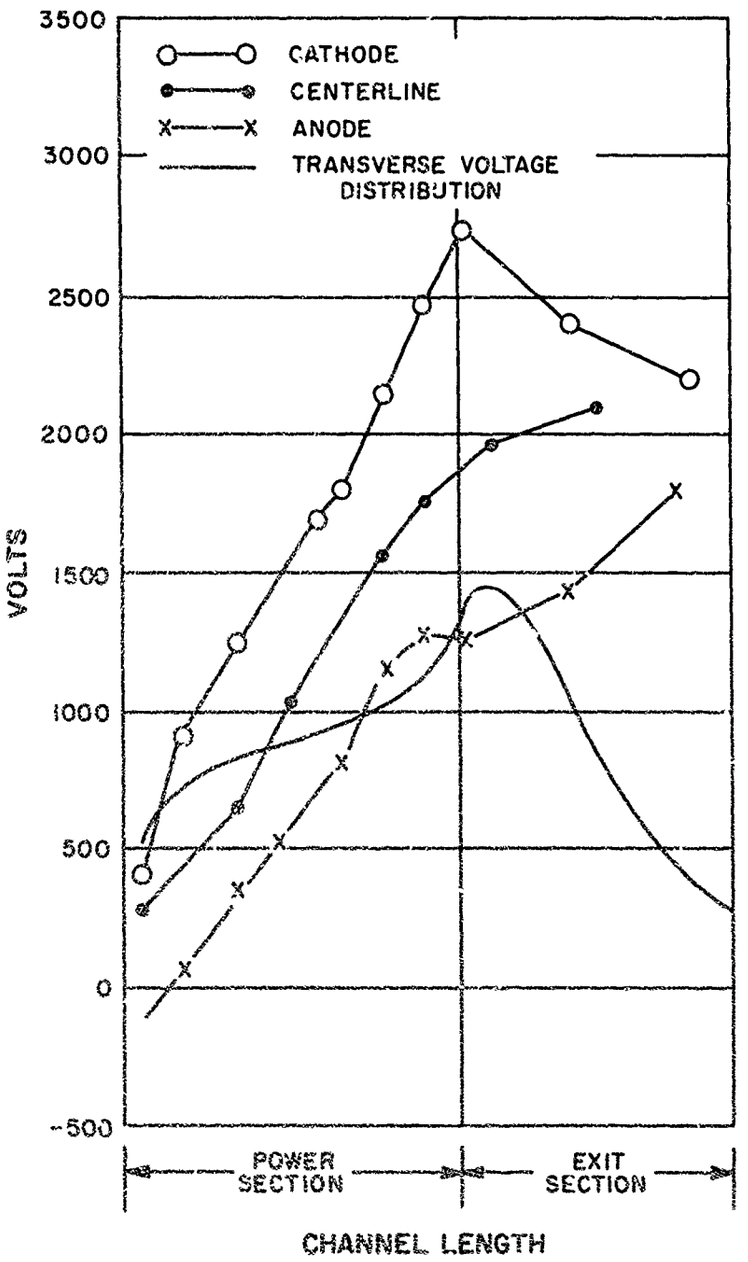

Figure IV-19 Voltage Distributions in the Net Power and Exit Sections for Power Test #50

A6433

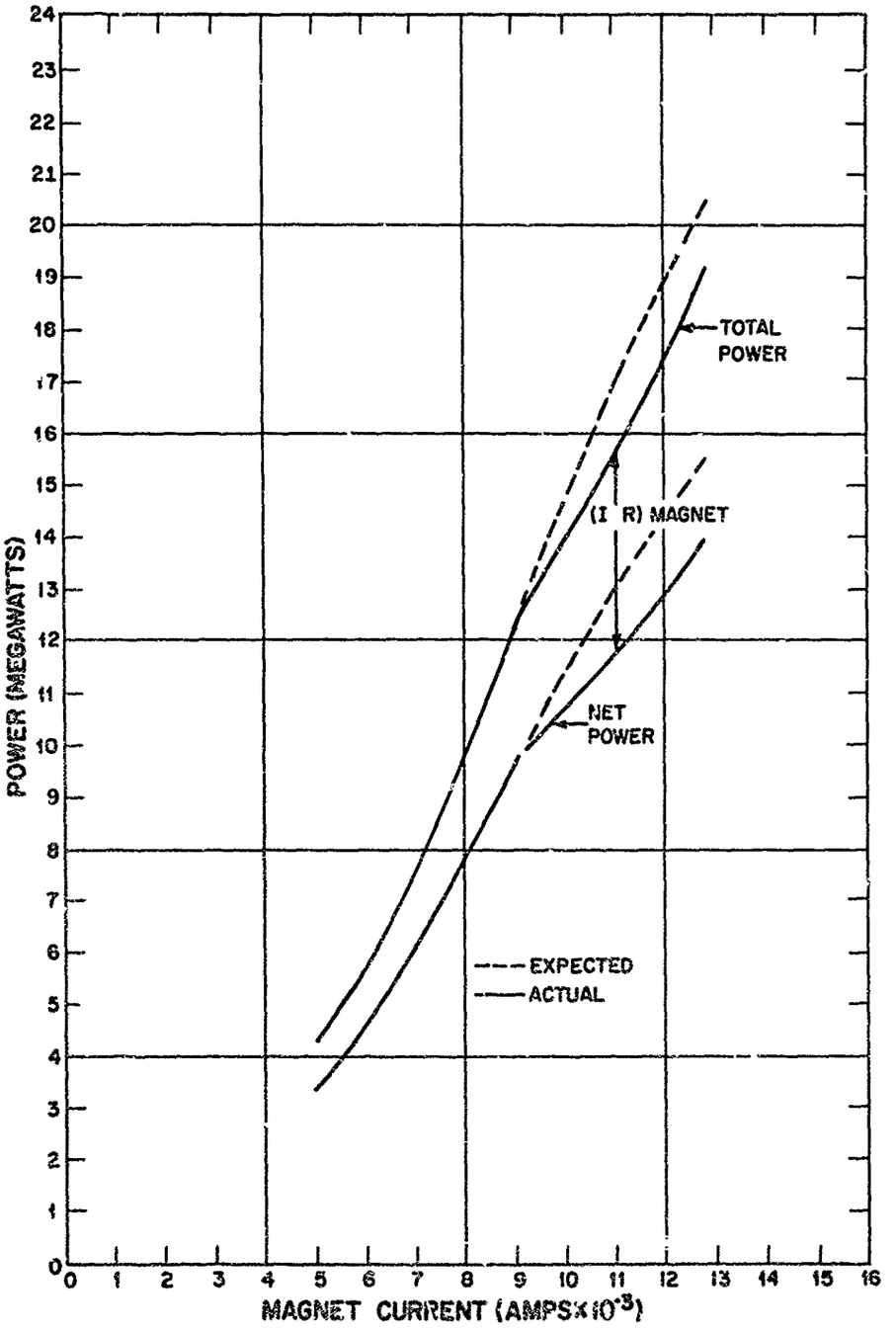

Figure IV-20 Power vs Magnet Current for Power Test #50

A4490

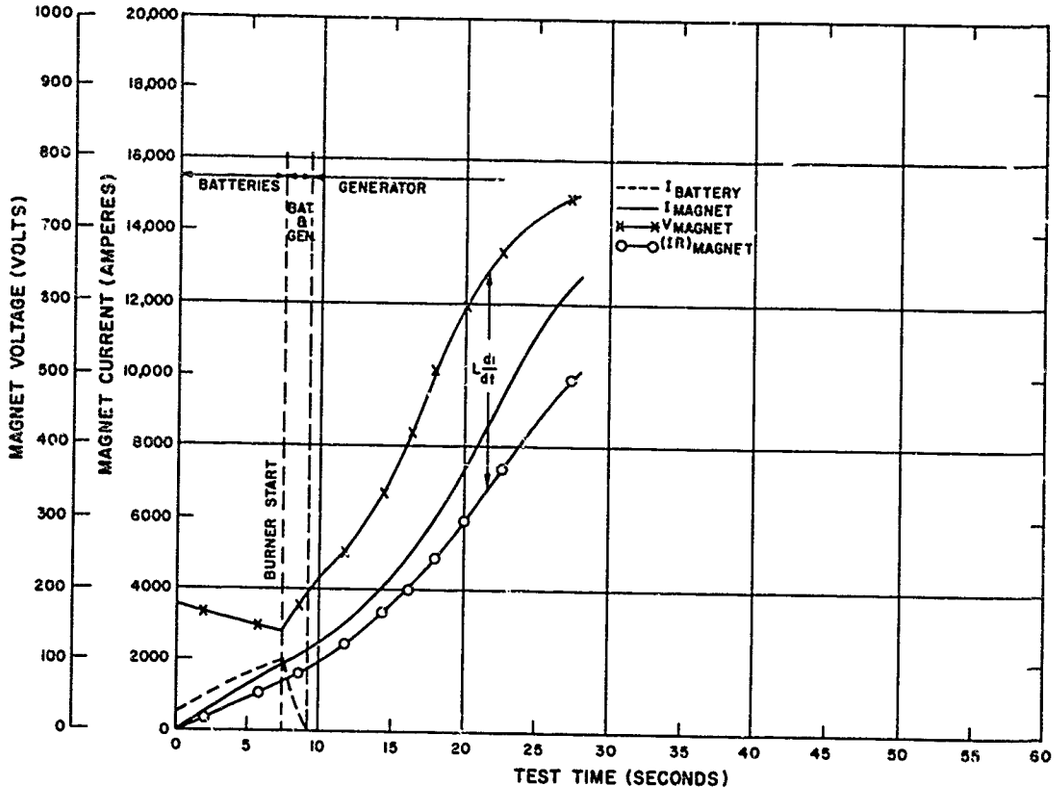

Figure IV-21 Excitation Characteristics for Power Test #51

A4465

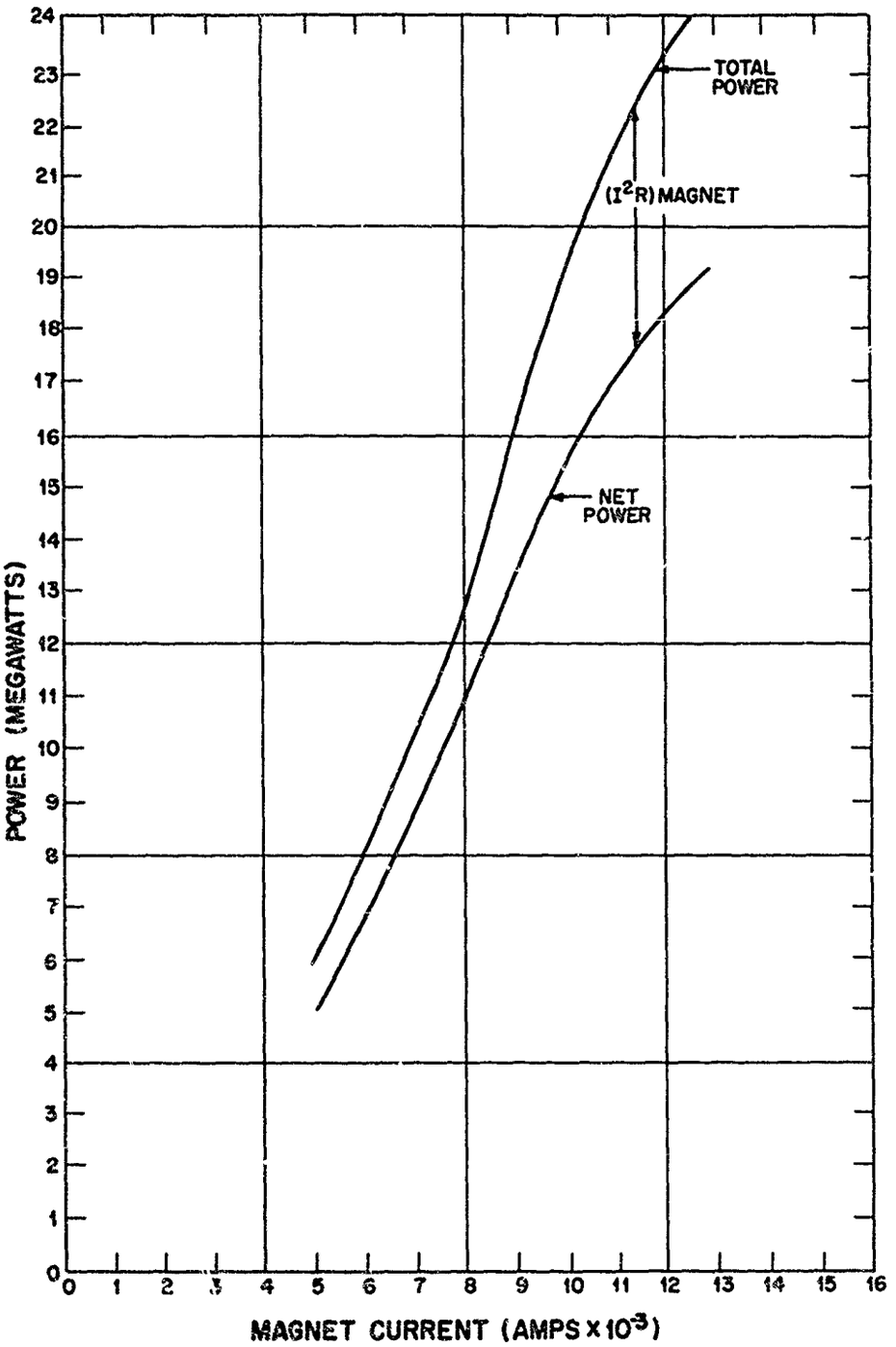

Figure IV-22 Power vs Magnet Current for Power Test #51

A4431

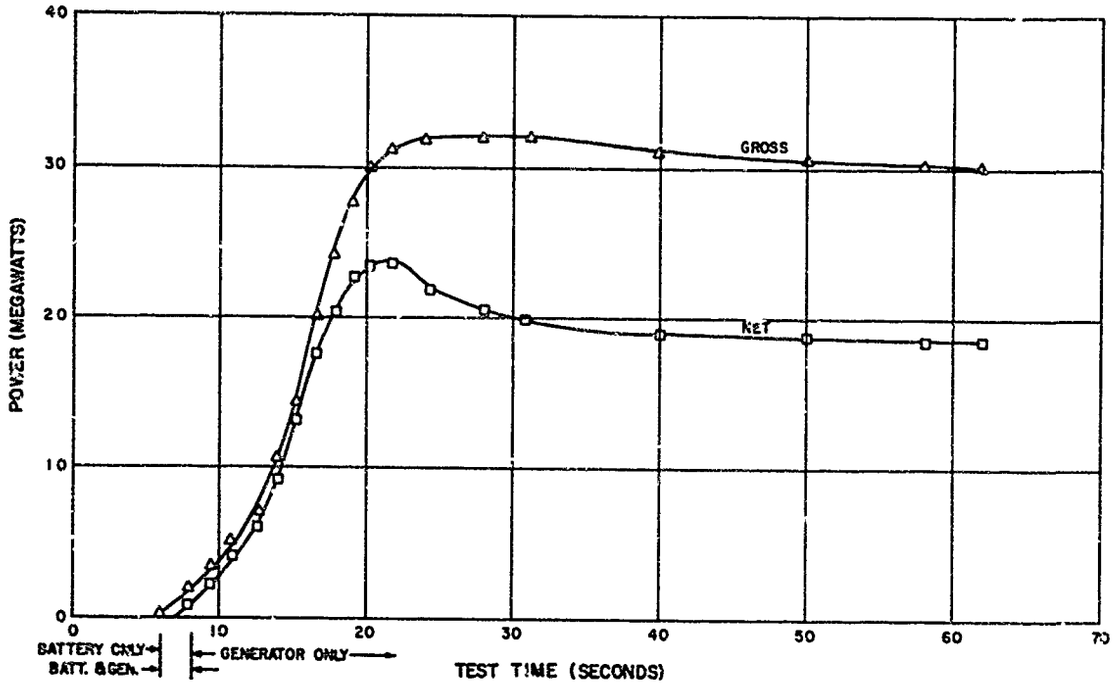

Figure IV-23 Power vs Time for Power Test #56

A3333X

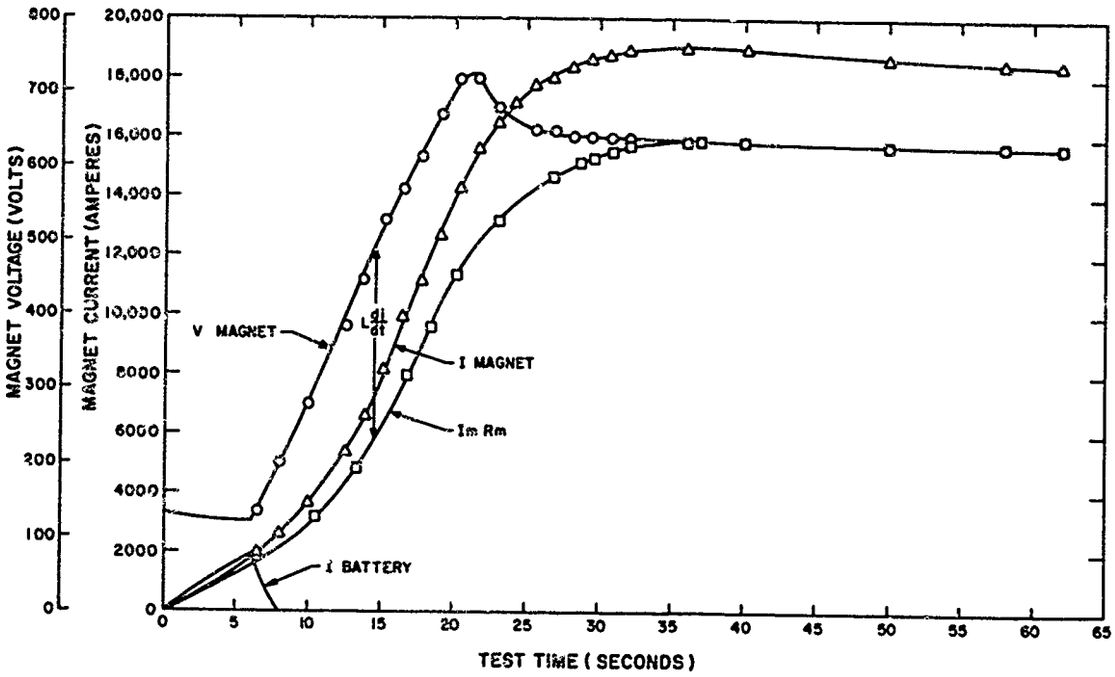

Figure IV-24 Excitation Characteristics for Power Test #56

A5934

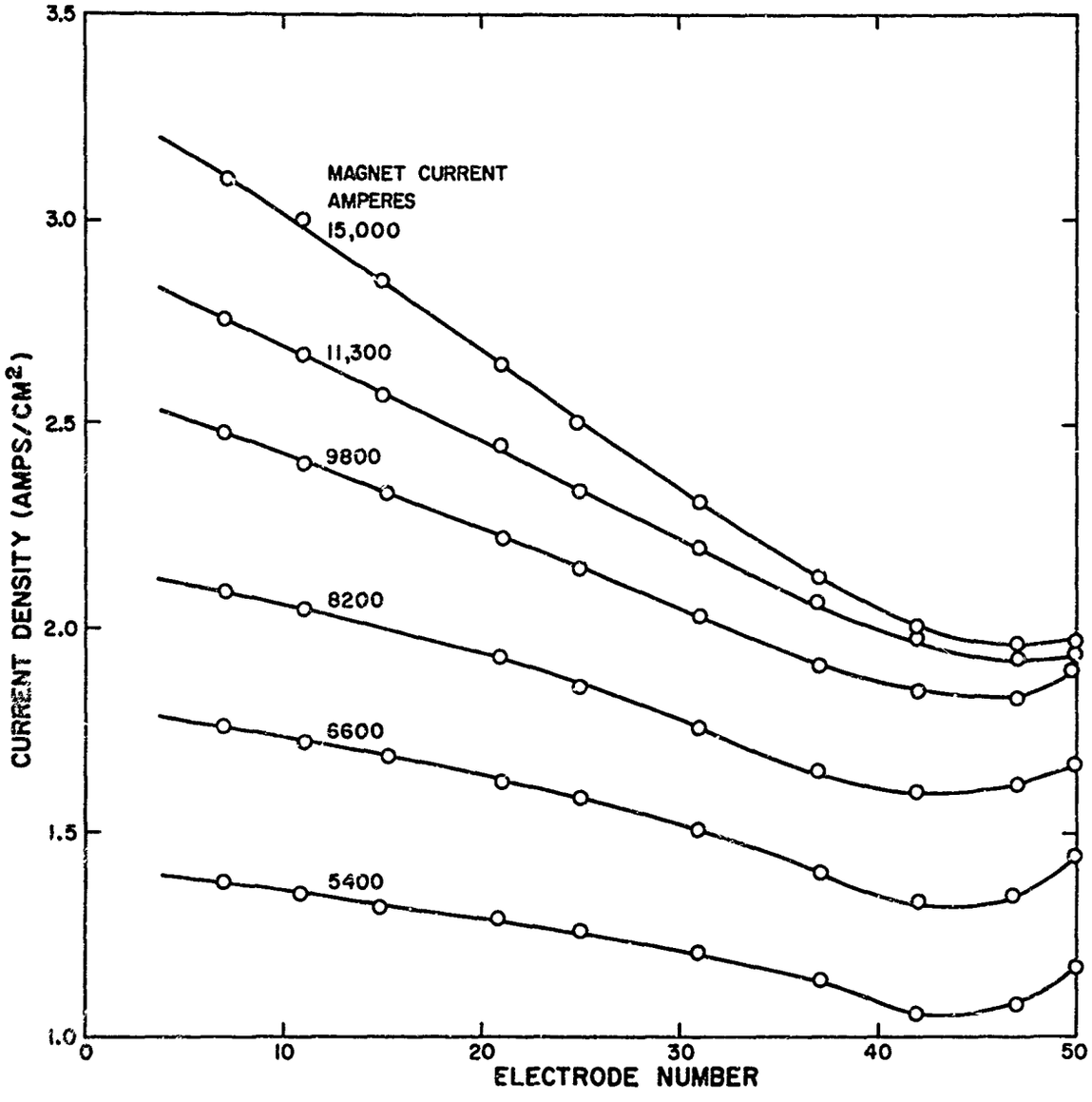

Figure IV-25 Current Density in the Net Power Section for Various Magnet Currents for Power Test #56

A3940

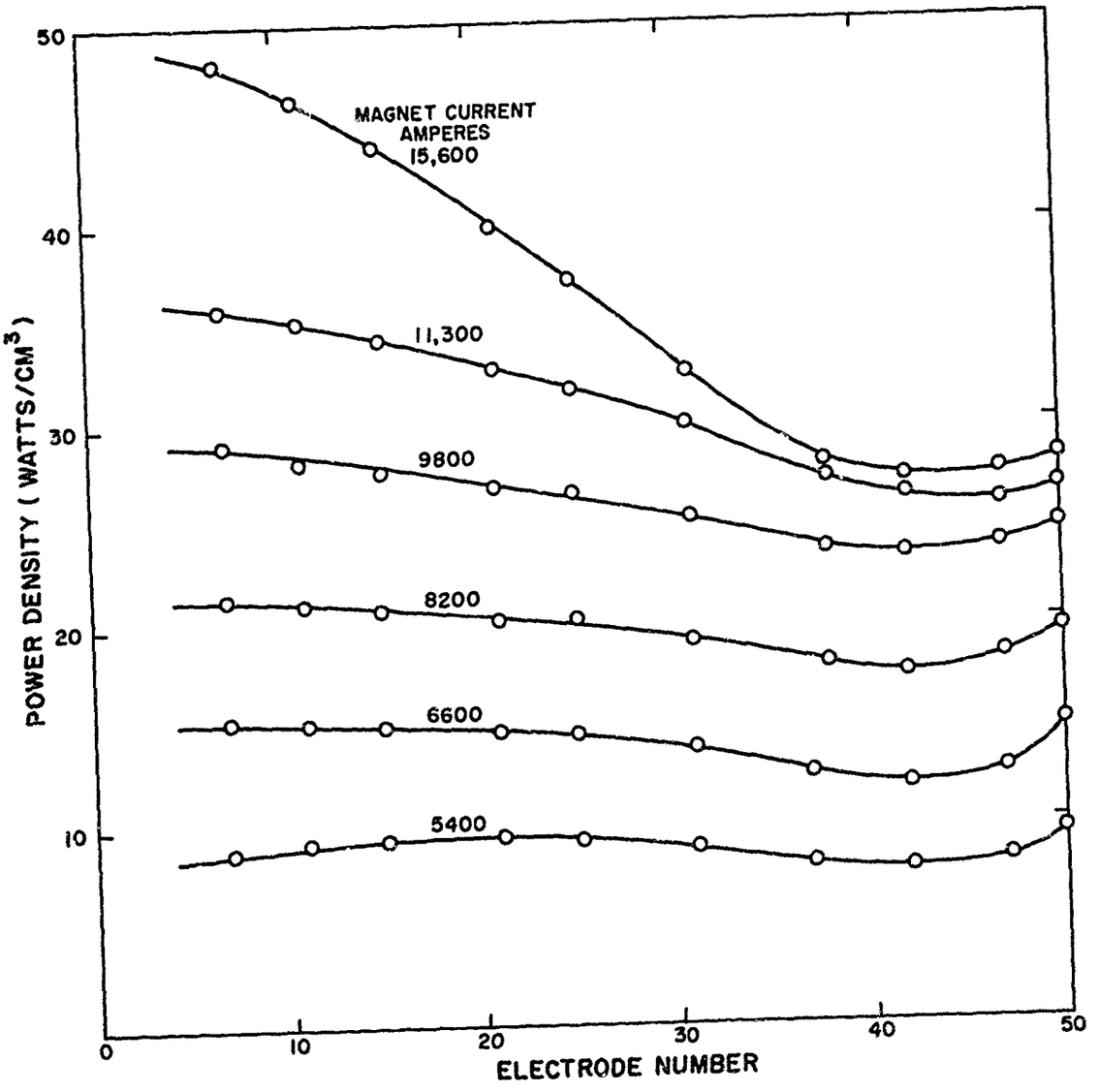

Figure IV-26 Power Density in the Net Power Section for Various Magnet Currents for Power Test #56

A3941

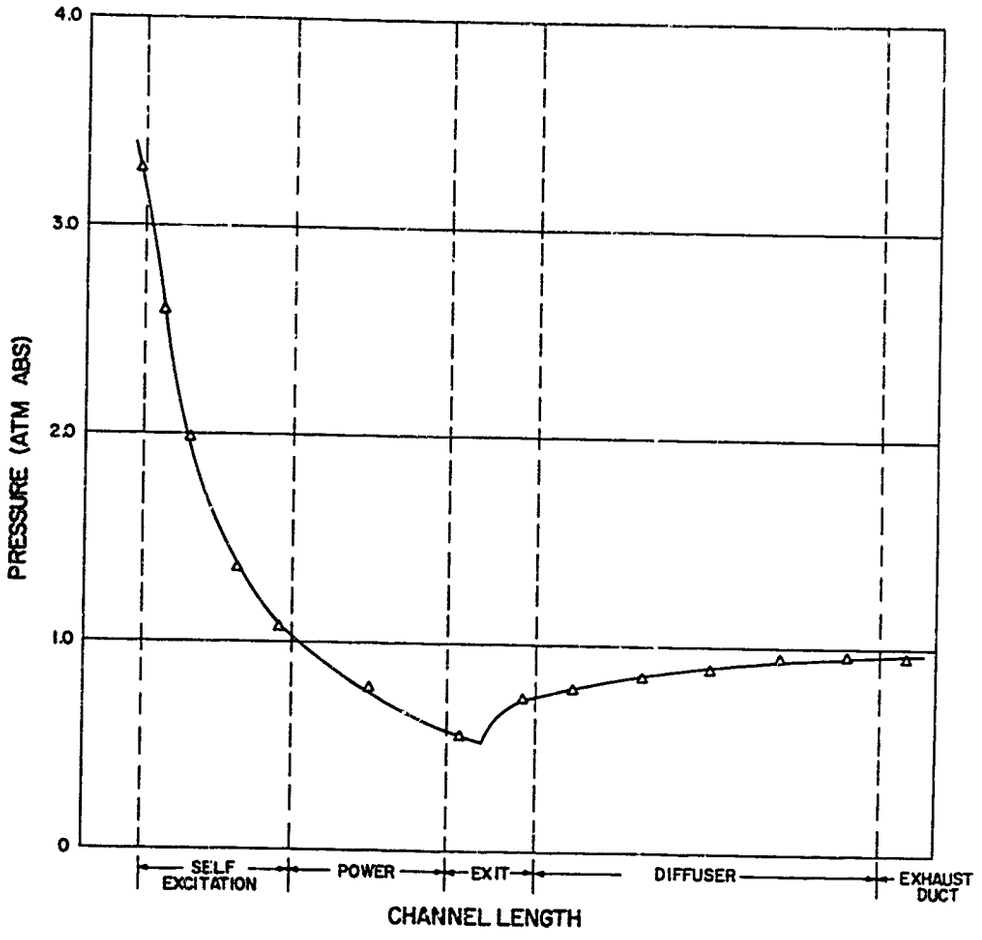

Figure IV-27 Typical Pressure Distribution Measured at a Magnet Current of 16,000 (A)

A4455

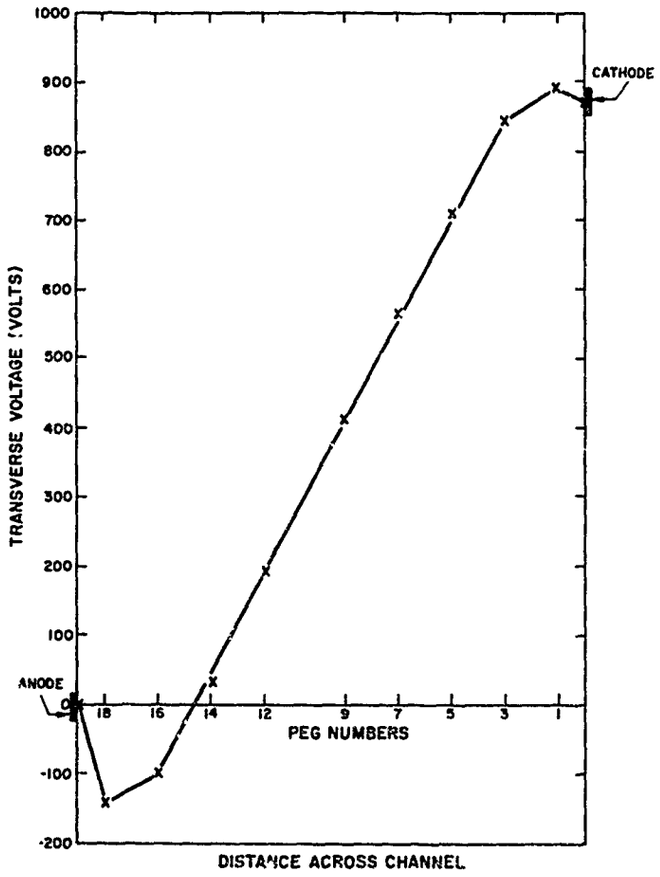

Figure IV-28 Transverse Voltage Distribution Measured for Electrode #21 at a Magnet Current of 16,500 (A) During Power Test #56

A3932

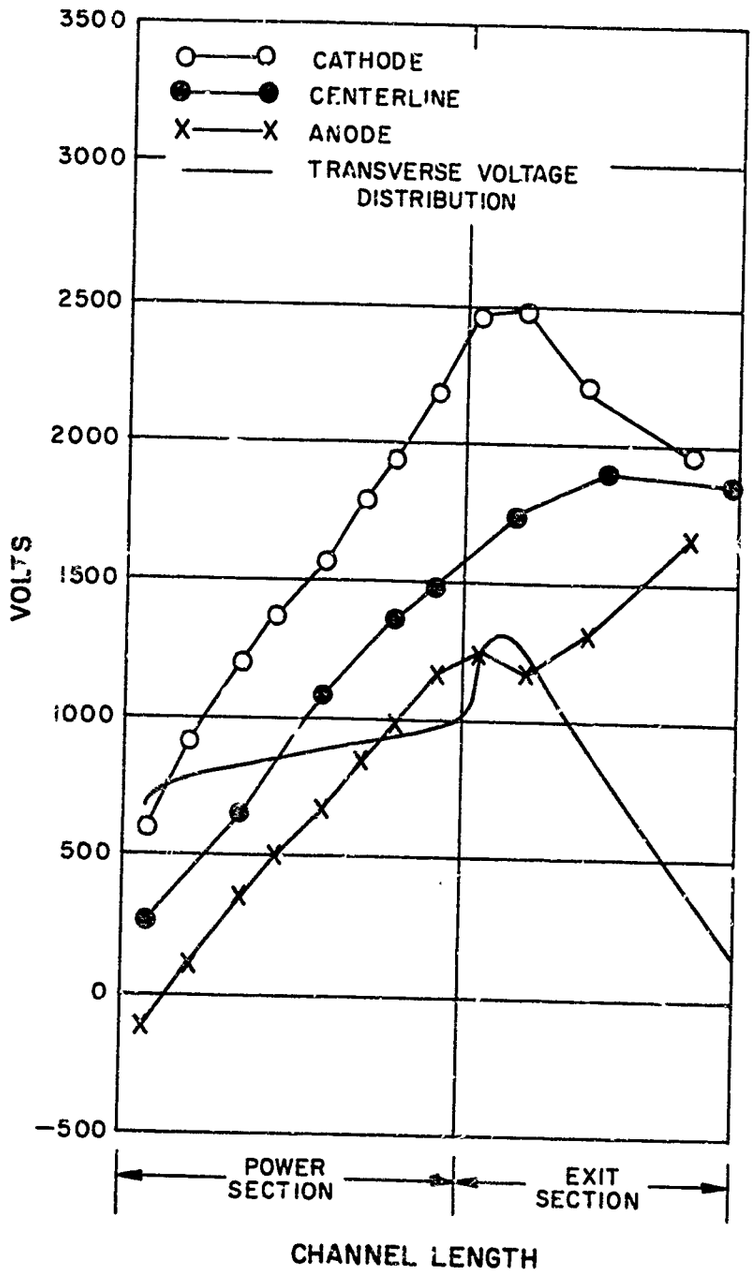

Figure IV-29 Voltage Distributions in the Net Power and Exit Sections for Power Test #56

A4453

V. SUMMARY

The progress during this testing program did not come easily, and many important problems were encountered and solved during the course of the test program. These included:

1. Internal Arcing in the Generator Channel

Internal arcing occurred particularly on the electrode walls. This, together with internal water leaks in the generator channel, has been the problem, manifested itself with the first test, and remained a prime consideration throughout the whole program. Destructive arcs which also destroy performance can be prevented only if the magnitude and polarity of the electric field, particularly the axial components are carefully controlled. The electric field in the generator causes a potential to exist between adjacent metal elements of both the electrode and insulating walls. In the electrode walls the potential difference is due to a combination of the Hall effect and a change in the induced voltage with distance along the channel. The latter component is due to the change both in the gas velocity and channel size. If an arc forms between adjacent elements of the insulating wall the j x B force on the arc is such as to blow the arc along the surface of the wall and extinguish it. Thus, the insulating walls can sustain relatively high interelement potentials of the order of 3^ volts. The situation on the electrode walls is more complicated and it has been found that "favorable" and "unfavorable" electric field gradients exist. A favorable voltage gradient exists for the case when an arc formed between adjacent electrodes is driven off the wall by the j x B force on the arc. The unfavorable gradient exists when the arc is driven into the wall by the j x B force. When the arc is driven into the wall it can cause extensive damage and water leaks. Therefore, the unfavorable voltage gradient should be avoided or minimized. The situations yielding favorable and unfavorable gradients on the two electrode walls are summarized in Table 1 below:

Table 1

	Anode (internal)	Cathode (internal)
$E_x > 0$	favorable	unfavorable
$E_x < 0$	unfavorable	favorable
$E_{Hall} < 0$	unfavorable	favorable

$\frac{dVy}{dx} > 0$	favorable	favorable
$\frac{dVy}{dx} < 0$	unfavorable	unfavorable

where E_x is the axial field and Vy the transverse voltage.

It is seen that a situation where $\frac{dVy}{dx} > 0$ leads to a favorable gradient. Thus, the generator loading should be such that the transverse voltages increase with length along the duct. This can be achieved except in the exit where the voltage must drop to zero. It is necessary to cease the loading in the exit where a favorable gradient can no longer be maintained.

Unlike the transverse voltage, the effect of which is symmetric along both electrode walls, the Hall effect produces an asymmetric favorable vs unfavorable situation. The Hall effect increases the favorable gradient on the cathode (positive electrode looking into the generator) and creates an unfavorable situation on the anode. By far the greatest difficulty has been experienced on the anode wall of the net power output section where arcs have caused substantial damage to the electrodes, steel backing for the electrodes, and the water seals. The unfavorable gradient must be maintained at less than approximately 30-40 volts between adjacent elements. Favorable gradients approximately twice this amount can be tolerated.

2. Internal Water Leaks in the Generator Channel

Internal water leaks occurred particularly on the electrode walls. The channel was built in 1963 with a 1962 technology. It represented an extreme advance in size over the excited water cooled channels of approximately 10 kilowatts output, and even over heat sink designs of one megawatt output (the Mark II). The channel, as built, contains thousands of water seals which, in retrospect, can become exposed to combustion gases, attacked by arcs, or opened due to flexing and thermal stress, and is extremely vulnerable to water leaks. The insulating peg walls have, in fact, performed adequately in spite of this vulnerability, but the problem has been ever present on the electrode walls where a water leak can insulate the electrode from the gas and cause an arc, or where an arc between electrodes can cause a leak. Present channel construction methods would largely eliminate water leak problems.

3. Electrodes

The electrodes originally installed were inadequate to handle the current which concentrated in spots and contributed to arcing and water leaks.

4. The Combustion Chamber Backplate Injector

As originally built, this piece was inadequate to handle the heat loads. After repairs and modifications failed, the backplate was discarded in favor of one fabricated of copper, and no further difficulties have been experienced.

5. Recirculation of Exhaust Quench Water in MHD Channel

It was discovered that during startup, and indeed during the steady state operation of the generator in the efficient high speed mode, the exhaust cooling water spray was recirculating into the channel due to boundary layer separation in the channel. On the electrode walls of the generator the decelerated flow in the impulse mode of operation corresponds to an adverse pressure gradient. Thus, the boundary layer on the electrode walls is somewhat more susceptible to separation than in the reaction mode of operation. It is believed that this fact, together with the relatively low pressure in the power section as compared with the design mode of operation necessitated the addition of the supersonic diffuser to the generator.

6. Electrical Arcs and Flashover External to Channel

The channel has been removed many times for repairs, and each time it is reinstalled, there is the possibility of an external arc from the channel due to the high potentials (up to 3 KV). The tailpipe has been a bad offender here. The problem is alleviated by very careful attention to details of channel installation.

Originally, it was intended to study the performance of the Mark V generator over a wide range of seeding, mass flow, and loading configurations. However, as the testing program progressed, the main problem was to find an operating configuration which would lead to rated power output without excessive voltage gradients or water leaks. From a strictly fluid dynamic point of view, it was evident from the beginning of the testing program that the generator had more than ample power capability and that the chief problems were of a practical nature.

The original design of the Mark V generator presented in the Final Report on Contract No. AF 33(657)-8380 envisioned operation of both the self-excitation and power sections of the generator at low supersonic

Mach number, $M < 1.2$. The design calculations first figured the performance of the self-excitation section and then used the gas conditions at the exit from the self-excitation section to calculate the performance of the power section. As designed, the output from the power section and excitation section was approximately equal. A much better mode of operation has been found during the testing program. In this mode of operation the power input to the magnet is substantially reduced below the design value. Because of this, the gas enters the power section at a relatively high speed near Mach 2, and for a given magnetic field this leads to higher power density. Thus, it has been possible to achieve ratios of net to exciter power of 3/1 to 5/1, as compared with the 1/1 ratio of the design. This new mode of operation has greatly influenced the design of new MHD generators, including the 20 MW LORHO Pilot MHD power supply at the Arnold Engineering Development Center.

It is interesting to speculate on the reasons why a more efficient mode of operation was not discovered during the design phase of the generator. We have already noted how the power section performance was calculated using only the exit conditions of the exciter at the design current. Secondly, at the time when the design calculations were carried out there was, for reasons which do not seem important now, considerable reluctance to operation on a high supersonic mode, and no experiments in that mode had been carried out. It is hoped that this excellent performance of the Mark V in the impulse mode will greatly add to the flexibility of the MHD generator design.

With the achievement of net output at greatly reduced magnet current, the penalty for self-excitation of an MHD generator has been greatly reduced.

VI. CONCLUSION

The Mark V has exceeded its design net output of 20 megawatts, and has provided a convincing demonstration of the ability to generate huge amounts of electric power with a rocket exhaust.

Specific important accomplishments during the program have included:

1. Demonstration of the capability to design a rocket-driven MHD generator to drive a specific load (the magnet).

2. Demonstration that self-excitation is easily achieved.

3. Achievement in excess of rated net output, but at only 87% of rated mass flow.

4. Achievement of higher ratio of net power to magnet power rather than design value through operation of the generator power output section in a high supersonic mode. This represents a very significant advance in fluid mechanics, and is already influencing design of new MHD equipment.

5. Very significant advance in the practical art and technology of MHD generators.

6. Demonstration of reliable and safe operation of rocket-driven MHD generators.

We believe that, as a result of the program, it should be possible now to provide such equipment for ground based applications, and to proceed to further development for specialized air or space borne applications. The results of this work should also be applicable in general to MHD generators using any polyatomic gas as the working fluid, and in particular to the hydrogen cooled nuclear rocket and to cases where the working fluid is hypersonic shock heated air, and to possible air or space force units employing special high performance combustion gases as the working fluid.

Unclassified

Security Classification

DOCUMENT CONTROL DATA - R&D

(Security classification of title, body of abstract and indexing annotation must be entered when the overall report is classified)

1 ORIGINATING ACTIVITY (Corporate author) Avco-Everett Research Laboratory 2385 Revere Beach Parkway Everett, Massachusetts	2a. REPORT SECURITY CLASSIFICATION Unclassified 2b GROUP

3 REPORT TITLE

Detailed Performance Evaluation of the Mark V Self-Excited Rocket Driven MHD Generator

4 DESCRIPTIVE NOTES (Type of report and inclusive dates)

Final Technical Report

5. AUTHOR(S) (Last name, first name, initial)

Avco-Everett Research Laboratory

6. REPORT DATE	7a. TOTAL NO. OF PAGES	7b. NO. OF REFS
October 1965	164	None

8a CONTRACT OR GRANT NO. AF 33(615)-1862 b. PROJECT NO. Project Code No. 6329 c. d.	9a. ORIGINATOR'S REPORT NUMBER(S) 9b. OTHER REPORT NO(S) (Any other numbers that may be assigned this report) AFAPL-TR-65-112 ARPA Order No. 291

10. AVAILABILITY/LIMITATION NOTICES

11. SUPPLEMENTARY NOTES	12. SPONSORING MILITARY ACTIVITY ARPA, AF Aero Propulsion Lab. Research and Technology Div. AFSC, Wright-Patterson AFB, Ohio

13 ABSTRACT

A rocket-driven self-excited MHD generator designed for a net power output of 20,000 kilowatts has been tested. The generator was designed to demonstrate the feasibility of using an MHD device to provide power at very high levels with relatively simple equipment. This report describes the generator and the testing program performed to study the characteristics of self-excitation and the combined operation of self-excitation and power output.

The initial test period was devoted to achieving self-excitation which is described together with the major problems involved. The stress is placed on the effect of L di/dt, loading, control of battery bank and test firing point, together with end effects experienced in the channel. After obtaining sufficient knowledge of the self-excitation and the control [illegible]of, the major effort was concentrated on the production of net power output.

The dynamics of the generator working fluid are discussed, together with the effects of various loadings of the generator. The transverse voltage distributions on the channel, together with the axial voltage and Hall voltage measurements taken, and their influence on generator performance, are presented. Power and current density and their variation are shown with power and magnet current relationships.

Significant results of the generator testing program were the production of a new power of 23,600 kilowatts with a gross power output of 32,000 kilowatts.

DD FORM 1 JAN 64 1473

Unclassified

Security Classification

Unclassified

Security Classification

14 KEY WORDS	LINK A		LINK B		LINK C	
	ROLE	WT	ROLE	WT	ROLE	WT
1. Generators, magnetohydrodynamic.						
2. Magnetohydrodynamic power generation.						
3. Mark V MHD Generator.						
4. Generators, Rocket driven.						
5. Power generation.						
6. Magnet, aircore.						
7. Electrodes.						

11

INSTRUCTIONS

1. ORIGINATING ACTIVITY: Enter the name and address of the contractor, subcontractor, grantee, Department of Defense activity or other organization *(corporate author)* issuing the report.

2a. REPORT SECURITY CLASSIFICATION: Enter the overall security classification of the report. Indicate whether "Restricted Data" is included. Marking is to be in accordance with appropriate security regulations.

2b. GROUP: Automatic downgrading is specified in DoD Directive 5200.10 and Armed Forces Industrial Manual. Enter the group number. Also, when applicable, show that optional markings have been used for Group 3 and Group 4 as authorized.

3. REPORT TITLE: Enter the complete report title in all capital letters. Titles in all cases should be unclassified. If a meaningful title cannot be selected without classification, show title classification in all capitals in parenthesis immediately following the title.

4. DESCRIPTIVE NOTES: If appropriate, enter the type of report, e.g., interim, progress, summary, annual, or final. Give the inclusive dates when a specific reporting period is covered.

5. AUTHOR(S): Enter the name(s) of author(s) as shown on or in the report. Enter last name, first name, middle initial. If military, show rank and branch of service. The name of the principal author is an absolute minimum requirement.

6. REPORT DATE: Enter the date of the report as day, month, year; or month, year. If more than one date appears on the report, use date of publication.

7a. TOTAL NUMBER OF PAGES: The total page count should follow normal pagination procedures, i.e., enter the number of pages containing information.

7b. NUMBER OF REFERENCES: Enter the total number of references cited in the report.

8a. CONTRACT OR GRANT NUMBER: If appropriate, enter the applicable number of the contract or grant under which the report was written.

8b, 8c, & 8d. PROJECT NUMBER: Enter the appropriate military department identification, such as project number, subproject number, system numbers, task number, etc.

9a. ORIGINATOR'S REPORT NUMBER(S): Enter the official report number by which the document will be identified and controlled by the originating activity. This number must be unique to this report.

9b. OTHER REPORT NUMBER(S): If the report has been assigned any other report numbers *(either by the originator or by the sponsor)*, also enter this number(s).

10. AVAILABILITY/LIMITATION NOTICES: Enter any limitations on further dissemination of the report, other than those imposed by security classification, using standard statements such as:

(1) "Qualified requesters may obtain copies of this report from DDC."

(2) "Foreign announcement and dissemination of this report by DDC is not authorized."

(3) "U. S. Government agencies may obtain copies of this report directly from DDC. Other qualified DDC users shall request through _____."

(4) "U. S. military agencies may obtain copies of this report directly from DDC. Other qualified users shall request through _____."

(5) "All distribution of this report is controlled. Qualified DDC users shall request through _____."

If the report has been furnished to the Office of Technical Services, Department of Commerce, for sale to the public, indicate this fact and enter the price, if known.

11. SUPPLEMENTARY NOTES: Use for additional explanatory notes.

12. SPONSORING MILITARY ACTIVITY: Enter the name of the departmental project office or laboratory sponsoring *(paying for)* the research and development. Include address.

13. ABSTRACT: Enter an abstract giving a brief and factual summary of the document indicative of the report, even though it may also appear elsewhere in the body of the technical report. If additional space is required, a continuation sheet shall be attached.

It is highly desirable that the abstract of classified reports be unclassified. Each paragraph of the abstract shall end with an indication of the military security classification of the information in the paragraph, represented as *(TS)*, *(S)*, *(C)*, or *(U)*.

There is no limitation on the length of the abstract. However, the suggested length is from 150 to 225 words.

14. KEY WORDS: Key words are technically meaningful terms or short phrases that characterize a report and may be used as index entries for cataloging the report. Key words must be selected so that no security classification is required. Identifiers, such as equipment model designation, trade name, military project code name, geographic location, may be used as key words but will be followed by an indication of technical context. The assignment of links, rules, and weights is optional

Unclassified

Security Classification